DIODE PUMPED Nd:YAG LASER DEVELOPMENT

C. W. Reno and D. G. Herzog

Advanced Technology Laboratories
Government and Commercial Systems
RCA
Camden, New Jersey

May 1976

Final Report

Prepared for

GODDARD SPACE FLIGHT CENTER
Greenbelt, MD 20771

TECHNICAL REPORT STANDARD TITLE PAGE

1. Report No.	2. Government Accession No.	3. Recipient's Catalog No.

4. Title and Subtitle	5. Report Date
DIODE PUMPED Nd:YAG LASER DEVELOPMENT	May 1976
	6. Performing Organization Code
7. Author(s)	8. Performing Organization Report No.
C. W. Reno and D. G. Herzog	ATL-CR-76-02
9. Performing Organization Name and Address	10. Work Unit No.
Advanced Technology Laboratories Government and Commercial Systems RCA Camden, N. J. 08102	11. Contract or Grant No. NAS5-23281
	13. Type of Report and Period Covered
12. Sponsoring Agency Name and Address National Aeronautics and Space Administration Goddard Space Flight Center, Greenbelt, Md. 20771	Final
	14. Sponsoring Agency Code

15. Supplementary Notes

16. Abstract

A low-power Nd:YAG laser was constructed which employs GaAs injection lasers as a pump source. Power outputs of 125 mW TEM_{00} CW with the rod at 250°K and the pump at 180°K were achieved for 45 W input power to the pump source. Operation of the laser, with array and laser at a common heat sink temperature of 250°K, was inhibited by difficulties in constructing long-life GaAs LOC laser arrays. Tests verified pumping with output power of 20 to 30 mW with rod and pump at 250°K. Although life tests with single LOC GaAs diodes were somewhat encouraging (with single diodes operating as long as 9000 hours without degradation), failures of single diodes in arrays continue to occur, and 50 percent power is lost in a few hundred hours at 1 percent duty factor. Because of the large recent advances in the state of the art of CW room temperature AlGaAs diodes, their demonstrated lifetimes of greater than 5000 hours, and their inherent advantages for this task, it is recommended that these sources be used for further CW YAG injection laser pumping work.

17. Key Words (Selected by Author(s))	18. Distribution Statement
Nd:YAG laser Injection laser Diode-pumped laser GaAs injection laser AlGaAs diodes	

19. Security Classif. (of this report)	20. Security Classif. (of this page)	21. No. of Pages	22. Price*
Unclassified	Unclassified		

*For sale by the Clearinghouse for Federal Scientific and Technical Information, Springfield, Virginia 22151.

PREFACE

A low-power Nd:YAG laser was constructed which employs GaAs injection lasers as a pump source. Power outputs of 125 mW TEM_{oo} CW with the rod at 250°K and the pump at 180°K were achieved for 45 W input power to the pump source. Operation of the laser, with array and laser at a common heat sink temperature of 250°K, was inhibited by difficulties in constructing long-life GaAs LOC laser arrays. Tests verified pumping with output power of 20 to 30 mW with rod and pump at 250°K or above. Although life tests with single LOC GaAs diodes were somewhat encouraging (with single diodes operating as long as 9000 hours without degradation), failures of single diodes in arrays continue to occur, and 50 percent power is lost in a few hundred hours at 1 percent duty factor. Because of the large recent advances in the state of the art of CW room temperature AlGaAs diodes, their demonstrated lifetimes of greater than 5000 hours, and their inherent advantages for this task, it is recommended that these sources be used for further CW YAG injection laser pumping work.

ACKNOWLEDGMENTS

The contributions of A. Limm and F. Hughes of RCA, Lancaster, PA, and of H. Lockwood, H. Kressell, and M. Ettenberg of the RCA Laboratories, Princeton, NJ, were particularly significant to this work in the realm of laser diode materials technology. The consultations with and support by H. Lockwood were of great assistance throughout the program.

TABLE OF CONTENTS

LIST OF ILLUSTRATIONS

LIST OF ILLUSTRATIONS (Continued)

LIST OF ILLUSTRATIONS (Continued)

LIST OF TABLES

Section I

INTRODUCTION AND SUMMARY

This report describes the results of a program that extended over a 30-month period, whose objective was the development and test of a laboratory model of an injection laser pumped Nd^{3+}:YAG laser. As a step in evaluating the usefulness of injection laser pumping for possible aerospace applications, this research and development program was undertaken to evaluate the performance of near room temperature operation ($\leqslant 250°K$) of pump and laser material. Injection laser diode pumping of Nd:YAG continues to be attractive although results in this program were not conclusive. The attractiveness of injection laser diodes is enhanced by their sma size, their ability to operate with very low input power, their long life (exhibited in selected samples and in CW diodes), and by their relatively graceful decline when the fail.

Because of the great improvements made in the state of the art in CW AlGaAs injection lasers during this contract, emphasis should now shift to CW AlGaAs pumps for this application. Although careful control of fabrication is stabilizing the lifetime of pulsed injection lasers, the advantages of CW diodes lead to system configurations that are ultimately more attractive than pulsed systems. Many of the benefits of these configurations are now demonstrable. Some of the advantages of CW diodes include 1) their ability to operate from a dc source without pulsed drivers, 2) the bette match of their wavelength to Nd:YAG, and 3) their demonstrated lifetimes exceeding 10,000 hours, which is much better than most pulsed units.

The emphasis of this program should shift to the development of CW pumping wit fiber optics as the probable coupling mechanism. Fiber optics coupling allows the selection of single laser diodes and leads to efficient coupling into a small rod volum which creates a relatively high pumping rate. This in turn reduces the effect of thermal changes. In addition, the excellent wavelength match now available for CW diodes into the 806 nm absorption band of Nd:YAG requires substantially lower Nd co centration and low scattering media.

The laser developed for this program has produced 125 mW TEM_{00} with a rod temperature of 250°K and a pump temperature of 175°K. Because of difficulties encountered in producing long life pump arrays for pumping at 250°K, effort was concentrated on array lifetime. The best power output at 250°K for pump and array was 20 to 30 mW because array life intervened and no adequate array was available for th full demonstration.

By operating at the end of cold fingers coupled to a liquid nitrogen dewar, the temperature of the laser rod and the laser diode arrays could be varied between 150°K and 300°K. This allowed rapid characterization of the various system parameters.

The laser diode outputs are coupled through a slit into a close wrapped integrating chamber containing the laser rod. This allowed multiple path absorption in the laser rod with ease of coupling to the laser rod.

Rods have been evaluated having both external and internal mirrors. Measurements made on rods with 1.3% Nd doping have indicated excessive scattering losses of approximately 0.3%/cm. Preliminary tests with a 1% Nd rod indicate a scattering loss of approximately 0.03%/cm. This latter rod should provide considerably higher efficiency when incorporated in the system. Experimental work with the Nd:YAG laser is discussed in Section II of this report.

Both laser rod and laser diodes are cooled to 250°K in the present system concept. This is considered a useful concept because of the relative ease of attaining spacecraft temperature stabilization at this temperature. This allows some notable advantages in wavelength tuning for GaAs large optical cavity (LOC) diodes.

GaAs LOC diodes were selected for this program because of their relatively high wavelength reproducibility, advanced state-of-the-art, and the accessibility of a usable (not optimum) pump absorption band in Nd:YAG at 885 nm. The diode pump arrays designed for this system have employed 14 to 18 subarrays of nine to ten 0.006-inch laser diodes in a linear array. More recent subarray concepts employ nine subarrays of 12 to 14 stripe contacted laser diodes in a linear array.

In support of the experimental work, calculations of Nd:YAG performance over a range of parameters were carried out, including pump repetition frequency, pump power, temperature, coupling, and loss parameters. This is discussed in Section III of the report.

Section IV of this report discusses the development of pulsed injection laser arrays for 250°K operation. Section V describes laser diode array hybrid drivers which were designed and fabricated. Conclusions and recommendations are presented in Section VI.

Section II

EXPERIMENTAL OPERATION OF INJECTION LASER PUMPED Nd:YAG LASERS

In this section, pumping by homojunction and heterojunction laser diode arrays is described. Experimental work began by using homojunction laser arrays (which were available at the beginning of this work) in configurations that would allow the required light power to be generated for pumping Nd:YAG at the desired levels. Because arrays were not available to allow such operation at room temperature, parallel efforts which were begun in rod pumping and in room temperature array development were merged at the appropriate time. For the purposes of concept verification, a path was chosen which did not first test lifetime properties because of the short time cycle. Thus, when lifetime was found to be a serious problem, a major shift in emphasis was required.

The apparatus used for pumping Nd:YAG rods using homojunction arrays is shown in simplified form in Figure 1. This has been employed in pumping using various injection laser arrays. Salient features of some of the experimental work are compared to the contract goals in Table 1.

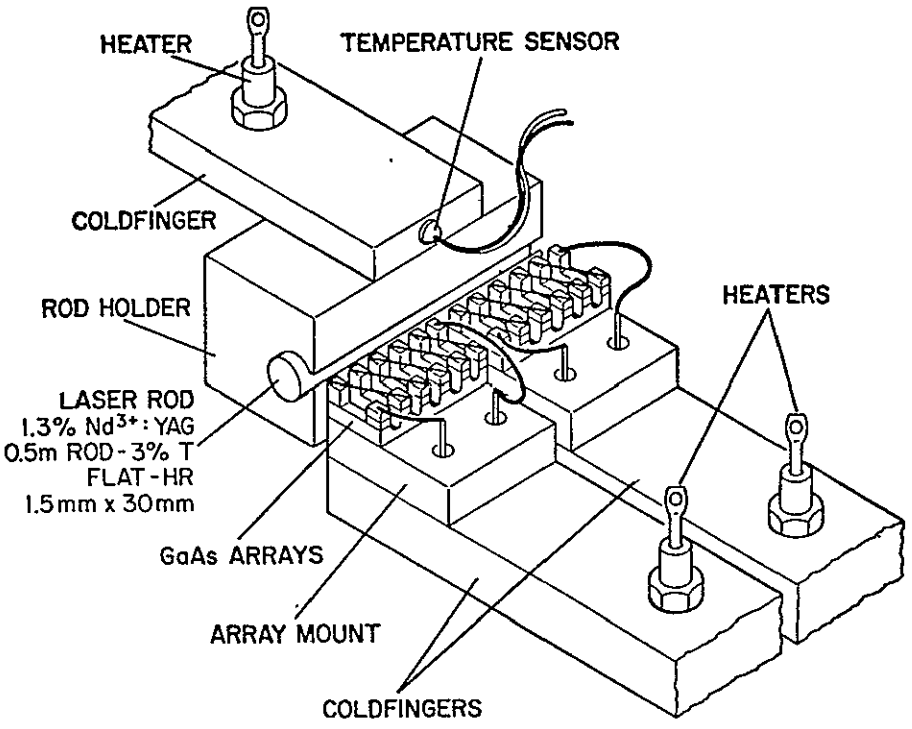

Figure 1. GaAs laser diode pumped Nd^{3+}:YAG laser assembly.

TABLE 1. SUMMARY OF LASER DIODE PUMP PROGRAM

	Output Power (mW)	Mode	Ripple (%)	Input Power (W)	Rod Temp. (°K)	Array Temp. (°K)	Pump Band (nm)
Performance Goals	125	TEM_{oo}	5	50	258	258	
Performance Achieved							
Pulse Pumped	125	TEM_{oo}	100	50	250	175	868
Ripple Pulse Pumped	40	TEM_{oo}	10	65	220	250	885

A. HOMOJUNCTION ARRAY PUMPING

The 150°K temperature required for homojunction arrays requires operating the GaAs laser arrays in a dewar cooled with liquid nitrogen. The assembly used is illustrated in Figure 1. The Nd:YAG rod is 5 cm long. A line source of approximately this length was required. Three 30-diode homojunction arrays in line make a line source of about 40 mm.

Each array is mounted on an individual copper plate 0.5 inch x 0.5 inch x 0.125 inch which contains the connectors for supplying power to the array. Each copper plate is mounted on the end of a copper finger, 0.5 inch x 0.125 inch x 4.5 inches. At the end of each finger, adjacent to the array are two 10-W zener diodes as heaters.

The fingers with these heaters are designed to allow the temperature of the array, operating at full power, to be maintained at any temperature between 100°K and 225°K. These fingers are attached to a copper block which is maintained at 77°K by liquid nitrogen in a metal dewar. The total width of the fingers (1-1/2 inches) required the partial reconstruction of an existing dewar. Experiments were conducted with the Nd:YAG rod in close proximity to the GaAs diode arrays. A brass box was mounted in place of one of the normal dewar windows. This box has windows at each end, at right angles to the normal dewar windows. The fingers containing the GaAs arrays extend into this box. An additional finger below these fingers carries the mount for the Nd:YAG rod. Heaters are included to allow temperature control of the rod. Adjusting screws, extending through the box wall, adjust the position of the Nd:YAG rod with respect to the GaAs arrays. The radiation from the rod is observed through the box windows.

Measurements of the array characteristics were made. The purpose of the measurements was the determination of the temperature at which the arrays would lase at the required wavelength of 868 nm and the determination of the bandwidth to be expected.

Measurements of the peak wavelength for the diodes in Array "B" were measured and are plotted as a histogram in Figure 2. These measurements were made at wavelengths comparable to those to be used in the experimental configuration. The wavelength spread varies from 2 nm to 3 nm. The change in shape reflects the difference in thermal contact between the diodes and the substrate.

Changes in wavelength with temperature were measured. The emissions from all the diodes in an array were imaged on the slit of the spectrograph for these measurements. Figure 3 shows the temperature vs. wavelength for Array A, an efficient array. The bandwidth variation with temperature was determined by recording the wavelengths at which the output power of the array was reduced to half the peak intensity. The wavelengths are shown by the dotted curve.

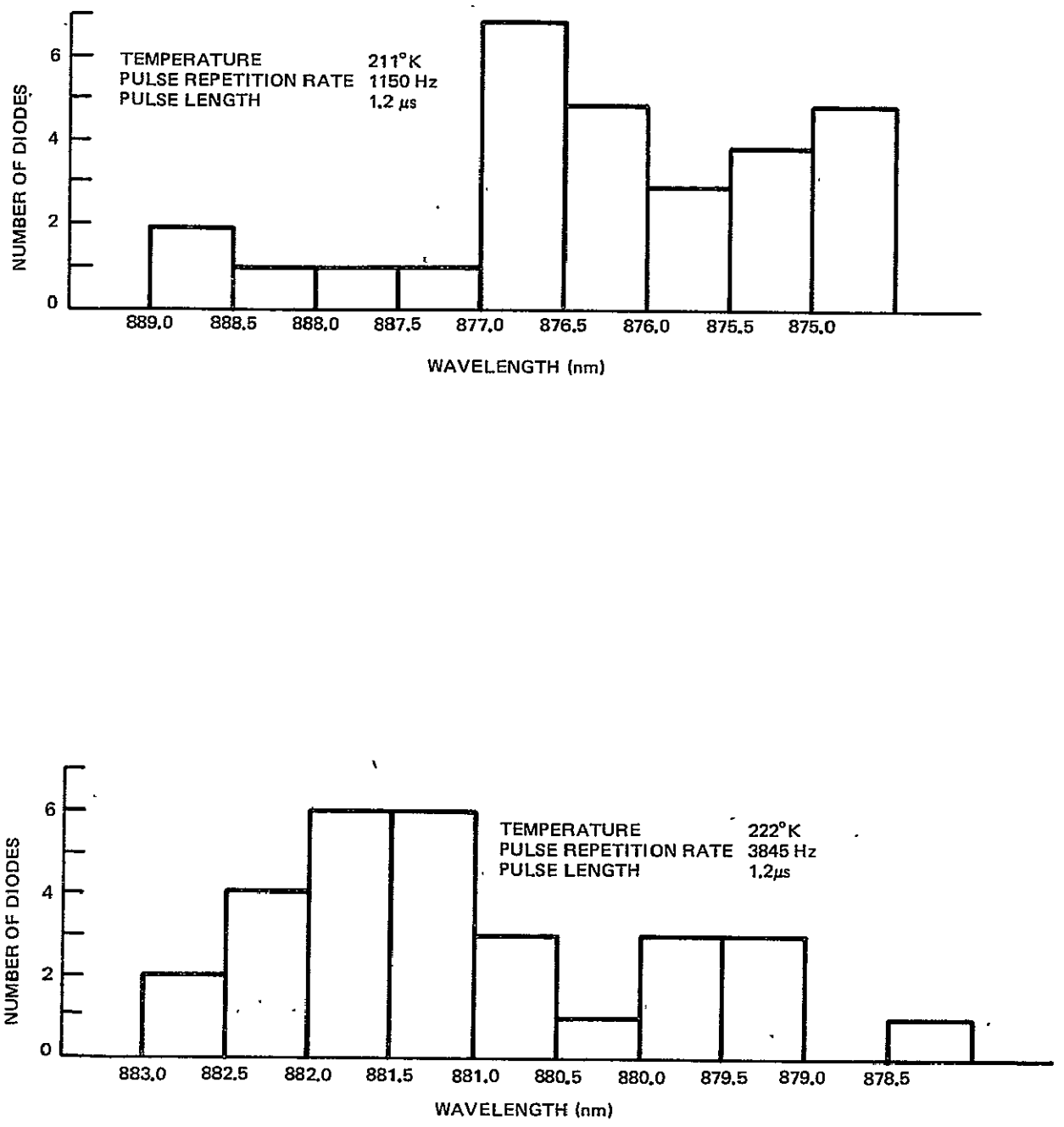

Figure 2. Histogram of wavelength of emission of individual diodes in Array B.

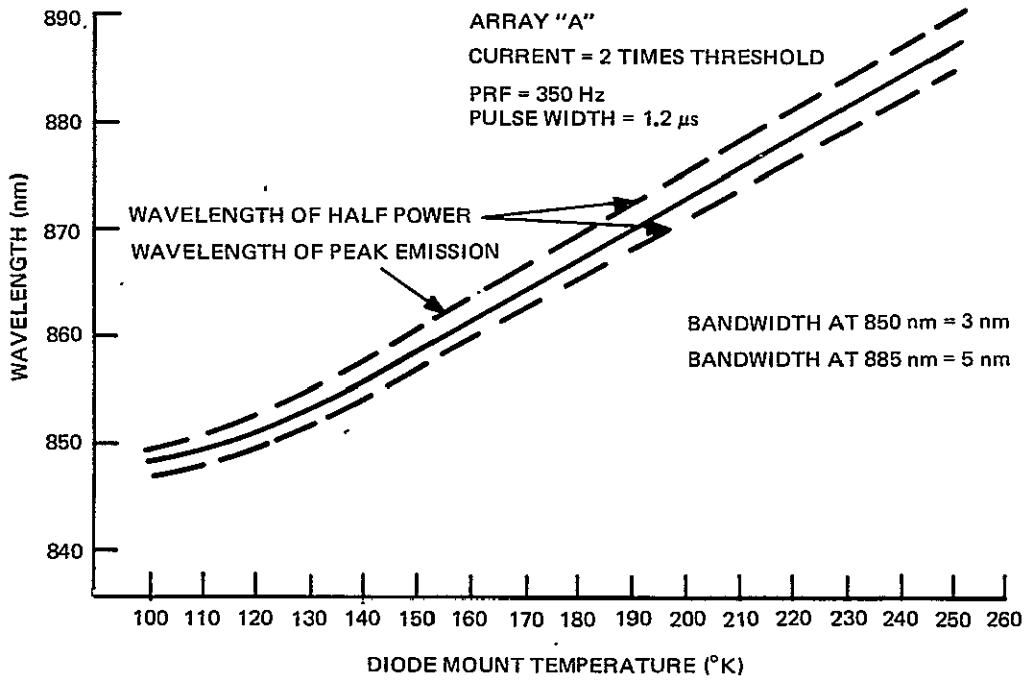

Figure 3. Temperature vs. wavelength for Array A.

As is noted, the bandwidth varies from 3 nm when the peak emission is at 850 nm to 5 nm. The rate of change of wavelength with temperature is 0.28 nm per °K. The temperature in all these measurements is the temperature of the end copper fingers supporting the actual diode mount. The actual diode temperature may be quite different from this temperature because of further ΔT's in the mount.

As a result of an observation that the temperature vs. wavelength curve varied with the duty cycle of the drive current, calibration curves of temperature vs. duty cycle for the arrays were run. The curves for Arrays A, B, and C are shown in Figure 4. The difference in slope in these curves results primarily from differences in thermal resistance due to variation in the mount characteristics between arrays.

1. Experiments with Flat-Flat Mirrors on Rod

Lasing of the Nd:YAG rod with a flat-flat mirror configuration at temperatures between 100°K and 300°K was achieved. The rod was pumped with the best of the three GaAs arrays which was driven in a burst mode, with a burst of 20 pulses, 10 μs apart, every millisecond. The pulses were 0.5 μs long. The GaAs array emitted approximately 60 W peak power. Both the GaAs array and the rod were brought to a temperature of about 170°K. After adjustment, lasing after eight pulses

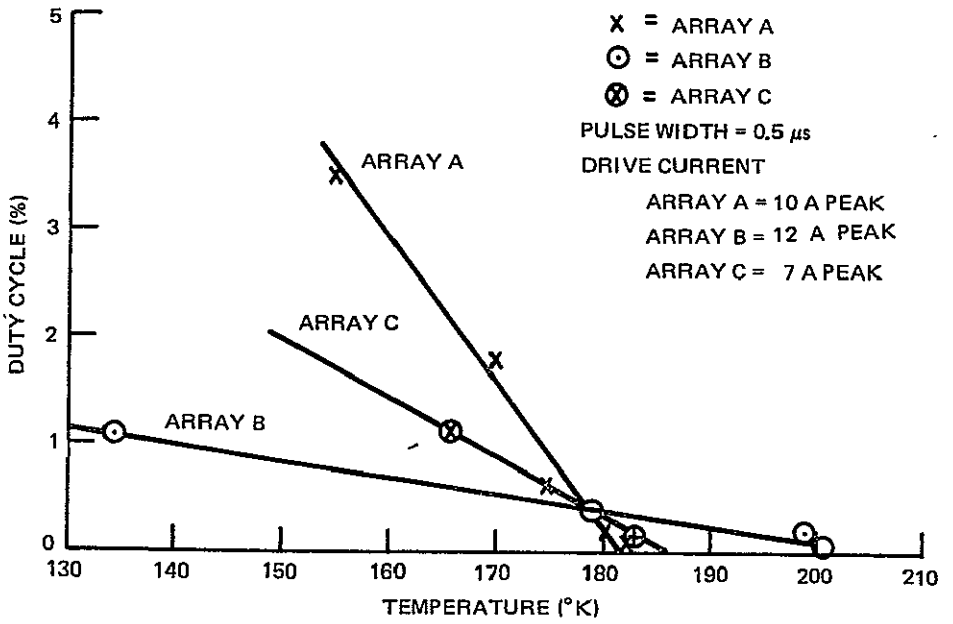

Figure 4. Required temperature for a wavelength of 869.5 nm for various duty cycles.

was accomplished. A photograph of a scope trace showing such lasing is shown in Figure 5. The photocell sensor whose output is shown was observing both the 868 nm radiation from the GaAs laser diodes and the 1.06 μm radiation from the Nd:YAG laser rod. The small regular pulses in the figure are the drive pulses from the GaAs laser diode. After the seventh drive pulse, additional spikes appear delayed in time from the driver pulses. These are the laser pulses from the Nd:YAG rod. They show the high frequency spiking typical of relaxation oscillations.

The following observations were made in this geometry:

a) Lasing was observed at Nd:YAG temperatures from 150°K to 300°K. No one region proved optimum.

b) There were null regions approximately 10°K apart where lasing was not observed, followed by peak regions where lasing was strongest.

c) Two major modes of operation were observed. One mode gave the normal bright small spot. The other mode showed concentric rings. The ring mode was observed most often at low temperatures.

d) Maximum lasing action seemed to occur when the mount was changing temperature slowly.

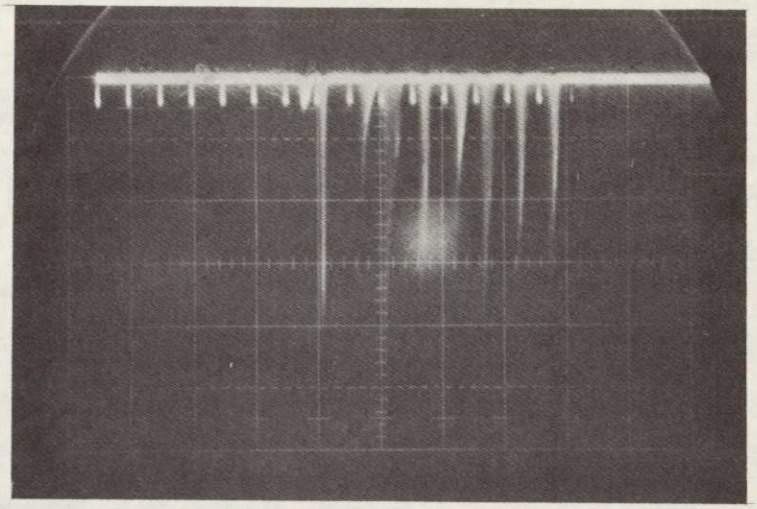

Figure 5. Scope trace showing lasing of Nd:YAG rod.

Analysis of these observations indicated that the Nd:YAG mount was causing bending of the Nd:YAG rod, thereby seriously decreasing the Q of the laser cavity.

2. Nd:YAG Rod Modification

After completion of the basic experiments outlined above, the Nd:YAG rod was broken in handling and was returned to the manufacturer for salvage (to be shortened to eliminate broken portion). Experiments in progress when the rod was broken indicated that more consistent operation could be achieved with less critical alignment. Therefore, a cavity consisting of a spherical surface of 0.5-m radius and a flat was specified for the shortened rod. Experiments on the modified rod showed a great improvement in efficiency.

For experiments with the shortened rod, one GaAs array was driven with 500-ns pulses at a rate of 35 kHz. Figure 6 shows multimode output power as a function of input power. Maximum power corresponds to a drive current peak of 10 A. A typical output waveform is shown in Figure 7. The first two pulses are leakage from the pump pulses. Input to the driver was 100 V at 200 mA. Output power as a function of rod temperature is shown in Figure 8 for one and two arrays driven. An indication of the efficiency of the integrating chamber was given by reducing the rod temperature to 132°K and tuning the pump source. Lasing was observed at pump source wavelengths between 868 nm and 881 nm; however, there was rapid reduction in the available pump power with increasing wavelength because of increased laser diode threshold.

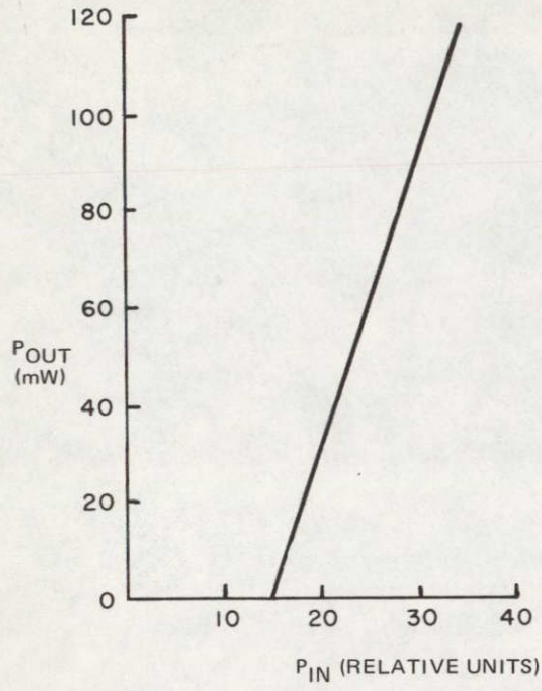

Figure 6. Output power vs. input power (peak power is at 10-A, 500-ns, 35-kHz input).

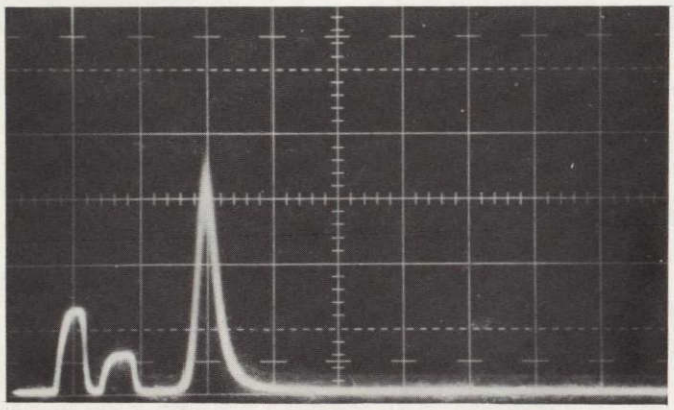

Figure 7. Output waveform (first two pulses are pump source). (0.5 μs/div, 0.1 V/div; average YAG laser power output was 200 mW.)

3. External Mirror Experiments

An Nd:YAG laser rod with an antireflection coating on one end and a highly reflective coating on the other was purchased. The rod was installed with the external mirror mount shown in Figure 9. Figure 10 shows the power output from the Nd:YAG

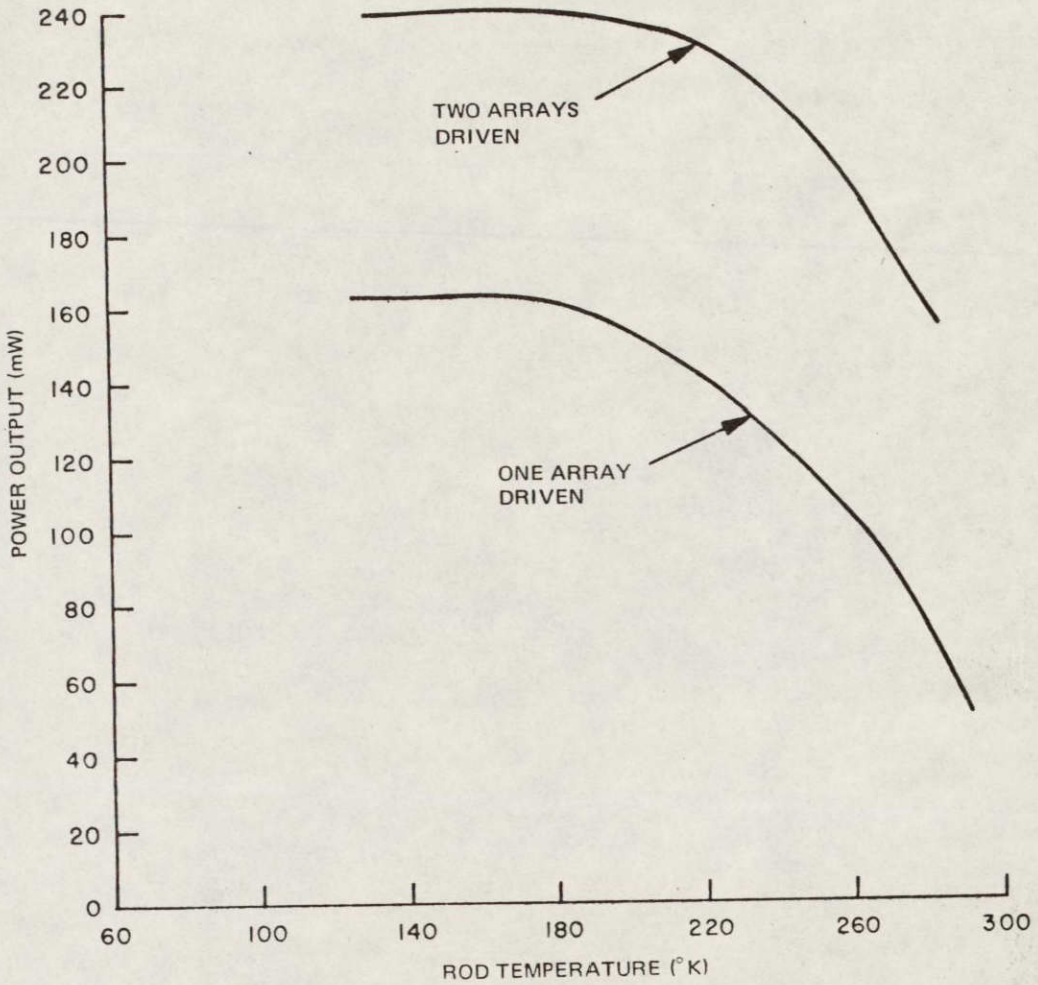

Figure 8. Output power vs rod temperature for one or two arrays driven. (Homojunction arrays, 180°K, short rod, 0.3% output coupling.)

laser vs. temperature for one and two driving arrays and when using a 670-mm radius, 1% laser mirror in the external mirror mount.

The pattern of the radiation from the rod took the form of two distinct nearly circular lobes. These lobes, at a range of 6 m, conformed to the expected size for the TEM_{01} mode, and the double lobing occurred in the plane of the pumping slit. Substitution of a 100-cm radius, 1% output mirror produced similar results with roughly 20% lower output.

Figure 11 shows the output waveform of the Nd:YAG laser driven at 868 nm with two arrays. The arrays were operating at 100 kHz pulse repetition rate with a duty cycle of 1%. The 1-m spherical mirror was used in the cavity. The output power was 80 mW. In the photograph, the top graticule is the base line. As will be

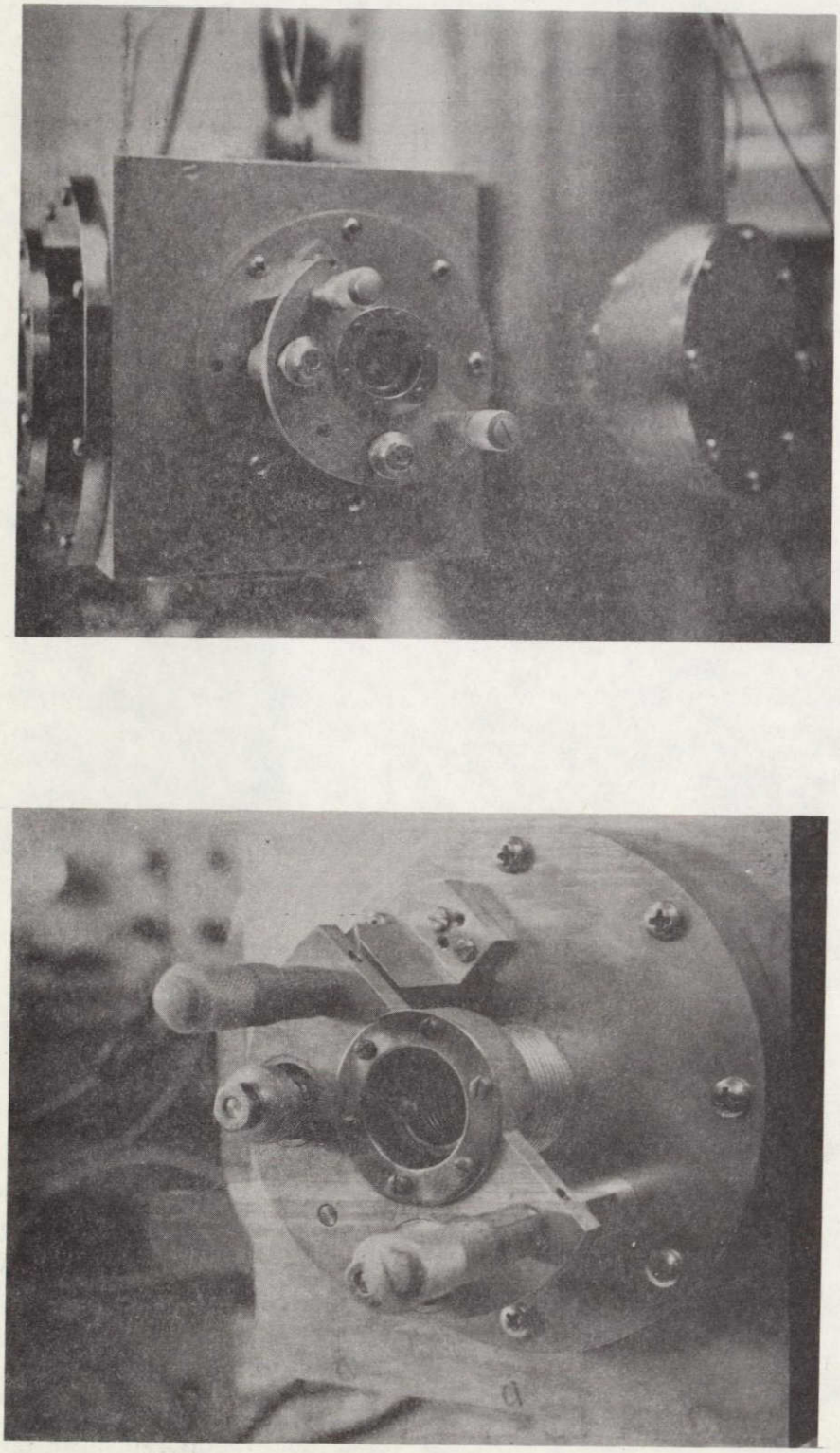

Figure 9. Laser mirror mount.

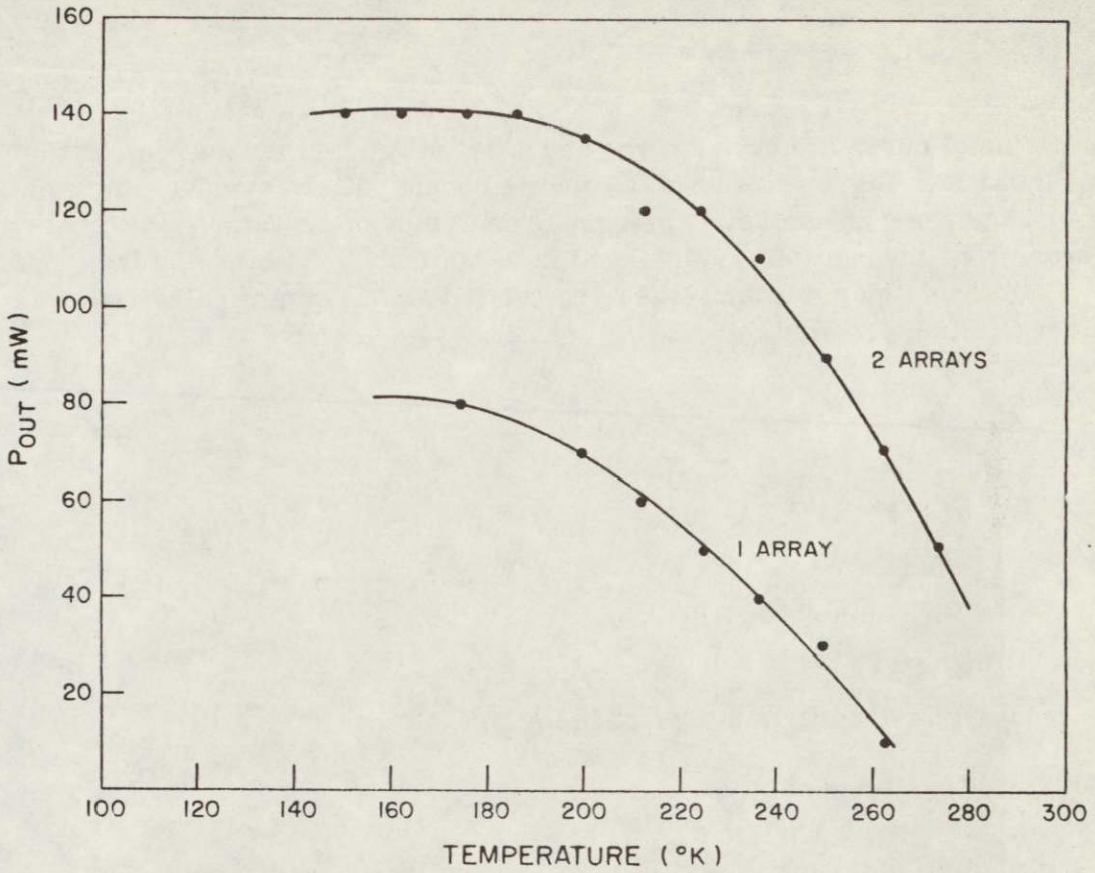

Figure 10. Power output from Nd:YAG laser. (Operating conditions: homojunction arrays, 180°K, 50-mm rod, 67-cm output mirror, 1% transmission, 2-m high reflectivity mirror on rod, 15-cm cavity length.)

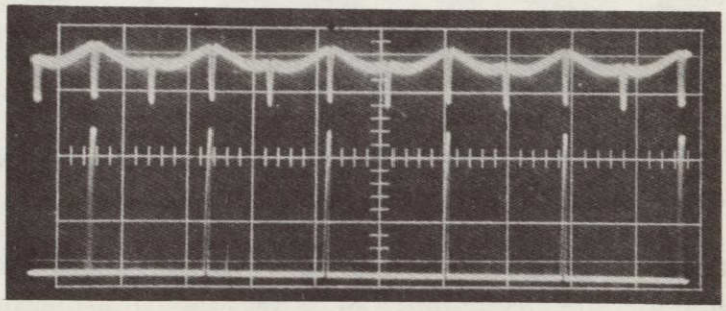

Figure 11. Output waveform of Nd:YAG laser pumped at 868 nm.

noticed, there is a very large amount of dc component in the signal. The ac modulation is less than 50%, and a large portion of this is the result of the difference in output from the two driving arrays. The spikes in the signal are pump pulse radiation leaking through.

4. Laser Mode Experiments

Experiments with the YAG laser were then directed at optimizing the cavity for TEM_{00} operation. TEM_{00} has been achieved for cavity lengths from 22 cm to 30 cm. Optimum length is 25 cm for the current integrating chamber type operation

using a 2-m radius of curvature upon the rod and a flat mirror at the remote location as shown in Figure 12. Figure 13 shows the scanned beam pattern measured at a range, z, of 4.25 m for a 25-cm cavity using a 10-m radius of curvature, 2% transmission mirror. The measured $1/e^2$ diameter is 0.345 inch (4.36 mm radius). For a 25-cm cavity, the minimum mode radius is calculated as 0.382 mm. The radius of the beam at range z is calculated by

$$w_z = \frac{\lambda z}{\pi w_o}$$

where

λ = wavelength (1.0641 μm)

z = range (4.25 m)

w_o = minimum mode radius (0.382 mm).

Substituting these values yields

$$w_z = 3.88 \text{ mm}.$$

The measured radius is 4.36 mm, which is about 12% oversize for a true gaussian beam. This result was expected since it is not a true gaussian beam (the wings are clipped).

Figure 14 shows the TEM_{oo} output power as a function of temperature for three mirrors with different transmissions. The best configuration was that which used 2% output coupling, except for very cold operation at which 3.5% coupling was best. The laser cavity was modified for these experiments by the addition of one or more adapter rings to extend the support for the external mirror.

The output power from the homojunction arrays was measured. A blackened brass block was mounted on the finger in the dewar which had previously held the Nd:YAG rod. A zener diode mounted on this black block permitted accurate control of its temperature. The black block was illuminated by the GaAs arrays operating

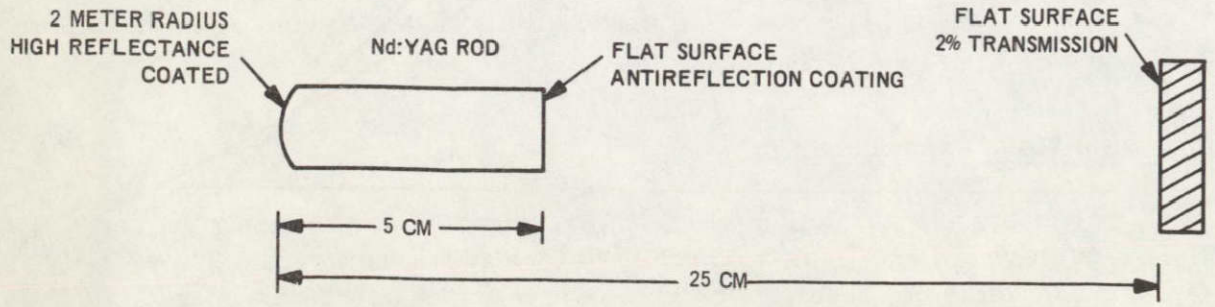

Figure 12. Cavity configuration.

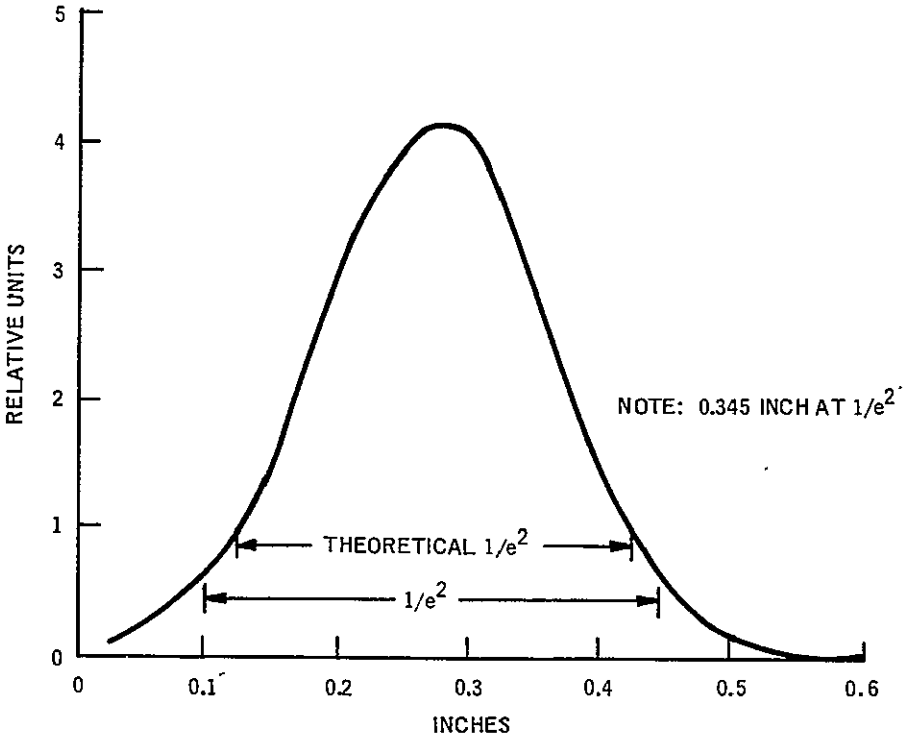

Figure 13. Nd:YAG laser beam pattern.

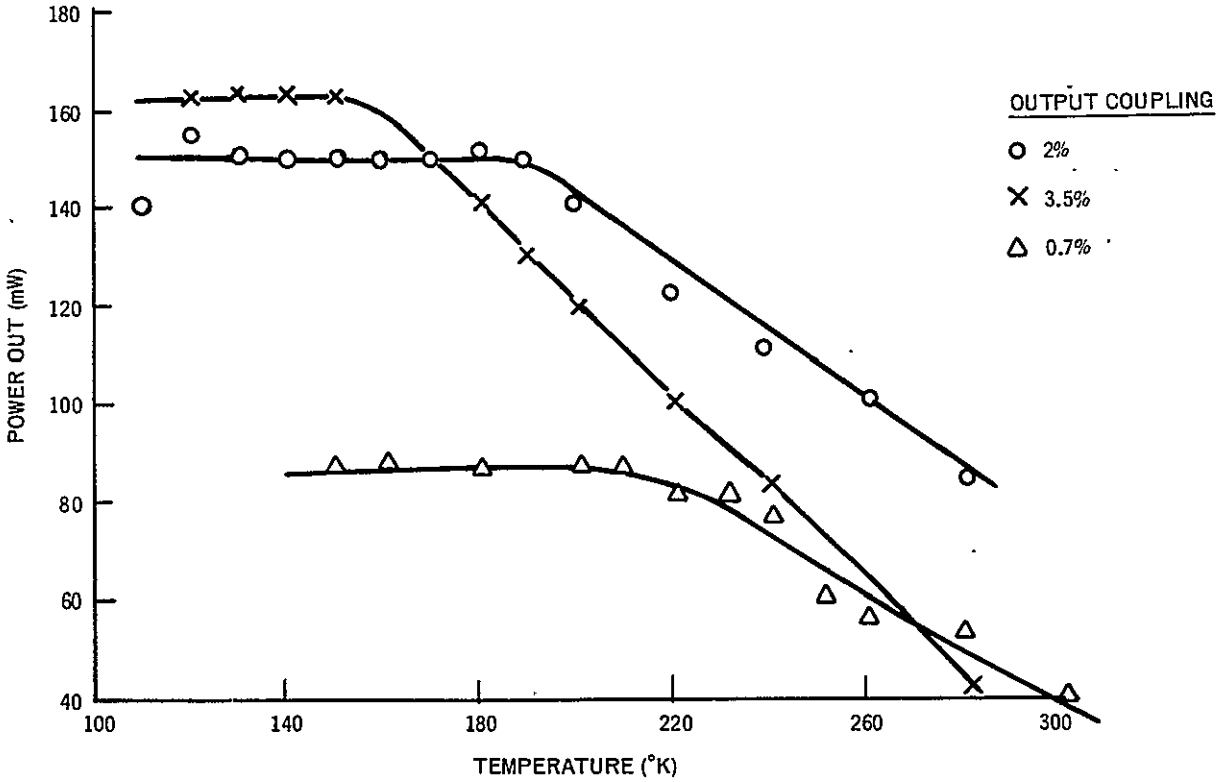

Figure 14. Power output vs temperature. (Operating conditions: 2-m high reflectivity on rod, 50-mm rod, 25-cm cavity length, TEM_{oo} operation.)

under the same conditions as they had been operated for the power output vs. temperature measurement. Then the array drivers were turned off and current was fed to the zener diode until the temperature of the black block was the same as when the array was operating. The absorbed power was determined to be 4 ±0.4 W. The input to the arrays at this time was 47 W.

The 4-W measurement is significant as it gives a direct measurement of the power required to drive the Nd:YAG rod in its holder under the conditions which yielded the output power versus temperature curves shown in Figure 14.

B. SILICON-DOPED GaAs LOC ARRAY EXPERIMENTS

Two GaAs LOC arrays were constructed from material available from stock to permit pumping of the Nd:YAG rod at the 886-nm line; this material was silicon doped. The arrays were labeled 185-1 and 188-1. The numbers 185 and 188 identify the source wafer. Array 185-1 is a 49-diode array, while 188-1 has only about 35 diodes. The threshold current and the emission wavelength were measured relative to the temperature of the mounting block at a duty cycle of less than 0.001. This data is shown in Figure 15. Array 185-1 rather surprisingly has a room temperature wavelength of 877 nm, a considerably lower wavelength than that of homojunction GaAs arrays. The amount of aluminum in the light-confining region must be at a few percent for these diodes. Array 188-1 has a room temperature wavelength of 898 nm, which was the anticipated value.

Figure 15 also shows the near field pattern for arrays 185-1 and 188-1. This pattern was obtained by moving a slit along the array and measuring the output vs. position.

The two silicon-doped LOC arrays have been used to pump the short Nd:YAG laser rod having integral mirrors. For 60 W into the drivers, output power ranged from 40 mW CW at a rod temperature of 180°K to 13 mW CW at 250°K. By measuring the power required to stabilize the rod temperature with and without the drivers in operation, it was determined the power delivered from the arrays into the rod and rod holder was about 500 mW.

The most significant result of these experiments is illustrated in Figure 16. By pumping at a repetition rate of 200 kHz on the array, this output waveform was achieved. Ripple is about 22% peak to peak with no tendency for spiking. A higher repetition rate is expected to greatly smooth the waveform.

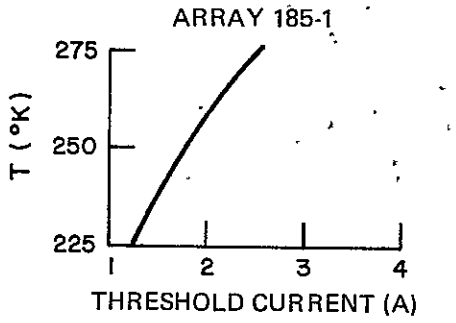

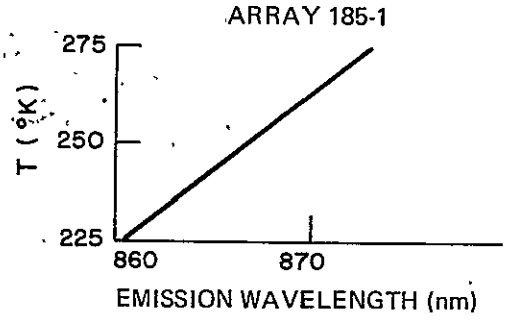

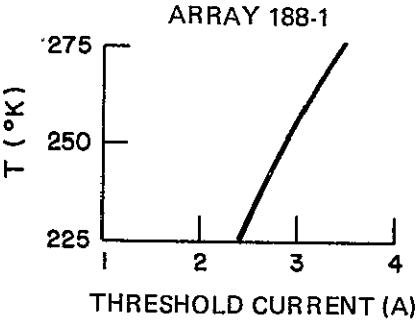

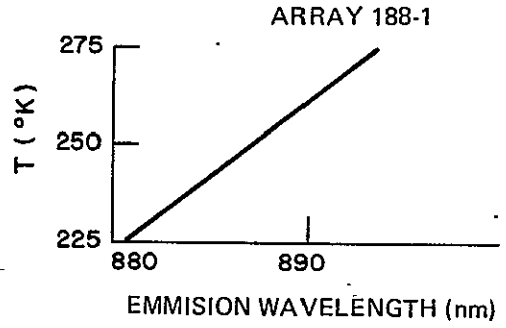

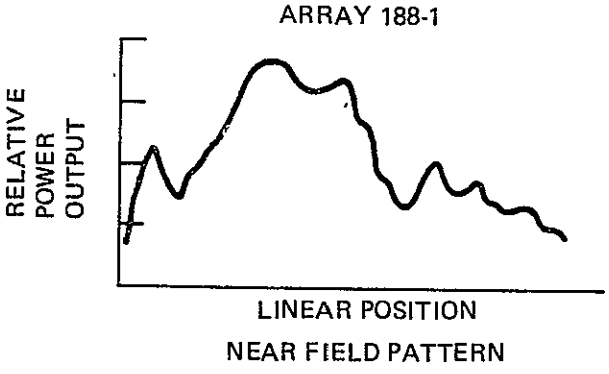

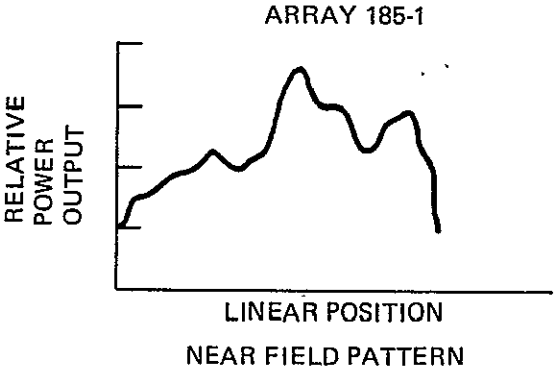

Figure 15. Performance of LOC arrays.

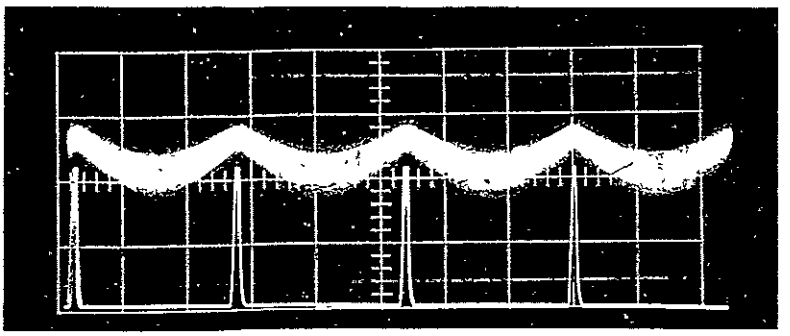

Figure 16. Output waveform of Nd:YAG laser pumped at 886 nm. (Hor. scale: 2 μs/cm)

C. LASER TESTS USING HETEROJUNCTION PUMPS

The major difference between the laser test unit and the previous experimental unit is that the Nd:YAG laser rod was driven by 16 subarrays of nine heterojunction diodes each rather than three arrays of 30 homojunction or heterojunction diodes each used previously. These 16 subarrays were pulsed consecutively, creating a much higher repetition rate.

Sequential driving of the subarrays requires a separate driver for each subarray. The narrow pulses of 50 ns or less require short leads between the arrays and the drivers. Therefore, the drivers are mounted within the vacuum chamber.

Figure 17 shows the fundamental mechanical assembly, with one subarray and one driver unit mounted. The Nd:YAG laser rod and its mount are shown in correct position. The rod is normally mounted on a separate support.

In the dewar the subarray-driver unit is rotated 90 degrees from the position shown. The base plate is mounted on a cold finger which conducts the array heat to the cold plate of the dewar. Heating units are also contained on this plate for temperature control of the GaAs arrays. The Nd:YAG rod and its holder have a separate heater and temperature control.

There are four array driver units on each mounting plate, which conducts the driver heat to the base plate and cold finger. The temperature of the base plate, subarrays and drivers is controlled as a unit. To temperature tune individual subarrays, the width of the pulse driving each array is varied, varying the input power.

To house the assembly shown in Figure 17, a box 8 inches on each side was constructed as an appendage to the dewar. The box has windows to permit the necessary optical measurements to be made.

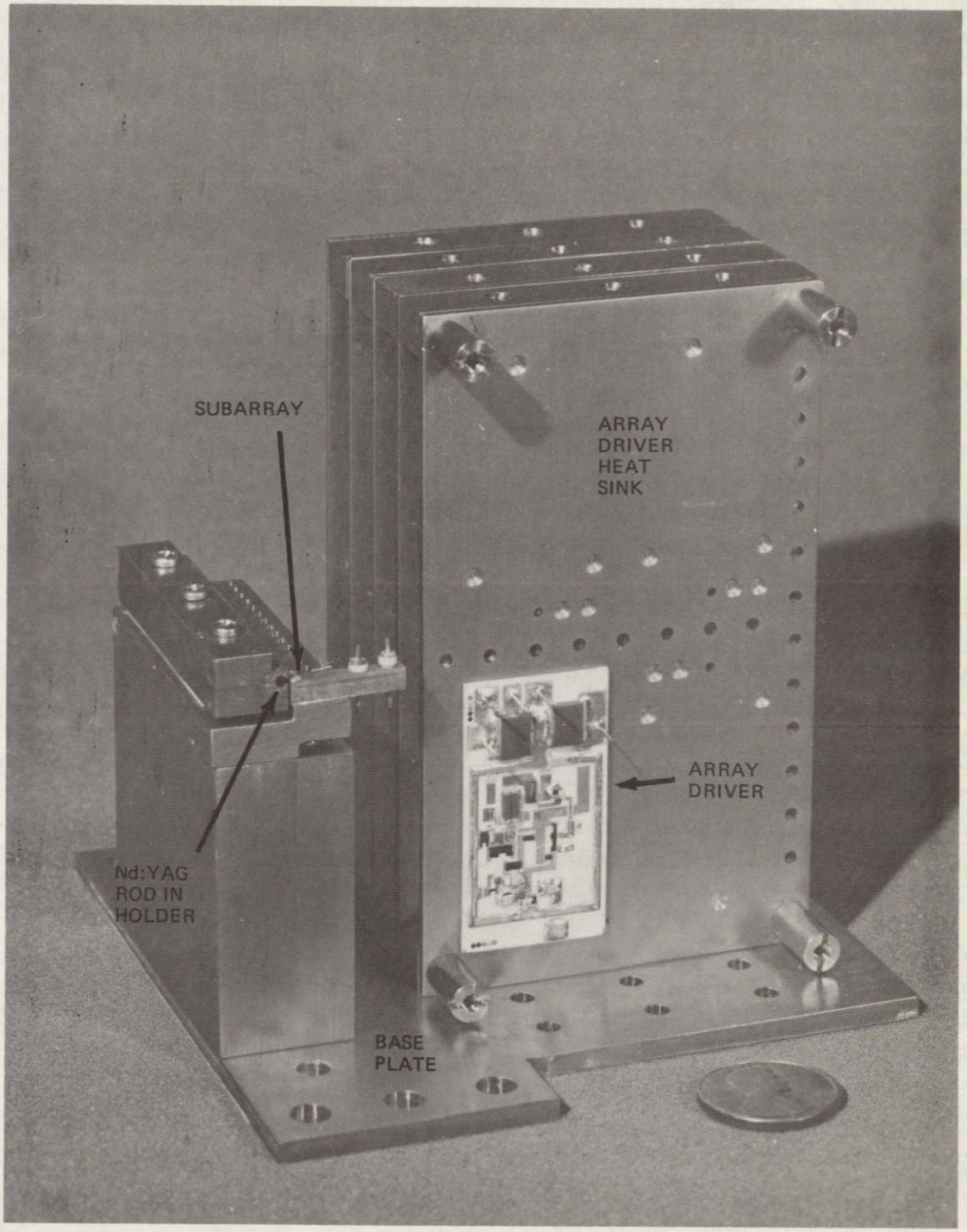

Figure 17. Diode pumped Nd^{3+}:YAG laser breadboard.

The results of tests on 14 subarrays which were made from wafer 132 to determine 1) their electrical characteristics for driving, and 2) the heat sink temperature to maintain a constant spectral peak versus duty factor are summarized in Figures 18, 19, 20, 21 and Table 2. Figure 18 shows the voltage and current waveforms across the laser subarray driven by a hybrid pulser. Of major significance is the 10-A drive achieved with 27 V across the array with a rise time of 50 ns. This confirmed that these mounts allow 10-A drive pulses through the arrays without significantly more voltage than that expected by adding single diode values.

The subarrays were mounted in the assembly shown in Figure 17. The sensor for the temperature controller is mounted in the block below the arrays. Figures 19, 20, and 21 show the operating temperature vs. duty factor for the subarrays mounted in the breadboard. With the exception of one subarray, not used, which showed a large $\Delta \lambda$, none of the spectra of these arrays shifted in width by more than approximately 20% of their nominal 3.5-nm half power width, indicating uniform heat sinking.

The arrays match wavelength at 255°K for duty factors ranging from 1.6% to 0.6%. The expected output power at 255°K block temperature is shown in Table 2. The change in output power from measurement to measurement is due to degradation of the diodes within the arrays. Investigation of this is discussed in Section IV.

The breadboard array was used to pump the laser rod placed in the same configuration used for TEM_{oo} experiments using the homojunction arrays. Maximum power output in this configuration was 40 mW at a rod temperature of 220°K. This low power is entirely attributable to the degradation of the pump arrays. For the laser rod employed in this experiment, 4 W of pump power are more than adequate to produce 125 mW of output. The degradation from 4 W to 2 W caused an inability to produce the required power. The continued degradation meant that even the low power (40 mW) could not be sustained. Development of arrays that can sustain 0.5 W/mil, as single diodes have over long periods of time (9000 hours), will allow use of this technique to provide a useful capability.

The output waveforms are shown in Figure 22. As can be seen, the ripple (approximately 10%) does not occur at the gross repetition frequency of the whole array. The ripple occurs at the frequency of the basic subarray repetition frequency. This is due to an inability to balance the power output for the various stagger fired subarrays in this assembly. The various subarrays had average powers that covered a wide range.

D. FIBER OPTICS COUPLING

Coupling from laser diodes into large numerical aperture fiber optics was investigated in order to demonstrate the feasibility of employing fiber optics as an efficient coupling medium. This in turn enables prediction of operational parameters of a laser system employing such coupling.

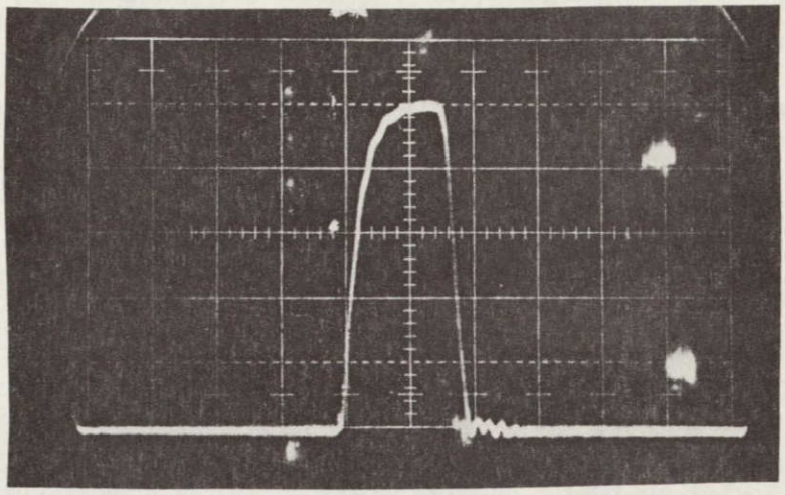

a. Current waveform. (Scales: vert. = 2 A/div, hor. = 100 ns/div)

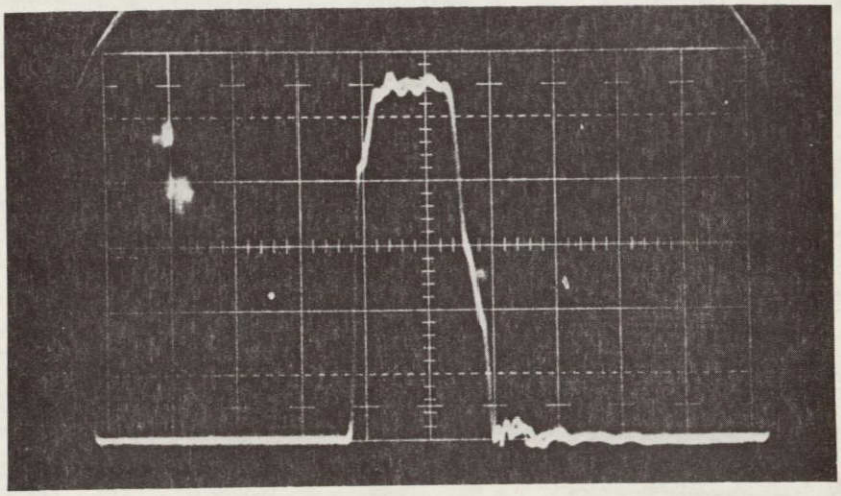

b. Voltage waveform. (Scales: vert. = 5 V/div, hor. = 100 ns/div)

Figure 18. Voltage and current waveforms for laser subarray drive.

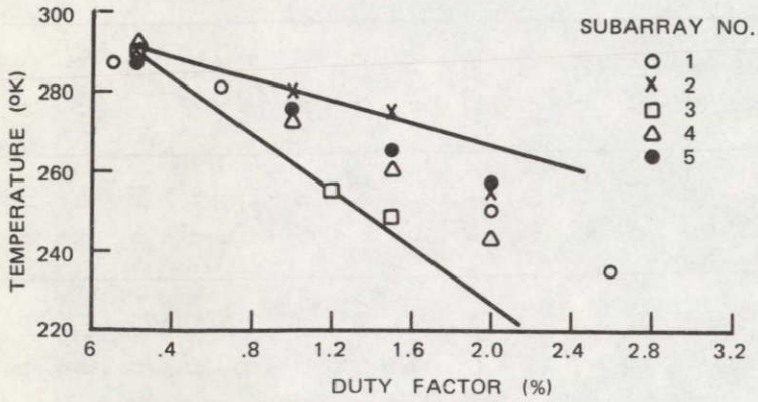

Figure 19. Heat sink temperature vs duty factor for constant wavelength of emission (for subarrays 1 through 5).

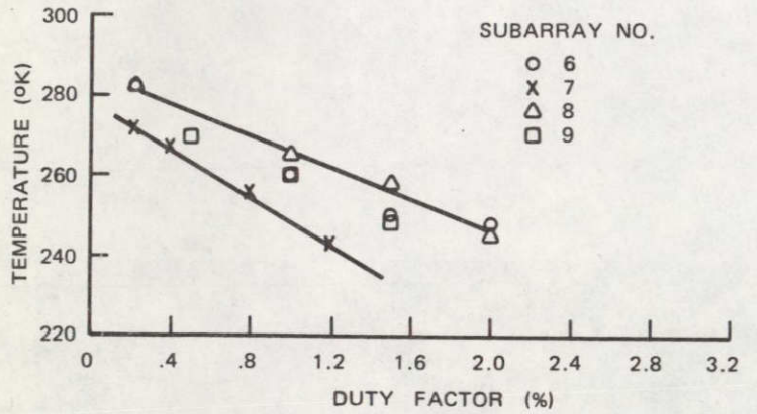

Figure 20. Heat sink temperature vs duty factor for constant wavelength of emission (for subarrays 6 through 9).

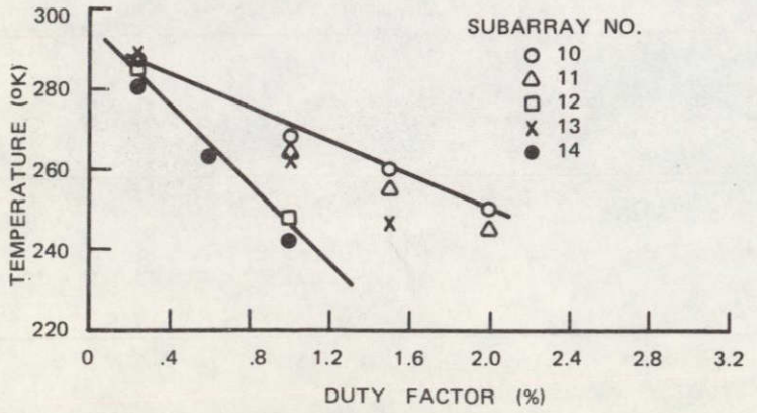

Figure 21. Heat sink temperature vs duty factor for constant wavelength of emission (for subarrays 10 through 14).

TABLE 2. SUBARRAY PERFORMANCE DATA

Array No.	Peak Output Power (W)				Maximum Duty Factor (%)	Average Output Power (W)			
	Orig.	Test No.				Orig.	Test No.		
		1	2	3			1	2	3
1	14	8	8	7	1.2	0.17	0.10	0.1	0.08
2	40	12	11	9	1.6	0.64	0.19	0.18	0.14
3	16	7	6.5	5.5	1.0	0.16	0.07	0.07	0.06
4	18	8	8	6.5	1.2	0.22	0.10	0.10	0.08
5	10	5	--	5.5	1.5	0.15	0.08	2.08	0.08
6	26	1.5	1.5	3	1.3	0.39	0.02	0.02	0.05
7	30	17	17	16	0.8	0.24	0.14	0.14	0.13
8	23	6	6	4	1.5	0.35	0.09	0.09	0.06
9	23	12	10	9.5	1.0	0.23	0.12	0.1	0.1
10	25	13	14	10	1.5	0.38	0.2	0.21	0.15
11	36	26	24	19	1.5	0.54	0.39	0.36	0.29
12	25	19	18	18	0.8	0.20	0.15	0.14	0.14
13	30	19	18	17	1.0	0.3	0.19	0.18	0.17
14	22	22	21	20	0.6	0.13	0.13	0.13	0.12
						4.09	1.96	1.89	1.64

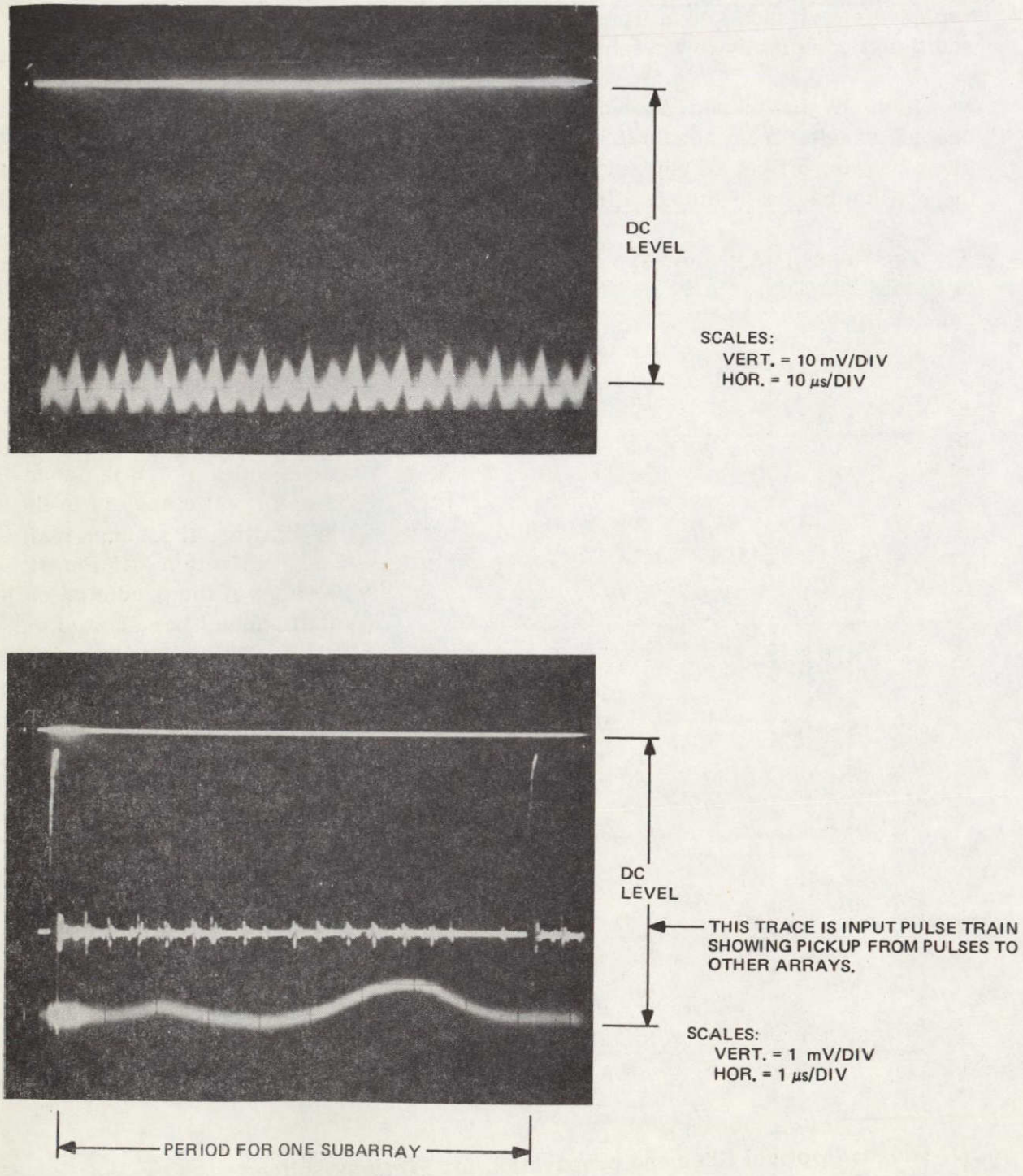

Figure 22. Ripple fire diode-pumped Nd:YAG laser waveforms.

The use of fiber optics to couple CW laser diode outputs to the Nd:YAG rod is a technique that offers the greatest promise for successful, efficient laser diode pumps. It allows construction of a bright source without increasing the thermal problems from CW diodes and makes practical selection of individually mounted lasers and the replacement of such single items. The principal disadvantage lies in adding an additional complexity to the fabrication cycle.

Both CW and pulsed laser diodes have broad, somewhat asymmetrical output beams, ranging from 10°x30° to 30°x40° at half intensity. Because of the breadth of these beams, a fiber of numerical aperture (NA) = 0.66 was chosen. In order to reduce the critical nature of the coupling, fibers of 0.010 inch aperture were used.

The fibers (NA=0.66) have been cut to length by cleaving the fibers[1] under tension. In Figure 23a a large area has an irregular surface; Figure 23b shows a flatter, cleaner break. Although the "mirror" zone of the cleave shown in Figure 23b has not covered the entire fiber and further experimentation is necessary to achieve high quality cuts, these cuts are of adequate quality for experimentation. Measurements comparing the light coupled into the fiber and into a photodiode placed in close proximity to a LOC diode identical to those on life test indicated 75% to 80% of the light from the diode is coupled through the fiber. If a core index of 1.6 is assumed and if Fresnel losses are compensated, the indicated coupling efficiency is in the range of 84% to 89%. Measurements with the photodiode limiting at a numerical aperture of 0.66 (the fiber NA) indicate approximately 90% collection efficiency. Thus, the upper bound of the measurement is within 1% to 2% of the predicted collection efficiency. Tests conducted coupling to a coated 0.010-inch fiber showed that 85% of the total emitted light was coupled through the fiber. This is at least 95% of the light available with the NA of the fibers coupled through a 6-inch fiber. Thus, efficient coupling from single laser diodes to a laser rod is predicted. Employing these numbers, it is then feasible to predict the performance characteristics of such a system.

---

[1] D. Gloge, "Optical fiber end preparation for low loss splices," BSTJ, vol. 52, pp. 1579-89, November 1973.

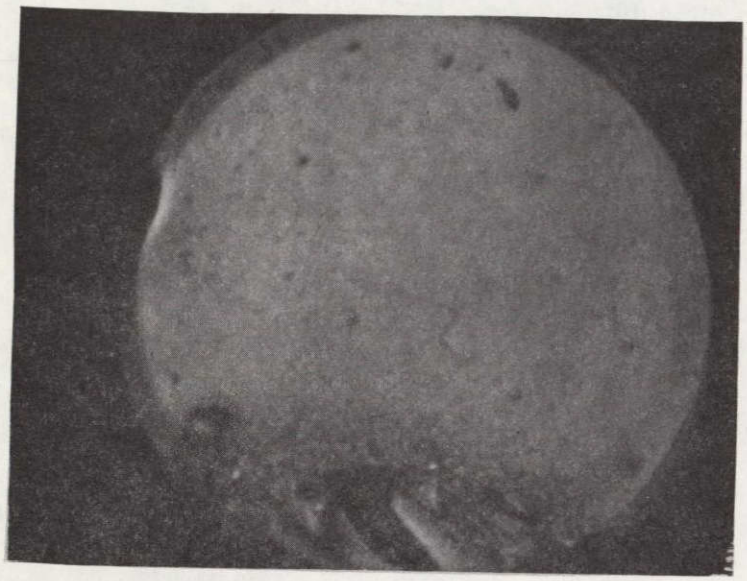

a. Fiber cleaved with excessive stress.

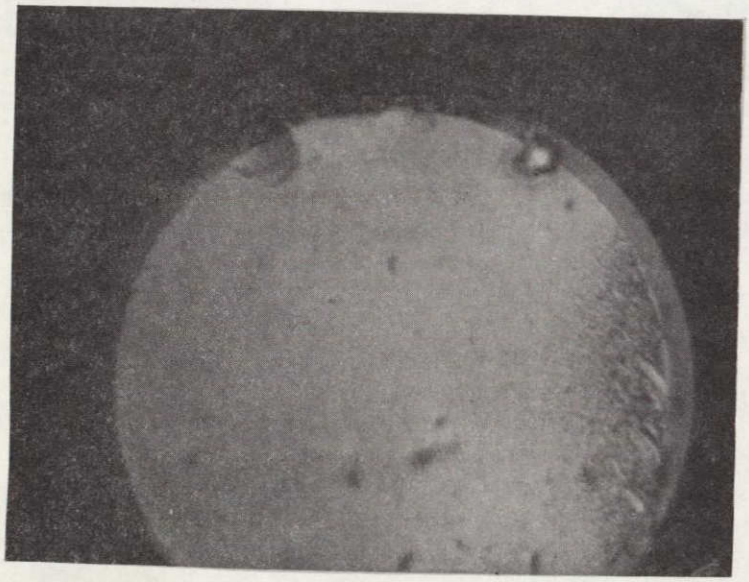

b. Fiber cleaved with slightly excessive stress.

Figure 23. Examples of cleaved facets.

Section III

Nd:YAG LASER THEORY

A. ABSORPTION AND SPECTRA OF MATERIALS

The fluorescent spectra of Nd:YAG shown by Koningstein and Geusic[2] are reproduced in Figure 24. Reference 2 states, "Ten lines are recorded between 860 and 950 nm. These lines are due to fluorescence which originates in levels of the $^4F_{3/2}$ manifold and terminates on levels of the $^4I_{9/2}$ manifold of Nd^{3+}:YAlG. The lines observed in the fluorescence spectrum appear in pairs which are separated on the average by 88 cm^{-1}. This pairing indicates that the $^4F_{3/2}$ state is split by 88 cm^{-1}. The positions of the Stark levels of the $^4I_{9/2}$ state are readily obtained....

"Twelve fluorescent lines are observed between 1075 and 1108 nm. These are assigned to $^4F_{3/2} \rightarrow {}^4I_{11/2}$ transitions. A part of the spectrum is shown in Figure 24a, and the energy levels of the $^4I_{11/2}$ state are given in Figure 24b. In addition, fluorescence has been observed from the $^4F_{3/2}$ levels to the $^4I_{13/2}$ manifold levels; this occurs around 1.3 μ."

Samples of Nd^{3+}:YAG 2.4 mm thick and of concentration 1% and 1.3% Nd_2O_3 by weight were procured from Lambda Airtron and scanned by using a Cary Spectrophotometer at RCA Laboratories at Princeton. Figure 25 shows a high-resolution scan in density for the 1% sample across the lines shown in Geusic's paper which occur between 850 nm and 900 nm. These are the strongest lines available lying within the spectral range obtainable using injection lasers (830 nm - 910 nm) at room temperature or less. Although the line lying at 868 nm (used by Rosenkrantz[3] for end pumping) shows a greater peak intensity, the width of the line lying at 885 nm is nearly twice as great. This fact, as well as its location, makes it of primary interest for pumping with GaAs diodes. Figure 26 shows data taken from the high-resolution scan of the two Nd^{3+}:YAG samples (resolution approximately 0.4 nm), which confirms the lack of any unresolved fine structure in the 885 nm absorption line in agreement

---

[2] J. A. Koningstein and J. E. Geusic, "Energy levels and crystal field calculations of neodymium in yttrium aluminum garnet," Phys. Rev., vol. 136, pp. 711-716, 2 November 1964.

[3] L. J. Rosenkrantz, "GaAs diode-pumped Nd:YAG laser," JAP, vol. 43, pp. 4603-4605, November 1972.

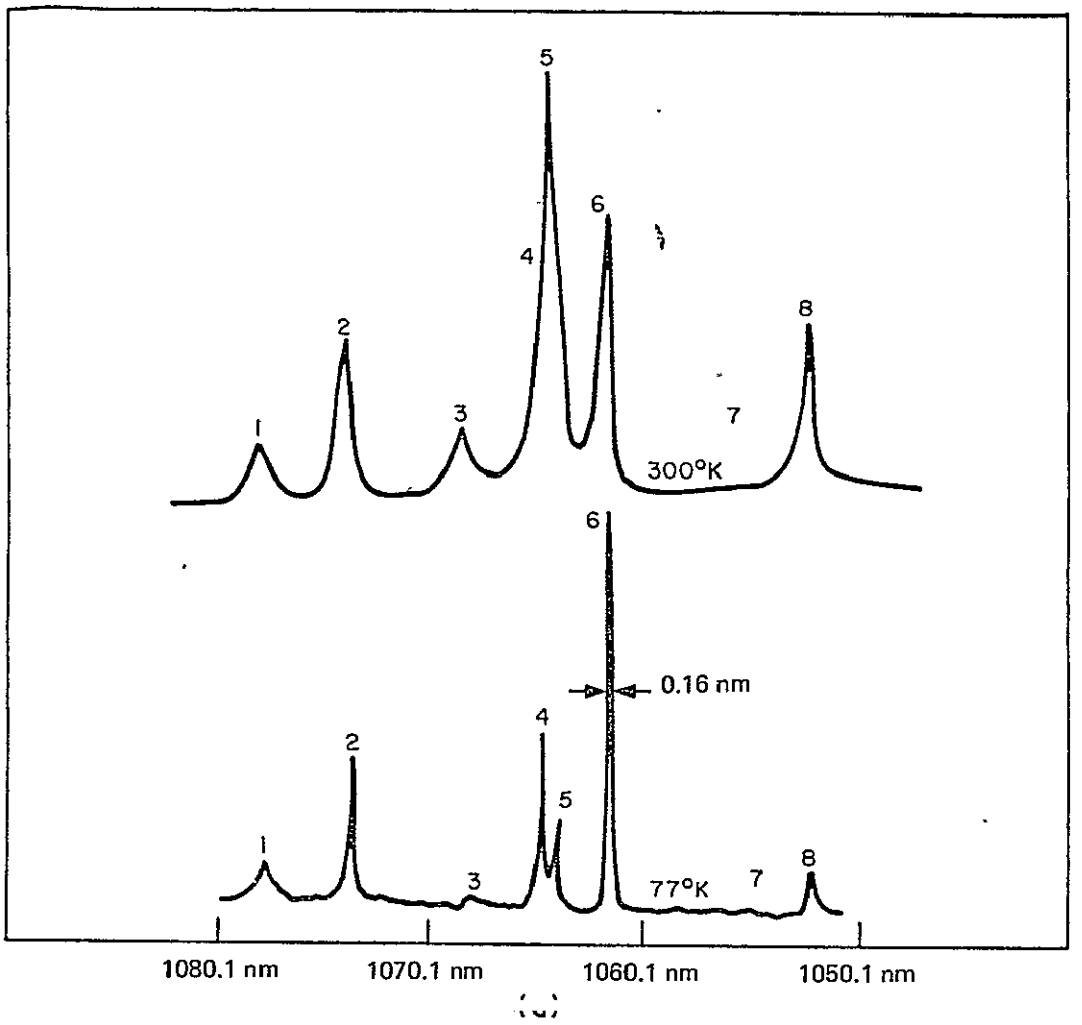

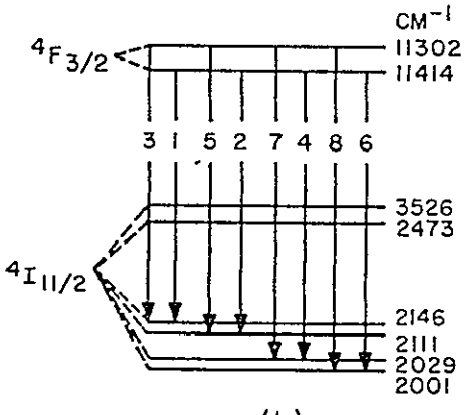

Figure 24. Spectroscopy of Nd:YAG emission lines.

(a) The fluorescence spectrum of Nd^{3+} in YAG at 77°K and 300°K in the region of 1.06 μm.

(b) The $^4F_{3/2}$ and $^4I_{11/2}$ energy levels of Nd^{3+} in YAG at 300°K.

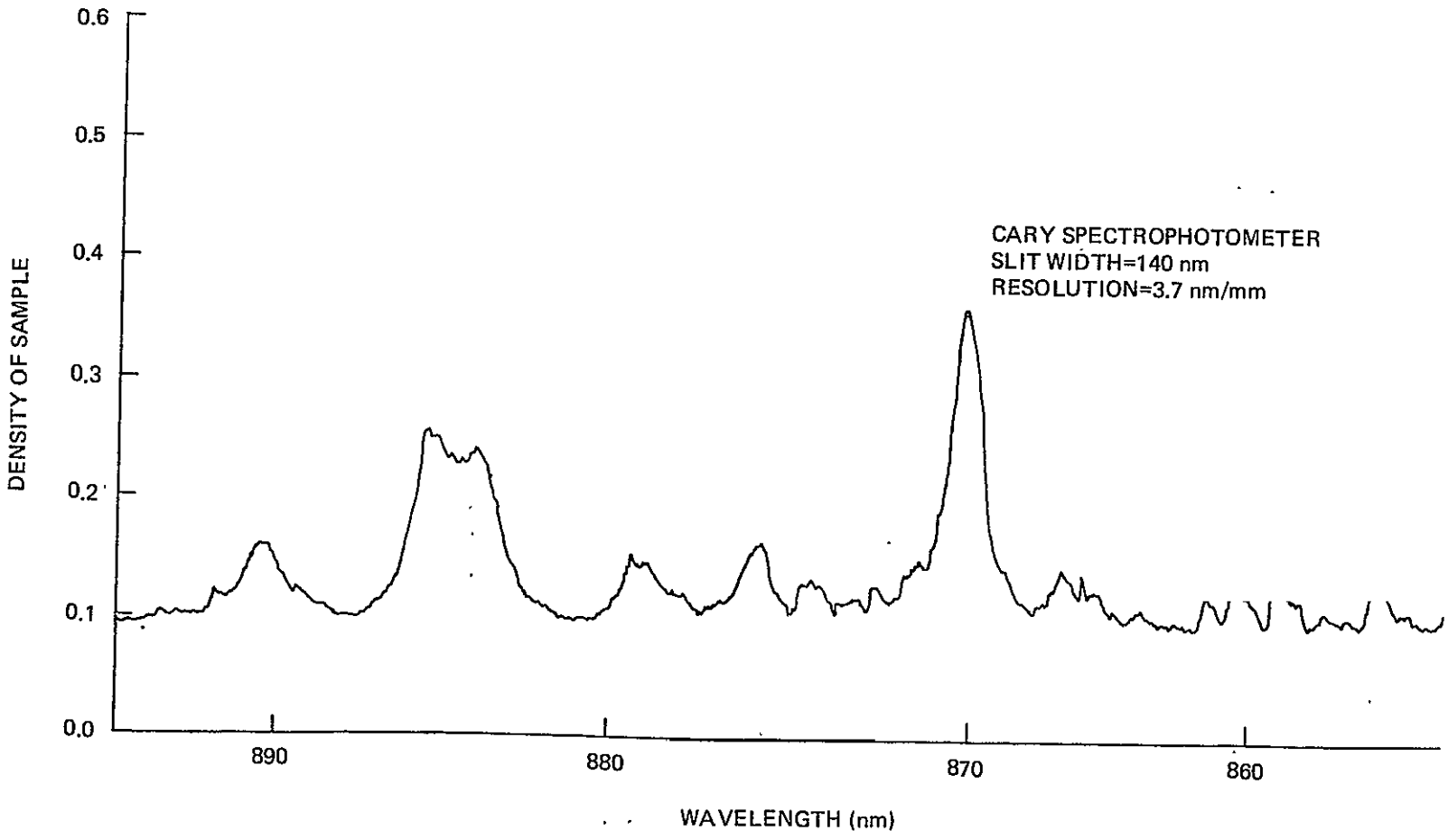

Figure 25. High resolution scan in density for 1% sample.

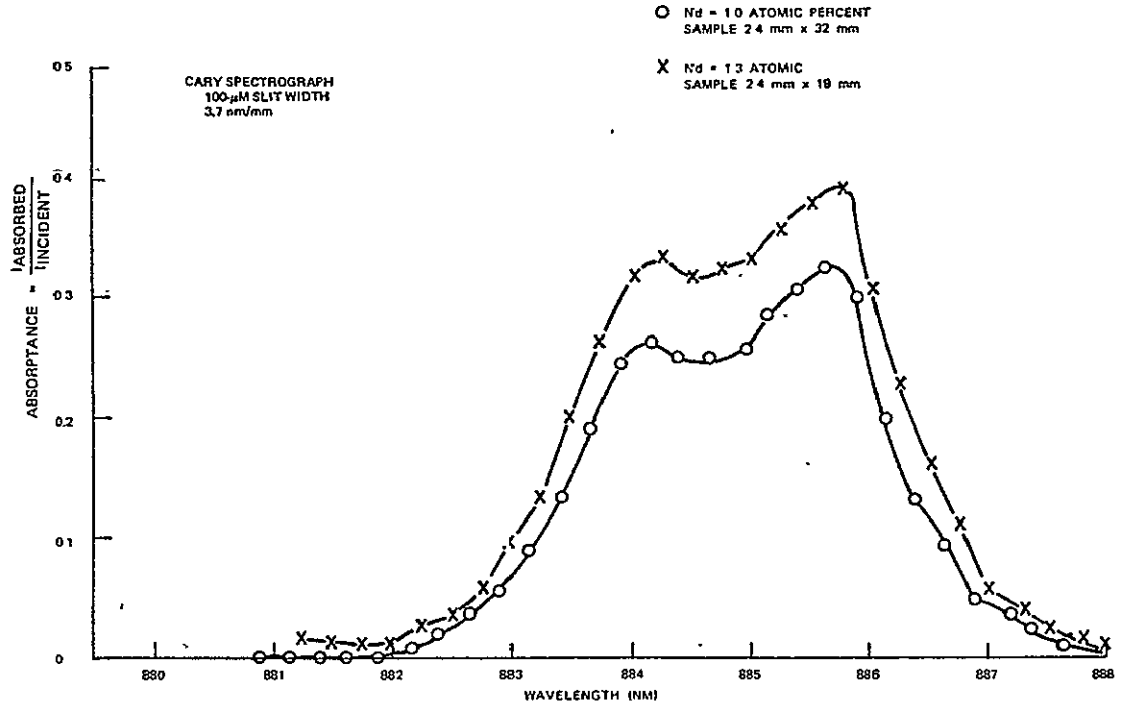

Figure 26. Transmission spectra of Nd:YAG near 885 nm.

with previous spectra with a width at half intensity of 2.9 nm. Within this line, in the 1.3% sample, the average absorption coefficient is about 1.49 cm^{-1}. The required path length to absorb 90% of the input light energy lying within the line is d = 1.55 cm. The data have been reduced on the basis of 100% transmission for both samples at 888 nm.

Additional absorption measurements have been made over the spectral range of 800 nm to 900 nm and over the temperature range of 200°K to 300°K. Curves for T = 260°K (the approximate operating temperature) and 300°K are shown in Figures 27 and 28, respectively. Figure 29 shows the spectra at 200°K.

A small (approximately 15%) increase was observed in the absorption strength of the 885 nm line over this range. The width of the 885 nm line decreased by about 0.4 n over this range (down to 200°K). The 868 nm line is about 1.25 nm wide at 300°K (50% intensity) and about 0.98 nm wide at 200°K. The absorption intensity changes in inverse order from 0.26 to 0.35 density for a 1% Nd^{3+} sample.

This results in loss of available pump power which is particularly accentuated in the temperature range below 200°K where the line is narrow enough that the absorbed power is decreasing at a rate which compensates for the increasing emission cross section of the laser line. This accounts for the experimental curves in Figure 14.

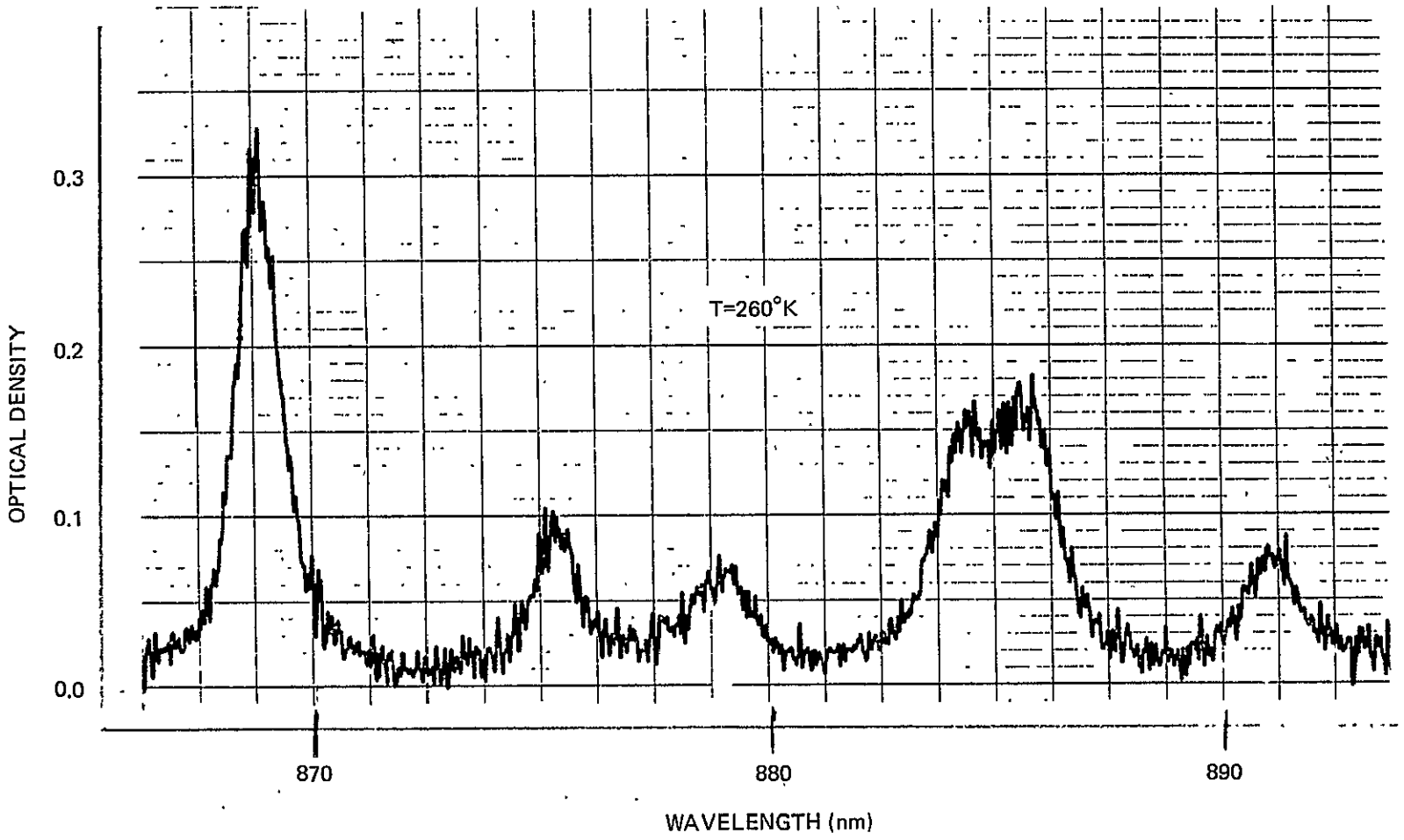

Figure 27. Absorption spectra 1% Nd^{3+}:YAG. (Sample thickness 2.4 mm. T=260°K.)

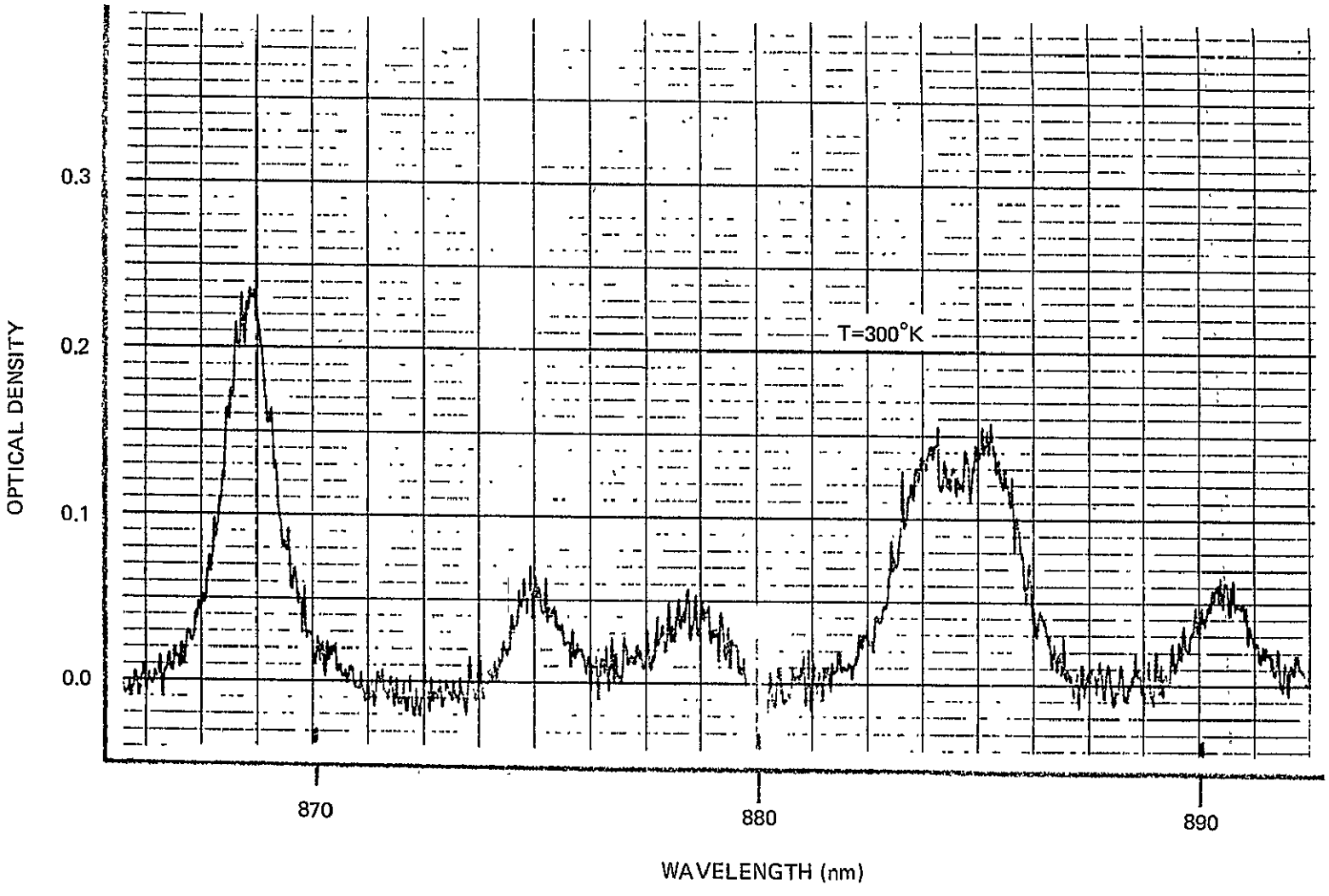

Figure 28. Absorption spectra 1% Nd^{3+}:YAG. (Sample thickness 2.4 mm. T = 300°K.)

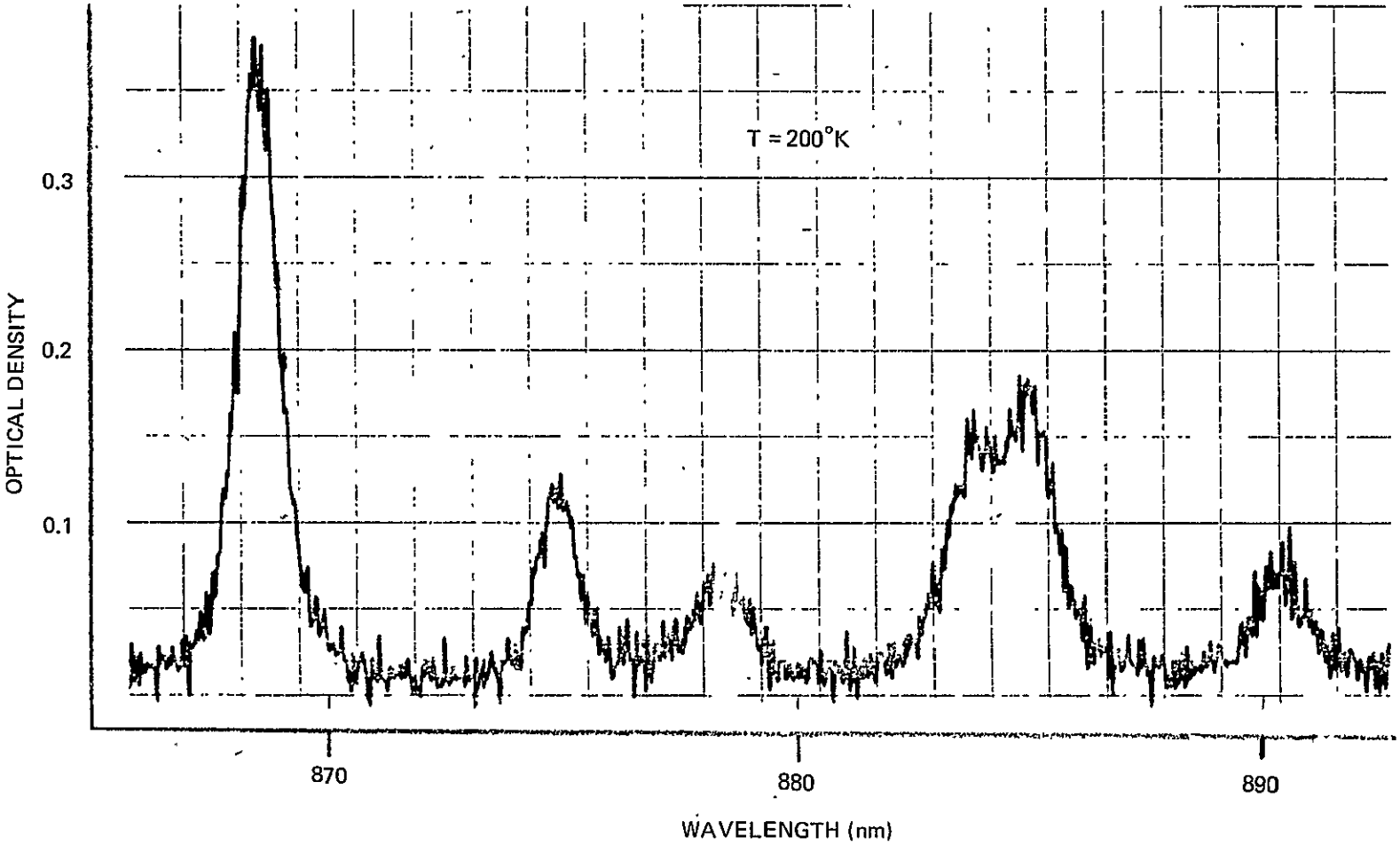

Figure 29. Absorption spectra 1% Nd^{3+}:YAG. (Sample thickness 2.4 mm. T = 200°K.)

A second wavelength band of particular interest is that near 800 nm. The peak of the absorption occurs at 806 nm and for 1% Nd^{3+} is a density of D = 0.25/mm (σ = 0.62). Figures 30 and 31 show the absorption for T = 200°K and T = 300°K, respectively. This absorption is a good match to CW AlGaAs diodes, but the LOC technology for pulsed diodes has not been demonstrated.

Data on quantum efficiency is found in the literature.[4] It confirms that the quantum efficiency of the $^4F_{11/2}$ fluorescence is high (60 to 70%). Although from Geusic[2] it is recognized that the two overlapping lines making up the absorption at 885 nm are transitions into two levels of the $^4F_{3/2}$ state separated by 112 cm^{-1} and although it is also observed that the laser line at 300°K represents a transition from only one of these levels, thermal cross relaxation will make the lines equally effective (112 cm^{-1} approximately equals 1/2 kT) as presented in Figure 24b.

Selection of the rod material for tests has been limited to tradeoffs between concentrations now commonly grown (i.e., 1% or 1.3% Nd_2O_3). As the absorption has been shown to increase for the line of primary interest and the optical quality is known to remain adequate, the only known factors which limit the use of the higher concentration material are the rod scattering and the fluorescent lifetime.[5] Scattering in the rod in the samples received is apparently 10 times as severe in 1.3% rods as in 1.0% rods. This offsets the apparent advantage in absorption for lasers with low couplings.

B. PERFORMANCE ANALYSIS

1. Output Power

Analysis of the operation of the Nd^{3+}:YAG laser power efficiency has been based upon the technique described by Chesler.[6] This analysis is required in order to predict the operation of a final system. The form of the equation used for comparison with experimental data taken using homojunction pump arrays is

$$P_{out} = \frac{w^2}{2R^2} \left(\frac{\nu_L}{\nu_p}\right) \frac{P_{abs}}{(1+\frac{\epsilon}{T})} \ln\left(1 + \frac{4\sigma\tau_s P_{out}}{\pi w^2 h \nu_L T}\right)$$

w = beam radius ($1/e^2$ intensity)

R = rod radius

---

[4] R. S. Brandewie and C. L. Telk, "Quantum efficiency of Nd^{3+} in glass, calcium tungstate, and yttrium aluminum garnet," JOSA, vol. 57, pp. 1221-1225, October 1967.

[5] R. F. Belt, "Nd concentration in YAG," Laser Focus, vol. 9, p. 51, August 1973.

[6] Ronald B. Chesler, "Optimized TEM_{00} output from a uniformly pumped four-level laser," JQE, vol. QE-8, pp. 493-496, June 1972.

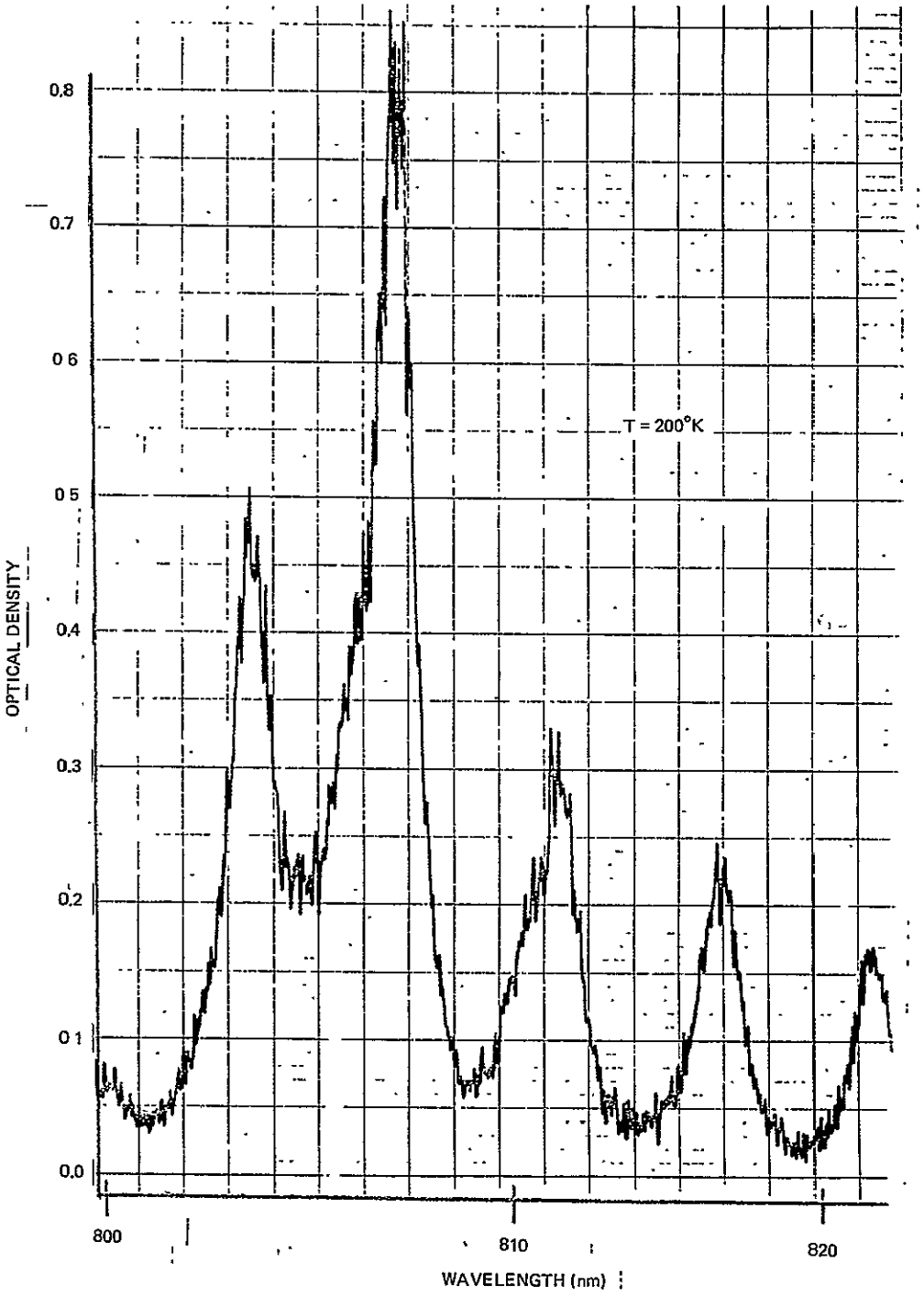

Figure 30. Absorption spectra 1% Nd^{3+}:YAG. (Sample thickness 2.4 mm. T = 200°K.)

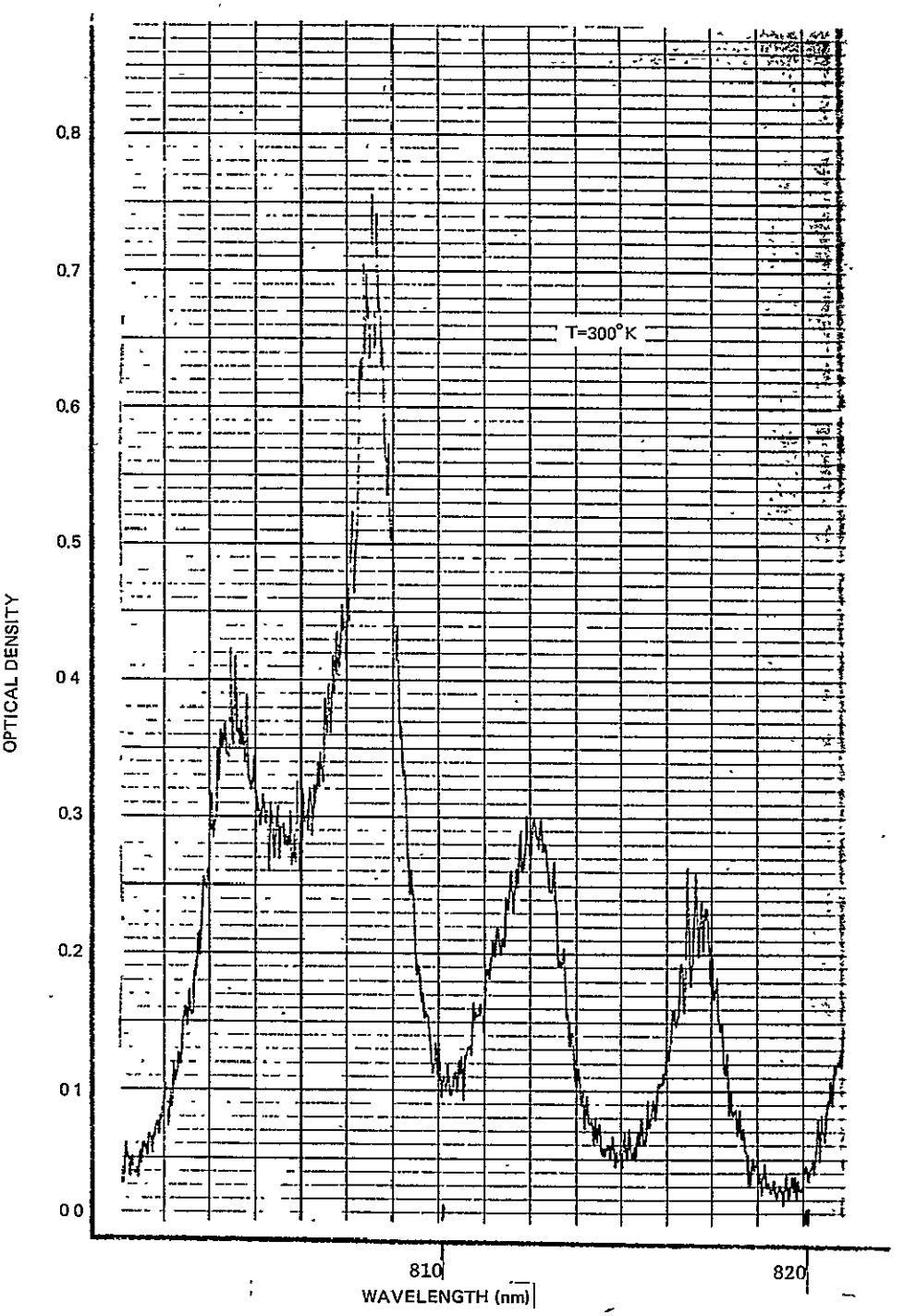

Figure 31. Absorption spectra 1% Nd^{3+}:YAG. (Sample thickness 2.4 mm. T = 300°K.)

ν_L = laser frequency

ν_P = pump frequency

P_{abs} = absorbed power

ϵ = round trip loss

T = mirror transmissic

h = Planck's constant.

τ_s = spontaneous lifetime, upper laser state.

One term (P_{abs}) of this equation varies with temperature as a result of thermalization of the lower laser state. This is estimated to increase the required P_{abs} by a value equal to

$$P_{LL} = \frac{Vn_o h\nu}{\tau_s} \exp(-hc\lambda'/kT)$$

where

P_{LL} = power lost in the lower laser state (W)

V = rod volume

n_o = impurity concentration

τ_s = spontaneous lifetime

h = Planck's constant

ν_P = pump frequency

c = speed of light

λ' = separation between ground state and lower laser state (cm^{-1})

k = Boltzmann's constant

T = temperature.

Two terms vary with temperature as a result of spectral linewidth changes: σ, and P_{abs}. Cross section (σ) is inversely proportional to the laser line width. (ΔV). For Nd^{3+} : YAG the laser line varies from about 0.7 to 1.5 cm^{-1} in width at 77°K to 6.5 cm^{-1} at 300 °K, and represents a shift in the transition (R_2-Y_3 at 300°K to R_1-Y_1 at 77°K). The R_1-Y_1 transition width has been measured by Kushida[7] from 77°K to approximately 400°K. The R_2-Y_3 transition is not represented in Kushida's data but is somewhat higher in cross section at 300°K. Calculations were made using the known values of σ at 77°K and 300°K, the saturation below 100°K, and the approximate slope to fit a function to the linewidth and do the calculation. By also assuming a decrease in absorbed power, a reasonable fit to data was obtained.

An additional difficulty found in fitting data to theory is that the theory assumes a uniformly pumped volume. On the basis of a simple analysis of the pumping scheme used, it appears that the effective pumped volume is somewhat less than the full rod volume. This influences the accuracy of the result.

2. Repetitively Pulsed Laser Pumps

The effect of the periodic disturbances upon the output of a Nd^{3+} : YAG laser has been reported in several papers.[8-10] To an approximation, the modulation index is

$$M = \frac{2a\hat{\beta}}{\tau_Q[(\omega_o^2 - \omega^2) + 4a^2\omega^2]^{1/2}}$$

where

$\hat{\beta}$ = pump modulation index

$a = 1/2\left(\frac{1}{\tau_s} + \frac{1}{\tau_R}\right)$

τ_s = spontaneous lifetime of laser state

[7]Takashi Kushida, "Linewidths and thermal shifts of spectral lines in neodymium-doped yttrium aluminum garnet and calcium fluorophosphate," Phys. Rev., vol. 185, p. 500, 10 September 1969.

[8]H. G. Danielmeyer and F. W. Ostermayer, Jr., "Diode-pump-modulated Nd:YAG laser," J. Appl. Phys., vol. 43, pp. 2911-2913, June 1972.

[9]H. G. Danielmeyer, "Low-frequency dynamics of homogeneous four-level CW lasers," J. Appl. Phys., vol. 41, pp. 4014-4018, September 1970.

[10]J. E. Jackson and R.R. Rice, "Output fluctuations of high-frequency pulse-pumped Nd:YAG laser," J. Appl. Phys., vol. 45, pp. 2353-2355, May 1974.

$$\tau_R = \frac{\pi w^2 T h \nu_L}{P_o \sigma}$$

w = beam radius in laser

T = mirror transmission

h = Planck's constant

ν_L = laser frequency

σ = emission cross section

P_o = output power

$$\tau_Q = \frac{2L}{c\epsilon}$$

L = cavity length

c = velocity of light

ϵ = total cavity loss.

For the regime where $\omega >> \omega_o$

$$f = \frac{1}{2\pi} \sqrt{\frac{2\ a\hat{\beta}}{\tau_Q M}}$$

and for

$\tau_s = 2 \times 10^{-4}$

$w = 0.4$ mm

$T = 0.02$

$\lambda_L = 1.06 \times 10^{-6}$ m

$P_o = 0.125$ W

$\sigma = 8.8 \times 10^{-23}\ m^2$

$M = 0.01$

$L = 0.5\ m$

$\epsilon = 0.04$

$\hat{\beta} = 1$

then $f = 570$ kHz.

Thus, repetition frequencies in excess of 1 MHz should reduce M to finite low values. Reducing the coupling to 1% (T) and the round trip loss to 1.5% (G) makes f = 340 kHz.

3. Nd:YAG Mode Studies

The TEM_{oo} mode size, its diffraction loss in an aperture the size of the laser rod in use on the project, and the relative efficiency of the laser mode in removing a uniform population inversion have been calculated by using standard equations. From the Handbook of Lasers,[11] the mode radius at one of the mirrors is

$$\omega_1^4 = \left(\frac{\lambda R_1}{\pi}\right) \frac{(R_2 - d)\, d}{(R_1 - d)\,(R_1 + R_2 - d)} \qquad (1)$$

where

λ = wavelength

R_1 = effective radius of one mirror

R_2 = effective radius of second mirror

d = the effective mirror separation.

The effective mirror separation is

$$d = d' - \ell\,\frac{(n-1)}{n} \qquad (2)$$

[11] Robert J. Pressley (ed.), Handbook of Lasers. Cleveland: Chemical Rubber Co., 1971, p. 434.

where

d' = physical cavity length

ℓ = length of higher index material

n = index of higher index material.

The effective radius of a mirror fabricated upon one end of the laser rod is

$$R_1 = \frac{R'}{n} \tag{3}$$

where

R' = real radius of curvature

n = index of the medium.

Then, using Equations 1, 2, and 3, with $\lambda = 1.064 \times 10^{-6}$ m, $R' = 2$ m, $n = 1.82$, $\ell = 5$ cm, and varying d' and R_2, the curves in Figure 32 were calculated.

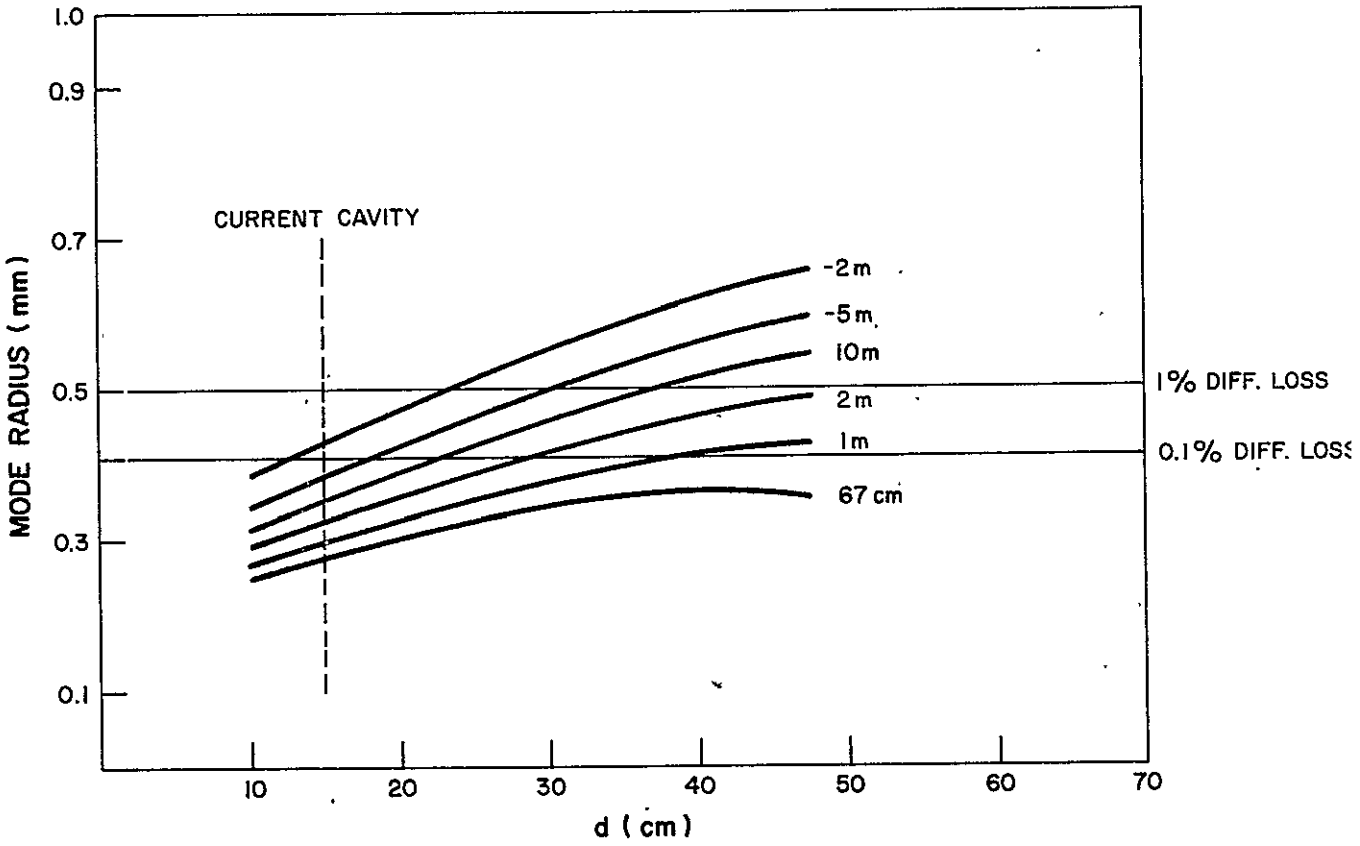

Figure 32. Laser mode radius vs cavity length.

The total flux in a Gaussian beam may be found as

$$P_o = I_o \int_0^{\rho} \int_0^{2\pi} \exp\left(-2\,\frac{\rho^2}{w^2}\right) \rho\, d\rho \quad d\phi$$

$$= -\frac{w^2\pi}{2} I_o \exp -2\rho^2/w^2 \Big|_0^R$$

From 0 to ∞

$$P_o = \frac{w^2 \pi I_o}{2}$$

The equivalent for a uniform beam is

$$P_o = \pi I_o R^2$$

The ratio is then (i.e., Gaussian filling efficiency η)

$$\eta = \frac{w^2}{2R^2}$$

The fractional loss (β) from a Gaussian beam at a circular aperture is simply

$$\beta = \exp - 2R^2/w^2$$

Figure 33 shows diffraction loss vs. mode efficiency for a Gaussian beam.

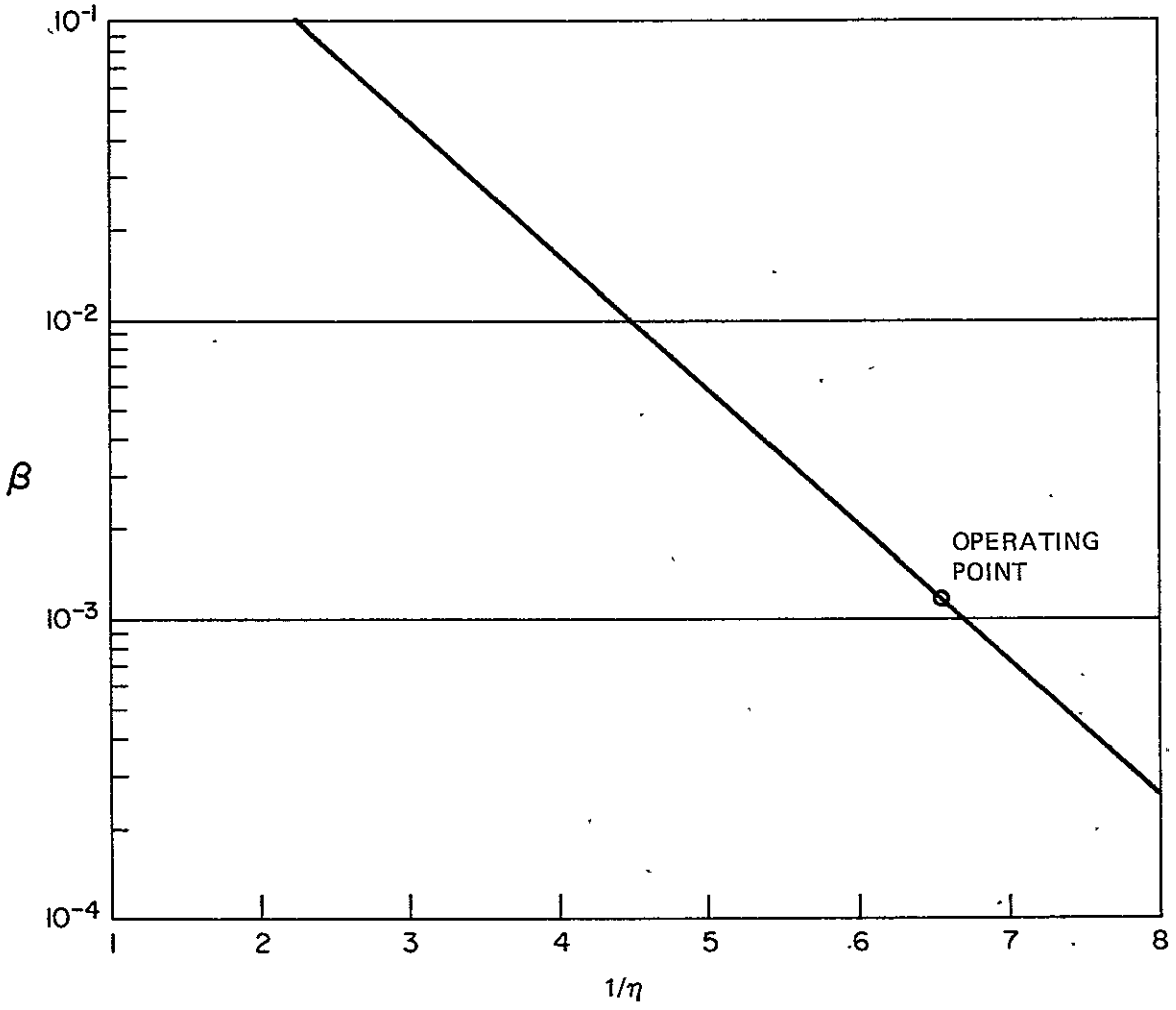

Figure 33. Diffraction loss vs. mode efficiency.

Section IV

PULSED GaAs PUMP ARRAYS FOR 250°K HEAT SINK OPERATION

The task defined for the injection laser pump source was to provide adequate pump power in a usable pump band of Nd^{3+}:YAG at a high enough repetition frequency to suppress laser ripple in a geometry conducive to coupling at a heat sink temperature of 250°K or higher. The pump wavelengths available are 810 nm, 868 nm, and 885 nm. Although the latter two absorptions are weaker than the former, their position makes them feasible for pumping by unalloyed GaAs laser diodes. The approach taken was to determine from among the state-of-the-art in semiconductor lasers at RCA those materials and constructions that could lead to a solution to the pump problem.

Only two forms of GaAs lasers (double heterojunction and LOC) are operable at high enough duty factor (1 to 2%), because of their low thresholds, to be useful in obtaining average powers in the 1-to-5 W range in moderate size arrays (1 to 200 diodes). Indeed, in double heterojunction diodes lifetime problems caused by the small emission thickness and by catastrophic destruction of the cavity ends due to high flux density lead to the conclusion that LOC diodes are the best available form for laser pump arrays.

A. MULTIPLE LAYER EPITAXY

As is well known, epitaxial growth of AlAs-GaAs alloys is greatly simplified by the almost perfect match in lattice parameter between these two compounds. The special task of multiple layer growth of laser structures involves growing adjacent layers with widely varying compositions and dopings. The interfaces between these layers must be extremely flat and well defined; there must be no contamination from one growth solution to the next; the layer thickness must be precisely controlled with submicrometer tolerances; and the final surface must be free of any solution when the wafer is withdrawn from the growing apparatus.

There are many possible designs of the growth apparatus, but the linear (as opposed to circular) multiple bin graphite boat has proven the most popular. Two of many possible designs are shown schematically in Figure 34. In Figure 34a, a GaAs source wafer, usually polycrystalline, precedes the substrate wafer into each bin and assures saturation of the solution before growth on the substrate is initiated. Figure 34b is an improvement over this design in that each solution has its own source wafer, and saturation of the solutions is maintained throughout the entire growth cycle. The source wafers are dropped onto relatively small solutions near the growth temperature and are spread over the entire wafer area by the quartz block weights. The resulting thin (typically $\leqslant$1 mm) solutions yield epitaxial layers the thickness of which can be

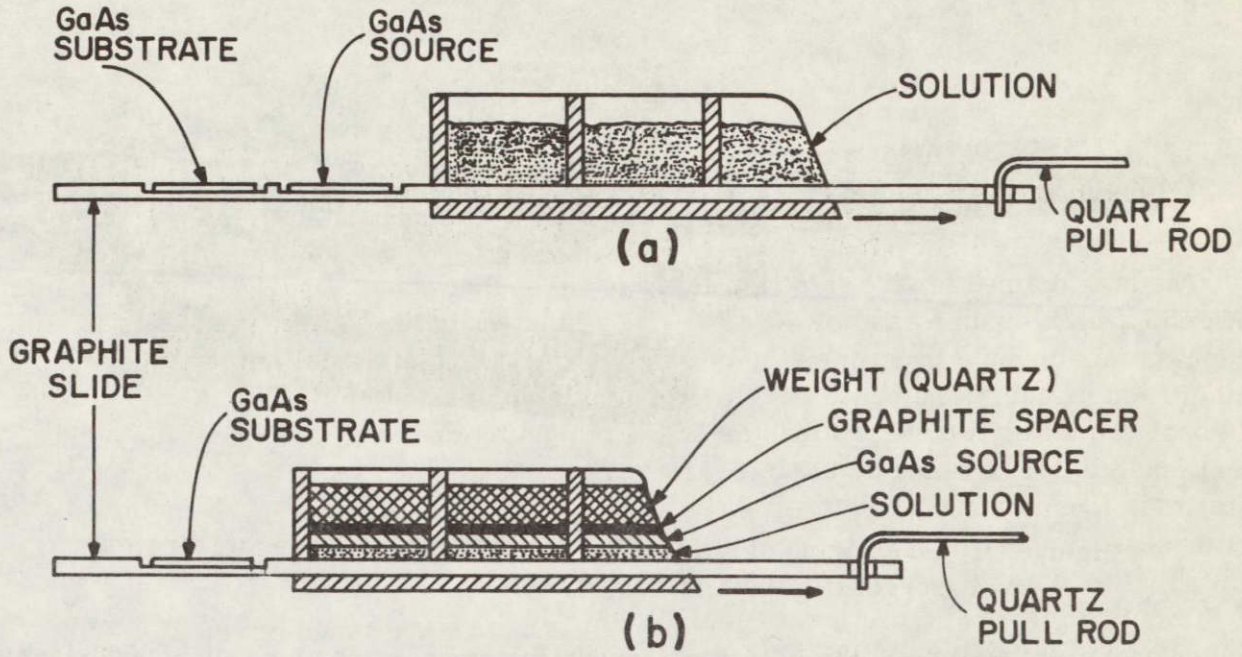

Figure 34. Schematic illustration of growth boat. In (a) the saturation of the solutions is completed by the source wafer preceding the substrate wafer whereas in (b) each solution is saturated by its own source wafer.

calculated directly from the phase diagram[12] because the formation of platelets in the solution is greatly reduced. Typical growth efficiencies, defined as the ratio of the thickness grown to that calculated from the phase diagram, range from 0.1 for 1-cm-thick solutions to >0.9 for solutions 0.2 mm thick. Still more precise saturation can be obtained by adding a bottom source wafer, as in Figure 34a, to the thin solution method of Figure 34b. Figure 35 is a photograph of a seven-bin boat (with one side removed) which combines the ideas of Figures 34a and 34b and is the boat used in all of the growth runs for this contract. The top sources are shown in their initial position above the 1-gram Ga solutions which will be flattened to 1-mm thickness by the action of the quartz weights.

The reason for this preoccupation with exact melt saturation is apparent if one considers the growth of layers on the order of 0.1- μm thickness. For this same reason, the longitudinal temperature gradient in the growth furnace is also important. If the substrate enters a bin at a temperature higher than the solution in that bin, there may be partial dissolution of the substrate because of undersaturation at the

[12] M. Ilegems and G. L. Pearson, "Derivation of the Ga-Al-As ternary phase diagram with applications to liquid phase epitaxy," Proc. Second Intl. Gallium Arsenide Symposium, Dallas, 16-18 October 1968, p. 3.

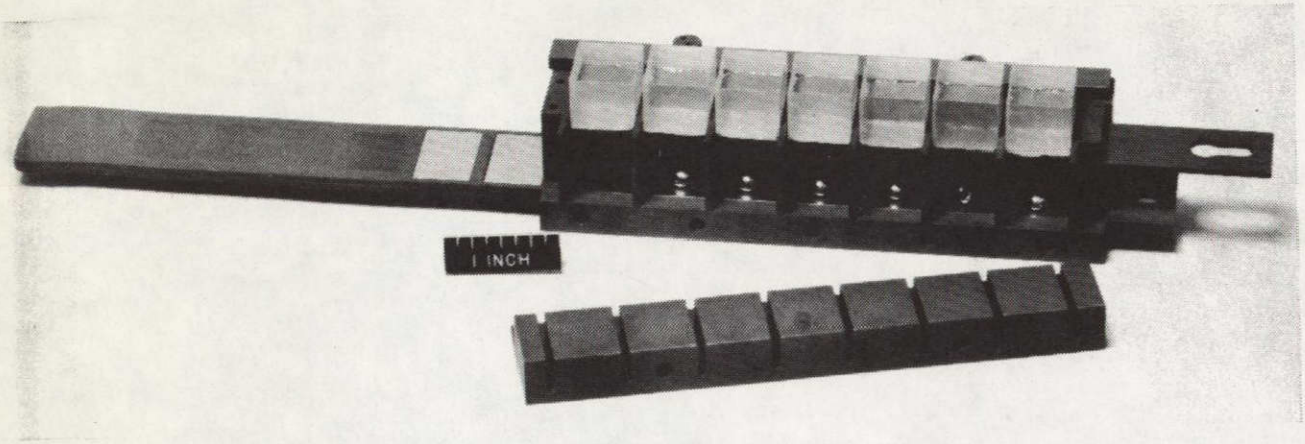

Figure 35. Photograph of seven-bin boat showing bottom as well as top sources in their initial position.

solid-liquid interface; therefore, a decreasing temperature gradient is undesirable when the control of extremely thin layers is involved. An increasing temperature gradient is more favorable because there will be deposition rather than dissolution when the substrate enters a bin which is at a higher temperature. In either case, large temperature gradients require more rapid cooling, thus aggravating the problem of layer thickness control. Typical optimum temperature gradients used for the work reported here are in the range of 0.1°C/cm along the length of the boat.

The major cause of (liquid) cross-contamination between solutions in adjacent bins is also the cause of poor wiping after the growth of the final epitaxial layer. Any geometric artifact such as a major defect or dendrite on the surface will cause the solution to adhere in that area. Figure 36 is a photograph of the surface of a multiple layer structure which shows some of these effects. Along both sides where the crystal is held in place, dendrites have grown and wiping after the last layer growth is incomplete. Since this inhomogeneity is confined to the edge of the crystal, it is not serious in terms of subsequent processing. However, along the leading edge there is a network of small defects which are made visible by the presence of gallium solution not removed by the final wiping.

Figure 37 is a photograph of multiple layer structure which is free of any surface irregularities. There are gradual steps in this surface with a typical height of only 0.03 to 0.05 μm; thus, the wafer can be processed for ohmic contacting without the need of a polishing step. This is especially important when the active layers of the structures are within a few micrometers of the surface as they are in the CW laser. For the pulsed device (to be described in more detail later in this report), the absence of a polishing step after growth increases the yield and reduces the cost, especially in a production environment.

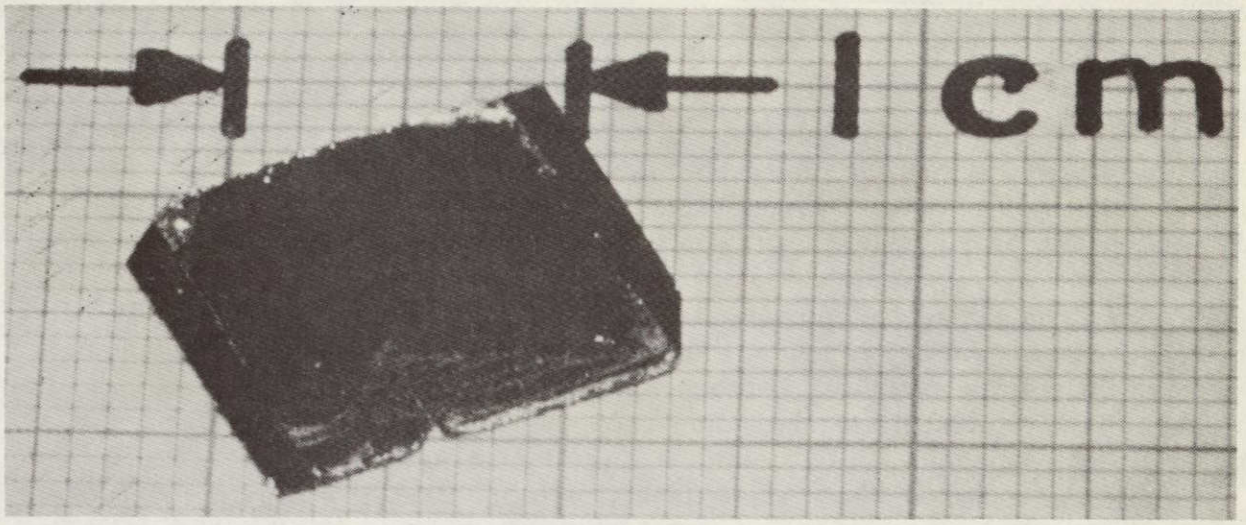

Figure 36. As-grown wafer showing solution adhering to edges and a network of defects along the leading edge. (The crystal has been cleaved through the defective region.)

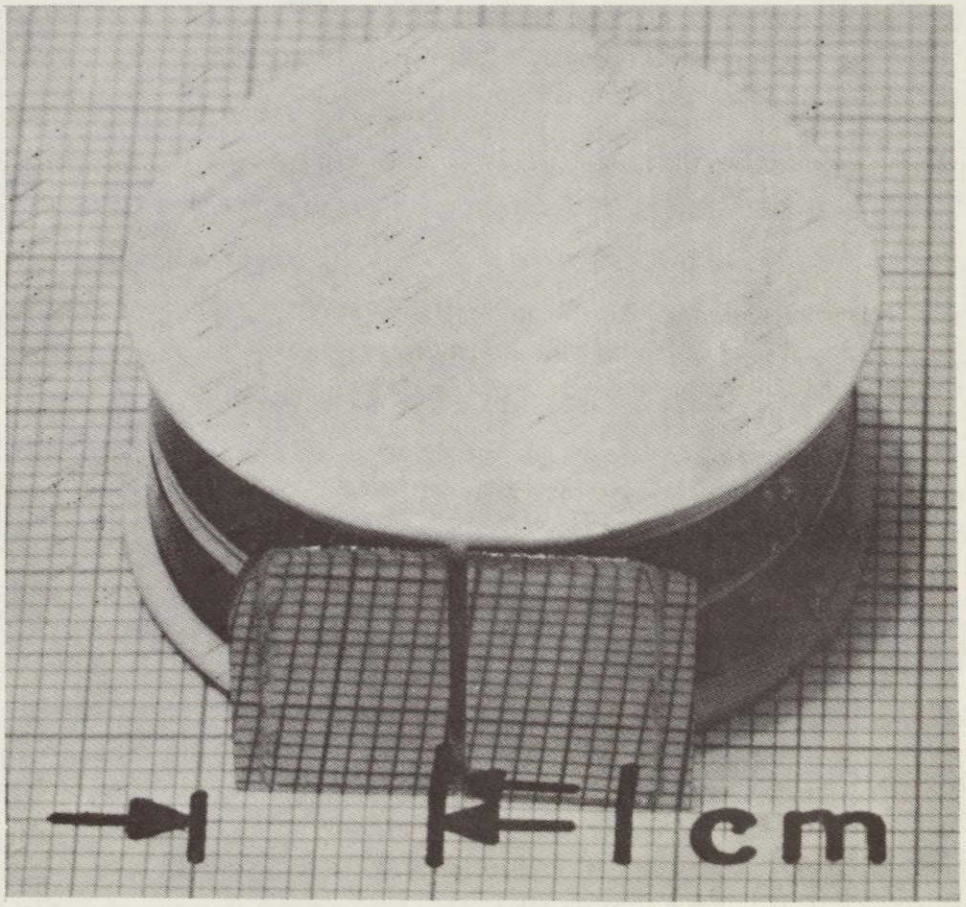

Figure 37. A cleaved wafer with defect-free surface. The absence of growth solution on the surface and its planarity is indicative of highly uniform growth.

B. LASER STRUCTURES

Figure 38 is a schematic diagram of a five-layer structure which can be considered the generalized GaAs injection laser. Multiple layer lasers under active study are variations of this structure and contain either some or all of the layers shown. Basically, the laser consists of a radiative recombination region 3 of width d_3, the "gain region," and a waveguiding region which is either equal to or thicker than the gain region. In Figure 38 the nominal waveguide region is of thickness $w = d_2 + d_3 + d_4$ with the higher bandgap regions 1 and 5 providing the walls of the waveguide because of their reduced index of refraction at the GaAs lasing photon energy. The difference in the Al content between i-numbered layers determines the refractive index difference Δn which, at the typical 300°K GaAs lasing emission wavelength of $\sim$900.0 nm, increases approximately linearly with the bandgap energy difference ΔE_g. For example, for $\Delta E_g = 0.4$ eV, $\Delta n \approx 0.2$ or $\Delta n/n \cong 0.2/3.6 \approx 6\%$.[13] Carrier confinement requires a potential barrier height of a few kT. At 300°K, a bandgap energy difference of $\gtrsim 0.1$ is adequate.

Various heterojunction laser structures are obtained by using selected layers in Figure 38. If $d_2 = d_3 = 0$ and $x(5) = x(1)$, we obtain the symmetrical double heterojunction (DH) laser.[14] With $d_2 = 0$ and $x(4) = 0$, the large optical cavity (LOC) laser diode is obtained.[15] A four-heterojunction laser is obtained when all the regions are used. Each of these structures is capable of a wide range of properties depending on the width of the various regions, their Al content, symmetry, and doping in the GaAs recombination region. We will discuss some of these properties later in the report but for identification purposes, a modification of the LOC structure is the device used for this contract.

The threshold current density of the laser depends on the width of the various regions and on the doping level in the recombination region. This becomes evident from basic considerations which are reviewed below.

---

[13] H. Kressel, H. F. Lockwood, and J. K. Butler, "Measurements of refractive index step and of carrier confinement at (AlGa)As-GaAs heterojunctions," J. Appl. Phys., vol. 44, p. 4095, September 1973.

[14] I. Hayashi, M. B. Panish, P. W. Foy, and S. Sumski, "Junction lasers which operate continuously at room temperature," Appl. Phys. Lett., vol. 17, p. 109, August 1, 1970.

[15] H. F. Lockwood, H. Kressel, H. S. Sommers, Jr., and F. Z. Hawrylo, "An efficient large optical cavity injection laser," Appl. Phys. Lett., vol. 17, p. 499, December 1, 1970. H. Kressel, H. F. Lockwood, and F. Z. Hawrylo, "Large-optical-cavity (AlGa)As-GaAs heterojunction laser diode: threshold and efficiency," J. Appl. Phys., vol. 43, p. 561, February 1972.

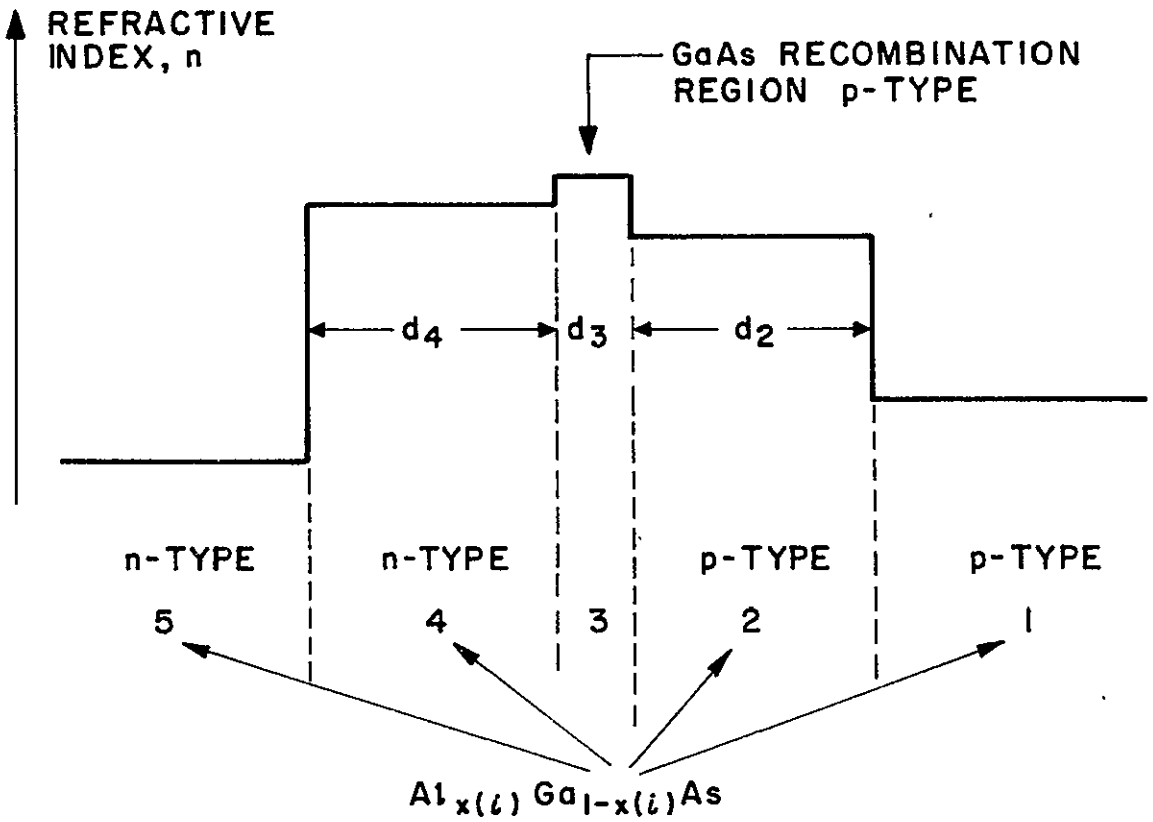

Figure 38. Cross section of generalized laser structure used in analysis of transverse modes. The radiative recombination occurs in region 3, while regions 2, 3 and 4 constitute the nominal waveguide.

At a given temperature, the laser threshold current density J_{th} is a function of the optical waveguide thickness w, the width of the recombination region d_3, the doping level, the facet reflectivity R, and the length of the laser L. The gain coefficient required to reach threshold, g_{th}, is

$$g_{th} = \bar{\alpha} + \frac{1}{L} \ell n \frac{1}{R} , \qquad (4)$$

where $\bar{\alpha}$ is the effective absorption coefficient. The major contribution to $\bar{\alpha}$ is due to free carrier absorption in well-designed heterojunction lasers.

The gain for a material of given doping is a function of the injected carrier density n in the recombination region (at threshold $n \propto J_{th}/d_3$), of the form $g \propto n^b$ where $b \geq 1$, and of the fraction, Γ, of the radiation which propagates through the recombination region

$$\Gamma \cong d_3/w \qquad (5)$$

Therefore,

$$g_{th} \propto \Gamma n^b \propto \Gamma (J_{th}/d_3)^b. \tag{6}$$

(A coupling factor which takes into account the position of the gain region within the waveguide region is neglected here.)

Combining Equations 4 through 6 yields an expression for J_{th}

$$J_{th} \propto w^{1/b} \; d_3 \; (1 - \frac{1}{b}) \left[\alpha + \frac{1}{L} \ell n \frac{1}{R} \right]^{\frac{1}{b}} \tag{7}$$

It is evident from Equation 7 that if b = 1, then J_{th} increases linearly with the width of the waveguide region w, assuming $\bar{\alpha}$ constant. However, if b >1, then for constant w, it is possible to reduce J_{th} by reducing the recombination region width d_3. Dependent upon the doping, LOC devices exhibit a value of b between 1 and 2.

C. EFFECTS OF p-DOPANT ON LIFETIME

The nature of the zinc diffusion, which is frequently used to improve the performance of ohmic contacts or to provide isolation in stripe contact geometries, affected the diode lifetime. This observation was made during experiments conducted during the contract period in support of other work.

The laser diodes studied were (AlGa)As double-heterojunction devices emitting at about 800.0 nm. This choice of wavelength is based on the availability of glass fibers with very low losses in that spectral region[16] and on the fact that previous work has shown that diodes containing $Al_{0.1}Ga_{0.9}As$ in the recombination region are more resistant to gradual degradation than diodes similarly fabricated with GaAs in that region.[17,18] The diodes were prepared by liquid phase epitaxy in a horizontal

---

[16] D. B. Keck, R. D. Mauer, and P. C. Schultz, "On the ultimate lower limit of attenuation in glass optical waveguides," Appl. Phys. Lett., vol. 22, p. 307, April 1, 1973.

[17] M. Ettenberg, H. F. Lockwood, J. P. Wittke, and H. Kressel, "High radiance, high speed $Al_xGa_{1-x}As$ heterojunction diodes for optical communications," Technical Digest, 1973 International Electron Devices Meeting, Washington, December 3-5, 1973, p. 317. M. Ettenberg, H. Kressel, and H. F. Lockwood, "Degradation of $Al_xGa_{1-x}As$ heterojunction electroluminescent devices," Appl. Phys. Lett., vol. 25, p. 82, July 1, 1974.

[18] H. Yonezu, K. Kobayashi, K. Minemura, and I. Sakuma, "GaAs-$Al_xGa_{1-x}As$ double heterostructure laser for optical fiber communication system," Technical Digest, 1973 International Electron Devices Meeting, Washington, December 3-5, 1973, p. 324.

multiple-bin boat. The recombination region, not deliberately doped, had an electron concentration of 5×10^{16} cm^{-3}. The spacing between the heterojunctions (i.e., the recombination region width) was 0.2-0.3 μm. The basic design concept of such narrow recombination region heterojunction diodes was previously described,[19] and is based on the controlled spread of the radiation beyond the recombination region into the adjoining low-loss, higher bandgap, p- and n-type (AlGa)As regions to reduce the far-field beam divergence.

Germanium was used to dope the p-type regions, while the donor dopants were Sn or Te. The spacing between the diode surface and the edge of the recombination region was ~3 μm including a p-type GaAs layer used to improve the ohmic contact. In subsequent discussion we will refer to this layer as the "cap" layer and the p-(AlGa)As layer (~30% Al) as the "p-wall". When processed in conventional broad-area form, the room temperature threshold current density was 1100-1500 A/cm^2 (with cavity lengths of 500 μm), and the differential quantum efficiency was 30-40%. The diodes were mounted p-side down on copper heat sinks using indium as the solder.

The effect of excessive zinc diffusion on diode life was studied in the following type of experiment. The p-surface of the wafer was protected with SiO_2 except for 13 μm-wide stripe windows. Zinc was next diffused to a depth of 1 μm using an excess zinc source in a sealed ampoule. The diffusion front, as revealed by etching, was located at the boundary between the p-wall and the cap layer. It is, however, possible that some Zn (or associated lattice defects), not revealed by etching, penetrates into the "p-wall" or even into the recombination region. This would be significant here since the p-wall had a thickness of only 0.5-0.8 μm, which makes the latter possibility more likely. Control sections of the same wafer were processed without diffusion. Both sections of the wafer were then metallized and assembled for operation by mounting on copper heat sinks. A typical threshold current for diodes 500 μm long was 550-600 mA.

A comparison of the life of the diffused and the nondiffused diode, shown in Figure 39, reveals a large difference. Diodes were operated at 500 mA which was below lasing threshold, in order to make the emission more directly dependent on quantum efficiency. Note that the diffused diode degraded to half its initial output in 40 hours while the nondiffused diode remained unchanged. Thus, Zn as a p dopant was no longer used for this work.

---

[19] H. Kressel, J. K. Butler, F. Z. Hawrylo, H. F. Lockwood, and M. Ettenberg, "Mode guiding in symmetrical (AlGa)As-GaAs heterojunction lasers with very narrow active regions," RCA Review, vol. 32, p. 393, September 1971.

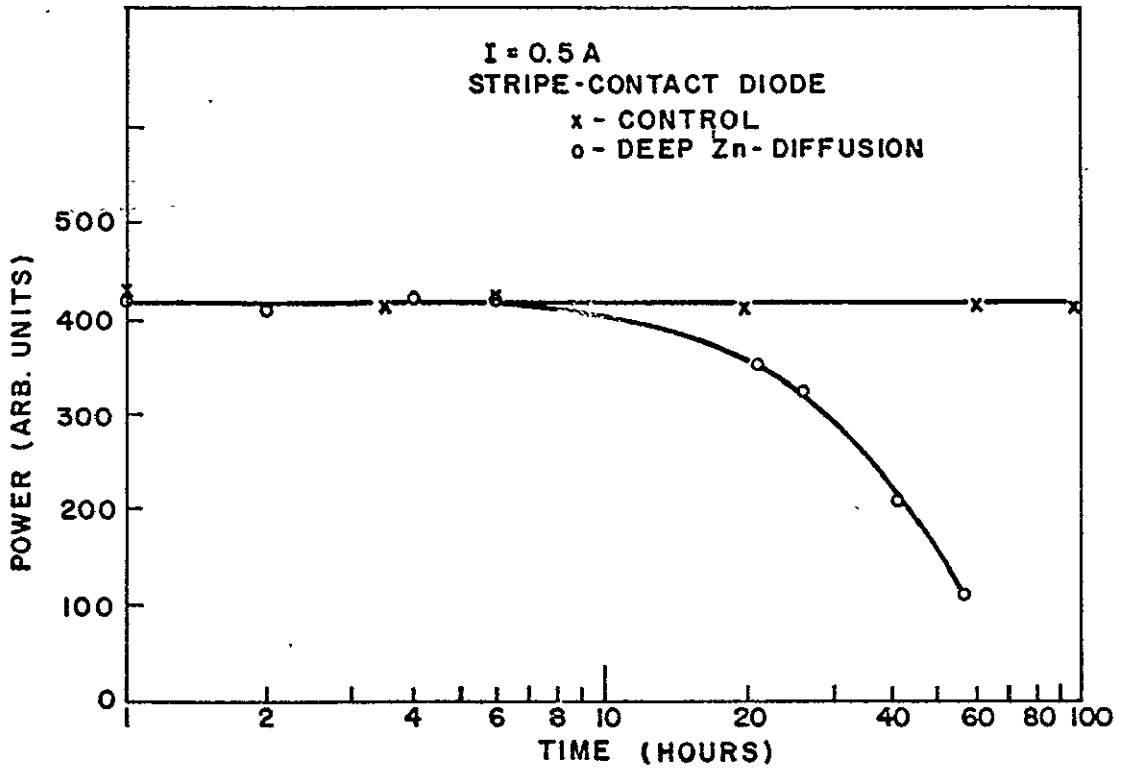

Figure 39. Power output as a function of time for two diodes fabricated from the same wafer but processed differently. One diode had a deep Zn diffusion ($\sim 1\ \mu m$) from an excess Zn source prior to ohmic contact application, while the other diode was not diffused.

D. EXPERIMENTAL RESULTS ON PULSED LASERS

Detailed results of a number of growth runs are tabulated in this section. From each run, slivers were chosen randomly after processing, and from these slivers 10 diodes were mounted on packages. Of these 10 diodes, two were fully characterized with respect to threshold current density, efficiency, temperature behavior, and beam pattern. Later in this section operating life is discussed.

1. Crystal Growth

All of the growth runs were made using a thin-solution method. Each wafer had a total of six epitaxial layers. The structure is shown in Figure 40. The first layer grown on the substrate is n-type GaAs, which serves as a new substrate for the subsequent layer growth. This layer is indispensable in the control of subsequent layer thickness, uniformity, and perfection; it is nominally 5 to 8 μm thick.

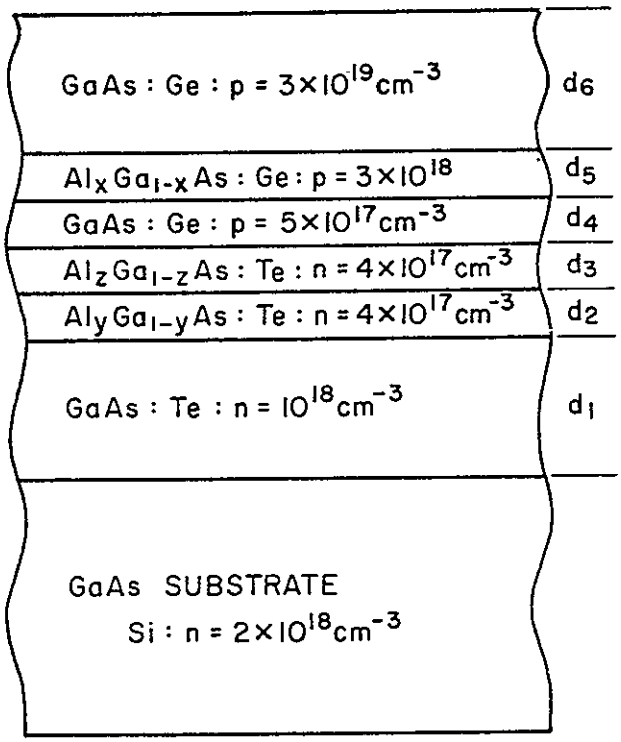

Figure 40. Schematic illustration of LOC laser. Typical parameters are d_1 = 5 to 8 μm, $d_2 = d_3 = d_4 = d_5 = 1\ \mu$m, $d_6 \simeq 15\ \mu$m; x = 0.15, y = 0.07, z = 0.015.

The optical cavity is located between layers 2 and 5, and since the radiation is rather well confined, thickness of these layers is not critical. Their nominal thickness is 1 μm each. The heavily doped "cap" layer of GaAs:Ge d_6 is generally about 10 μm. For very high-duty-factor operation, this layer is made as thin as 1 μm.

The cavity itself, layers 3 and 4, has critical dimensions in terms of beam control. To assure fundamental transverse mode operation, $d_3 + d_4$ is kept at 2 $\pm$0.1 μm with the p-n junction placed approximately ($\pm$ 0.2 μm) in the middle. In addition, the value of z in $Al_zGa_{1-z}As$ is kept at z = 0.015 to give a beam width (FWHM) of approximately 30°. If z = 0, the device will revert to the next higher transverse mode with a double-lobed beam requiring larger numerical aperture optics for efficient collection. The Al concentrations in the guiding layers are given by x = 0.15 and y = 0.07. The beam can be made considerably narrower than 25 to 30° by adjusting z and y, but there is a price to pay in threshold current, especially at the higher temperatures required for the current work. The exact melt compositions for the entire structure are given in Table 3.

TABLE 3. MELT COMPOSITIONS

Layer	1	2	3	4	5	6
Al	---	0.22	0.05	---	0.5	---
Ge	---	---	---	5.0	50	100
Te	0.35	0.15	0.15	---	---	---

All weights are in mg for 1-g Ga melts at a growth temperature of 800°C.

The growth schedule consists of raising the temperature to 850°C, cooling to 800°C, and holding for 1 hour. The source wafers are then dropped, after which the temperature is again held at 800°C for 1 hour to assure saturation of the melts. The substrate is then introduced into the first solution, and the temperature is raised 15°C to partially dissolve the substrate. Growth of the first layer starts at 815°C and ends at 800°C at which time the substrate enters the second bin. This process is repeated for all the subsequent layers at a continuous cooling rate of 0.5°C/min. The temperature changes (in °C) necessary to grow each layer are: $\Delta T_1 = 15$, $\Delta T_2 = 2.3$, $\Delta T_3 = 1.54$, $\Delta T_5 = 3.1$, $\Delta T_6 = 30$.

2. Performance Data

Table 4 lists the relevant physical measurements of a number of lasers tested. The lasing wavelength at 23°C is 890.0 ± 5.0 nm; at 75°C, it is 905.0 ± 5.0 nm. Threshold current densities (J_{th}) and differential quantum efficiencies (η) were measured with the aid of a calibrated ITT-4000 photodiode, with the lasers driven by a 200-ns current pulse. The output of the lasers is single-ended; i.e., there is a reflective coating on the rear and a near antireflective coating (SiO) on the front facet. The reflective coatings on runs L-192 and P-638 were defective for the particular diodes randomly chosen, and this explains their poor performance. Thus, radiation is emitted strongly from the rear of these diodes and the far-field pattern is distorted by reflections from the header. Naturally, the efficiency is also reduced because this scattered light is not collected by the detector.

The variability in performance seen in Table 4, although not excessive, does not truly represent the far greater uniformity inherent in the epitaxial process itself. The two most important contributions to scatter in the data are precise control of elemental Al in the melt and control of the optical thickness (index of refraction x actual thickness) of the antireflective coating. Both of these problems were essentially solved during the last weeks of the contract period and are not reflected in the data of Table 4.

TABLE 4. RELEVANT PARAMETERS OF DELIVERED LASERS

Run	J_{th}(23°C) kA/cm^2	η %	J_{th}(75°C) kA/cm^2	η %	θ_1 deg	θ_{11} deg
L-175-1	11.9	52	24.6	32	32	14
L-175-2	11.9	52	23.5	32	32	16
L-176-1	8.64	52	16.3	41	32	15
L-176-2	8.47	52	15.8	41	32	15
L-188-1	9.8	50	17.3	44	23	13
L-188-2	9.6	50	16.6	44	23	12
L-190-1	9.6	53	15.4	37	31	19
L-190-2	9.8	53	16.6	34	37	18
L-192-1	9.5	14	20.8	12	30	(a)
L-192-2	9.6	20	19.2	16	35	(a)
P-630-1	8.9	43	18	32	30	12
P-630-2	10	50	19	32	27	12
P-634-1	11.9	57	25.8	35	28	14
P-634-2	11.7	49	23.5	36	28	13
P-635-1	10.5	50	19.8	34	29	14
P-635-2	10.9	53	20.7	41	26	14
P-636-1	12.4	47	25.8	44	25	16
P-636-2	12.6	57	24.5	35	28	14
P-638-1	13.7	19	17	15	29	(a)
P-638-2	12.3	7	18	10	32	(a)

NOTES:

(a) See text for discussion.

(b) Lasing wavelength: λ_L(23°C) = 890.0 ± 5.0 nm; λ_L(75°C) = 905.0 ± 5.0 nm.

(c) J_{th}(100°C) = 25 to 35 kA/cm^2 for all lasers.

From the compositions shown in Table 3, it is clear that extremely small concentrations of Al are required in the melts. This is particularly true of layer 3, the layer having the most profound effect upon the far-field radiation pattern. Two factors influence the accuracy of the Al incorporated into the $Al_zGa_{1-z}As$: (1) oxygen contamination with the subsequent formation of Al_2O_3, and (2) operator error in handling microgram quantities of substances, a factor eliminated by appropriate training. By redesigning the input (H_2) gas flow system, oxygen contamination has been reduced considerably below 1 ppm. The removal of oxygen also noticeably improves the crystal quality and permits defect-free growth.

Variations in the optical thickness of the antireflective coating account for most of the run-to-run variations in threshold current density. For a given run, the typical variation in threshold current density from lasers taken from the entire wafer is less than 10%, with a somewhat larger variation in the external quantum efficiency.

3. Reliability

The first reliability question that arises for high-power lasers is one of facet damage rather than bulk degradation. That is, given high-quality defect-free crystal growth and good control over impurities, short term failures in lasers operated at high power levels occur mechanically at the facet and not through the generation of bulk defects which might lower the internal quantum efficiency.

Experiments were performed to determine (1) the mechanical factors affecting the onset of facet damage, (2) pulse duration dependence of facet damage, and (3) the specific damage threshold of those diodes delivered under the present program.

It has been established over the years that facet damage is associated with peak optical intensity. Many mechanisms, including stimulated Brillouin scattering, piezoelectric-induced strain, and electrostriction, have been invoked to explain surface damage, but definitive experiments to isolate the cause have not been devised.

It has been discovered that there are preferred nucleation sites for catastrophic damage. These sites are inevitably mechanical in nature. For instance, in relatively narrow (100 μm) lasers with apparently perfect facets, damage frequently initiates at the edge of the laser where it has been wire-sawed. The resulting surface disturbance appears to occupy an area less than 1 μm x 1 μm, but this region serves as the lowest threshold nucleation site for additional damage. As a result, a line of damage travels across the laser facet and destroys the mirror of the Fabry-Perot cavity and reduces the optical output. Occasionally the damage stops before destroying the entire facet, and the diode continues to lase at a lower efficiency. This cessation of damage may be related to the lateral homogeneity of the optical field in the cavity at the surface.

If the sawed edges are physically removed from the lasing region, which is the case for the stripe geometry used through the latter stages of this contract, there is a dramatic improvement in the threshold for catastrophic damage. When damage does occur, it will start at any scratch crossing the optical cavity and radiate in both directions.

If the surface is free of scratches (in the sense of not being visible at 2000X magnification with differential phase contrast), there is a further increase in the threshold for damage. The next surface feature for damage nucleation is the cleavage striation. This surface defect appears to be present to a greater or lesser extent in all diodes, and the more obvious the striation, the lower the damage threshold.

These effects are not small. Scratched diodes have been found to damage at one-sixth the optical power of similar unscratched diodes in a stripe configuration. Diodes with cavities defined by sawed edges tend to damage at powers one-half to one-third that of stripe-geometry diodes.

The second factor affecting limitations imposed by facet damage is the pulse duration. It is known from previous work that the onset of facet damage is dependent on the pulse length.

A series of experiments were performed using four-heterojunction lasers having $d_1 = d_5 = 1.13\,\mu m$, $x_1 = x_5 = 0.3$; $d_2 = d_4 = 0.5\,\mu m$; $x_2 = x_4 = 0.2$; $d_3 = 0.2$, $x_3 = 0$. Because of driver limitations, the pulse shape was not quite "square" but did reasonably approximate the desired shape. Figure 41 shows the current pulse used to obtain the damage data at each pulse width together with the appearance of the facet after damage. Note that the facet is usually not uniformly damaged, with the edge of the diode frequently (but not always) showing damage first, suggesting the propagation of damage from the edge of the diode inward. The damage data as a function of pulse width are shown in Figure 42 and indicate a damage limit which is inversely proportional to the square root of the pulse width. Also shown in Figure 42 are earlier data for single-heterojunction laser diodes. While having higher limits than the four-heterojunction device tested, the same $t^{-1/2}$ damage limit is indicated. The range of operation for diodes in the pump arrays is also indicated. Additional data published for double-heterojunction lasers[20] also suggest the same behavior, therefore indicating that it is possible to extrapolate the damage limit for a wide range of pulse duration values from limited experimental data.

Figure 42 also shows data obtained with a 100-ns-wide pulse. The uncoated diodes damage at ~400 W/cm, comparable to the single-heterojunction diodes. However, after coating with an antireflecting SiO film, the damage limit was increased to 1200 W/cm. Figure 43 shows the facet of the laser damaged at the 1200-W/cm level. The damage starts near a flaw at the edge of the laser and propagates along the facet toward the center. Although this represents a rather high damage limit, still greater reliability is achieved with the use of stripe geometry.

Finally, it should be noted that the instantaneous or catastrophic damage limit serves only as an indication of the upper limit of operation of the laser. For long-term reliability, operation at a considerably lower level is essential. However, it can be said that lasers have been operated at the 400-W/cm level at a repetition rate of 1 kHz with no appreciable drop in output after 350 hours.

---

[20] P. G. Eliseev, Semiconductor Light Emitters and Detectors (A. Frove, ed.). Amsterdam: North Holland Publishing Co., 1973.

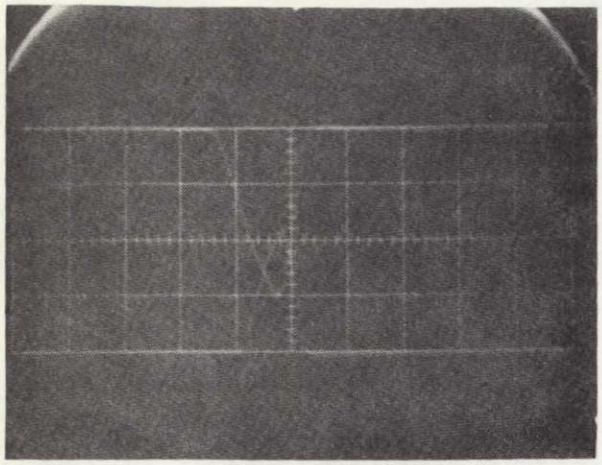

50 ns/div→

(a)

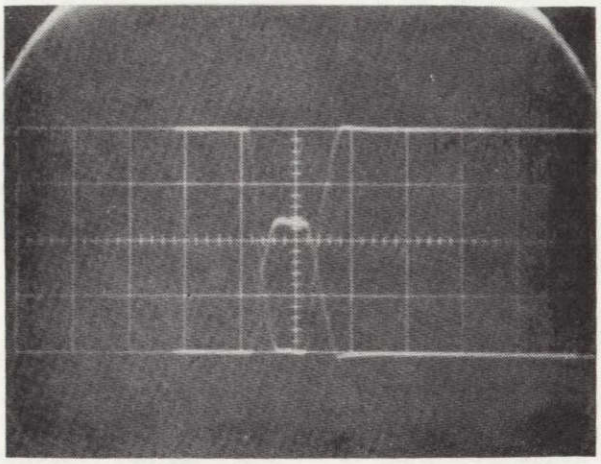

100 ns/div→

(b)

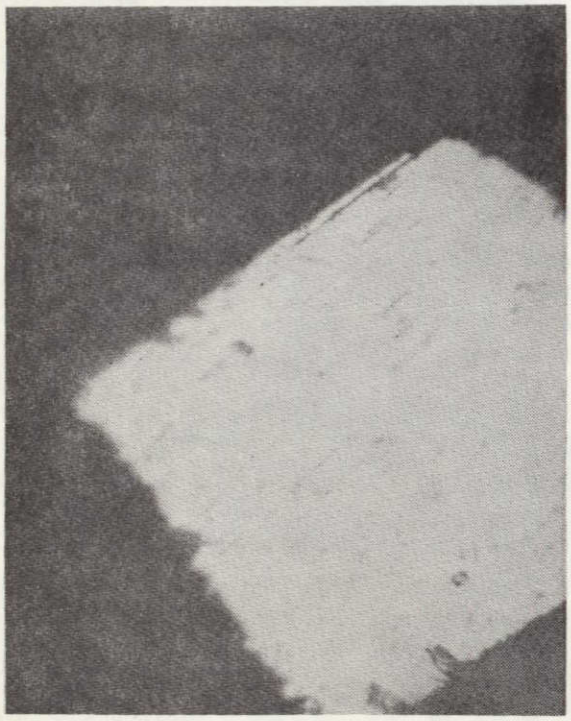

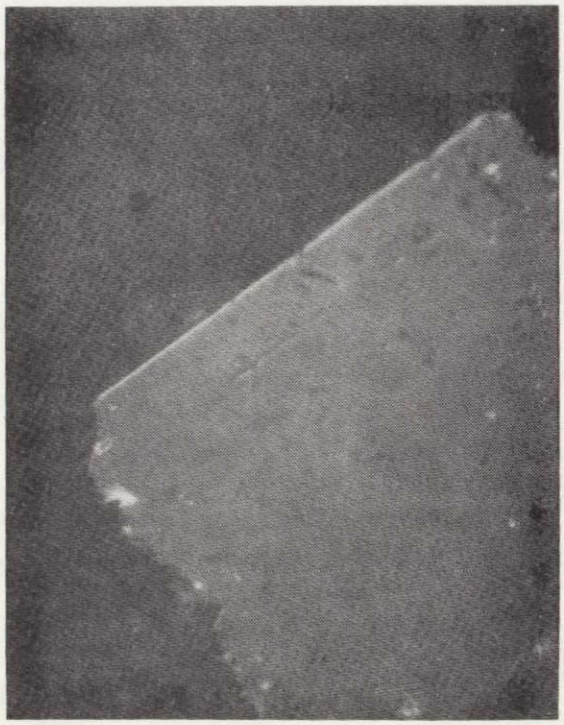

Figure 41. Instantaneous or catastrophic facet damage with pulse width increasing from 50 ns (a) to 2 μs (f). The photomicrographs (780X) of the facets show the line of damage in the optical cavity.

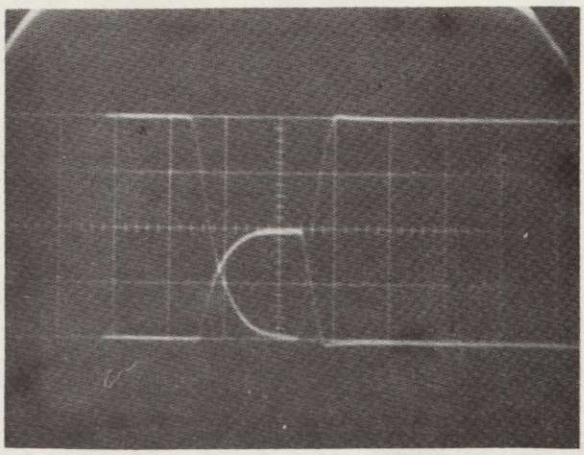

100 ns/div→

(c)

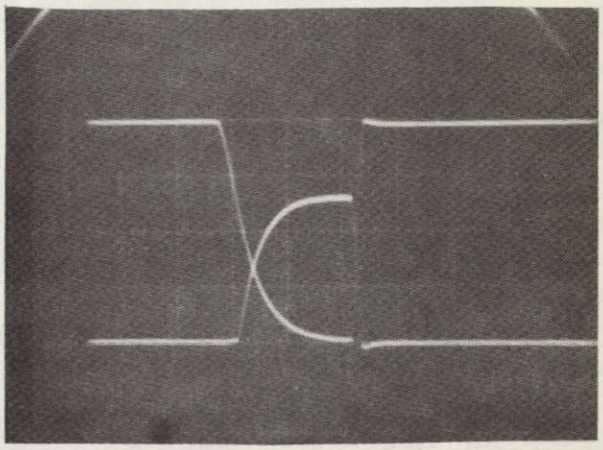

200 ns/div→

(d)

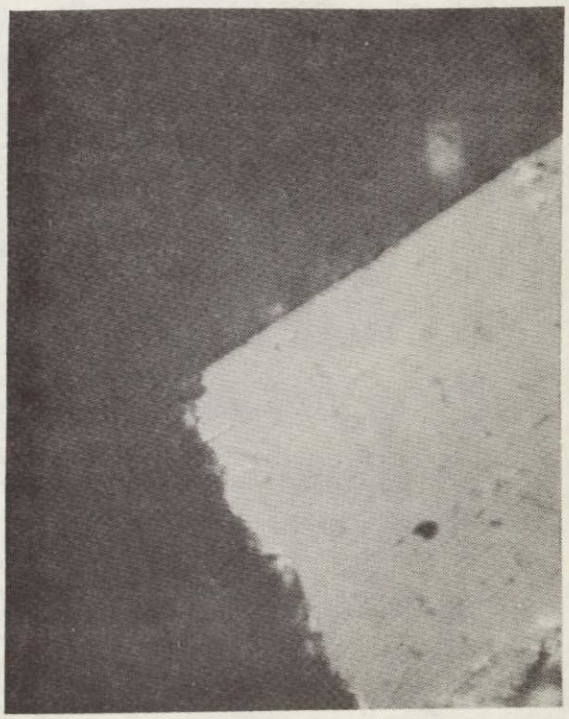

Figure 41. Continued.

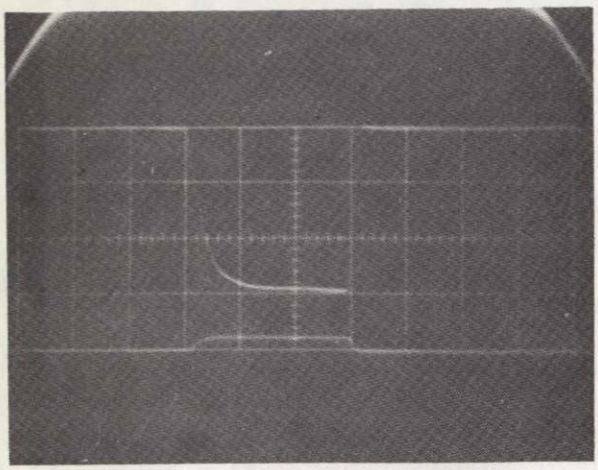

200 ns/div→

(e)

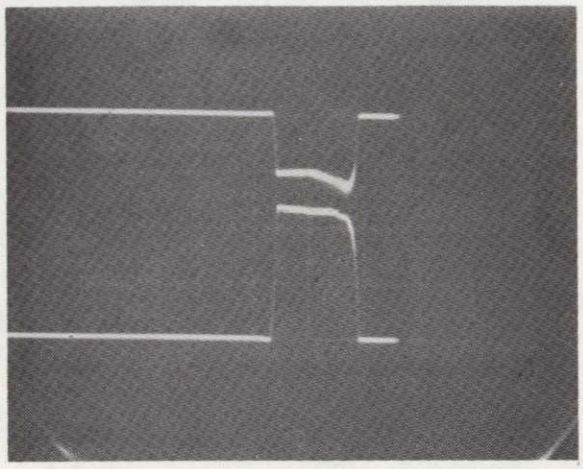

.5 μs/div→

(f)

Figure 41. Continued.

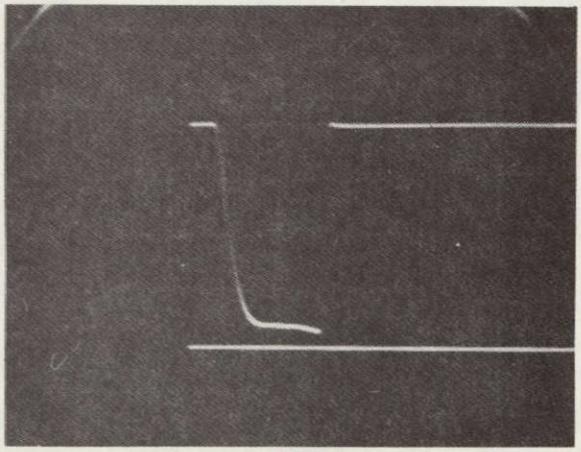

0.5 μs/div→

(g)

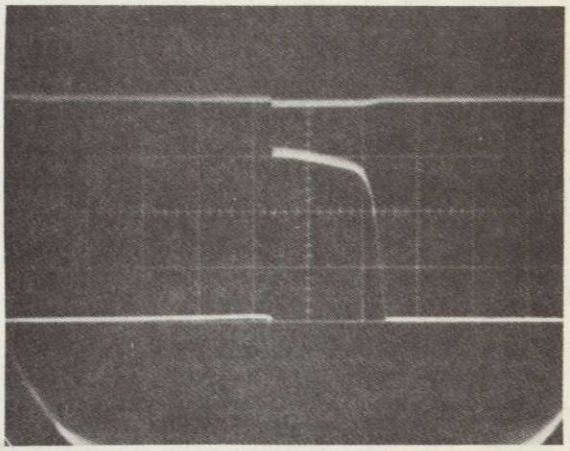

1 μs/div→

(h)

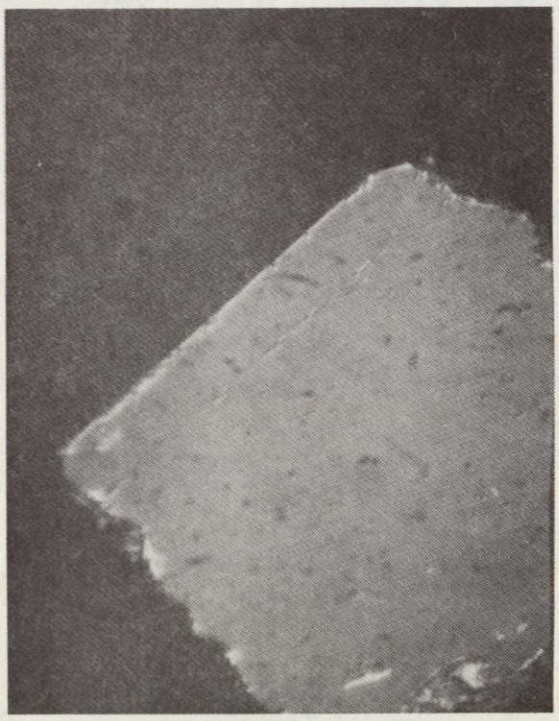

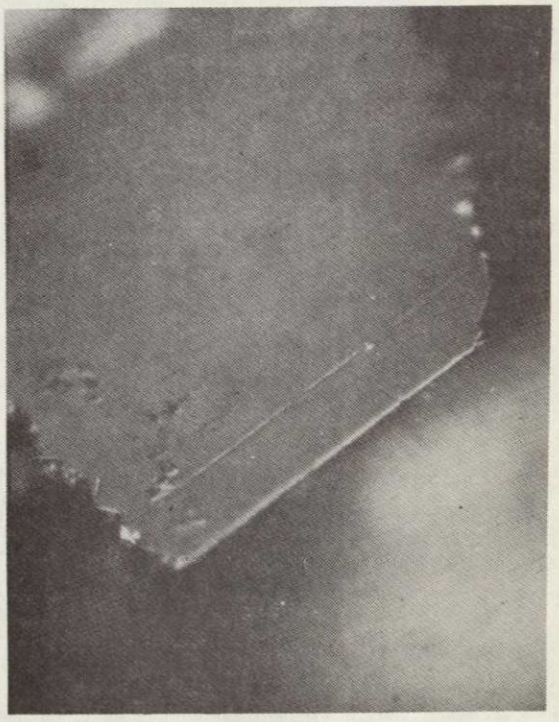

Figure 41. Continued.

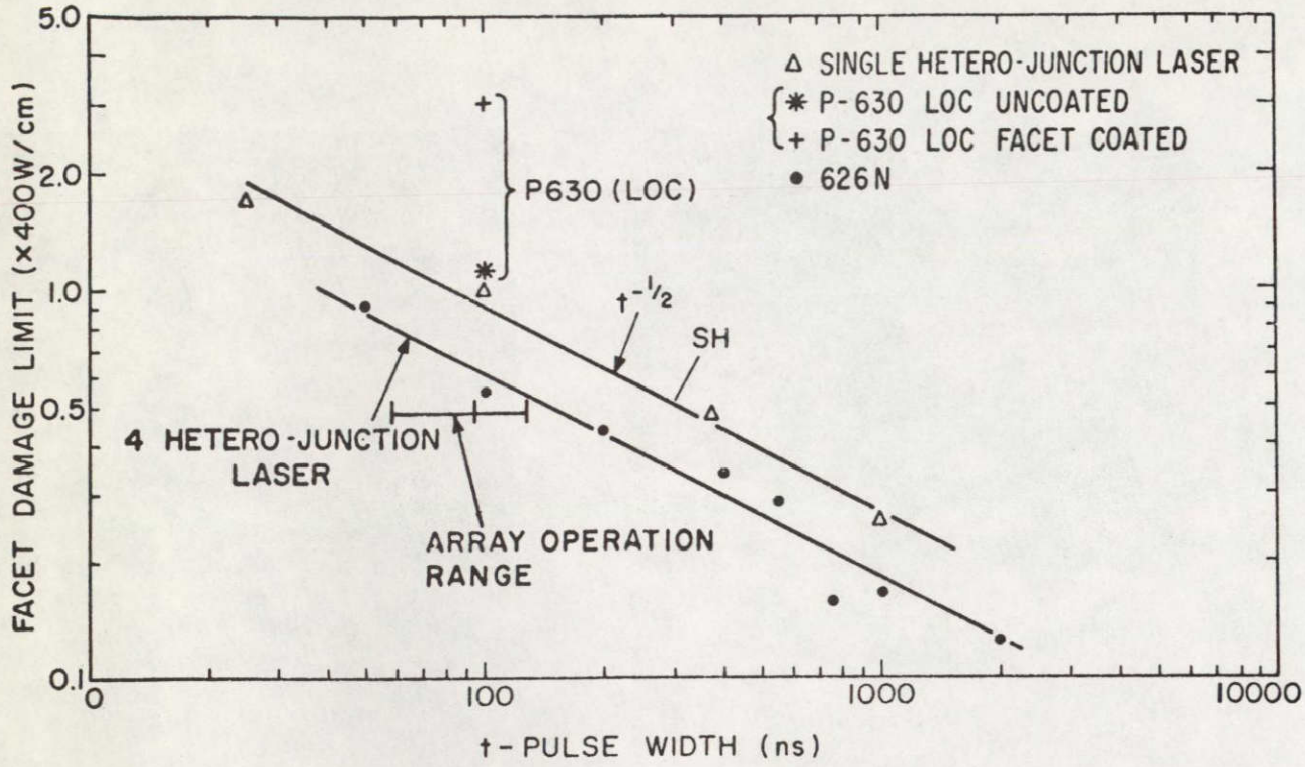

Figure 42. Dependence of facet damage on pulse width for uncoated lasers. The data points for P-630 LOC type lasers are given for coated and uncoated structures and correspond closely to previously obtained data for single-heterojunction lasers (upper curve). The lower curve is data taken on four-heterojunction lasers.

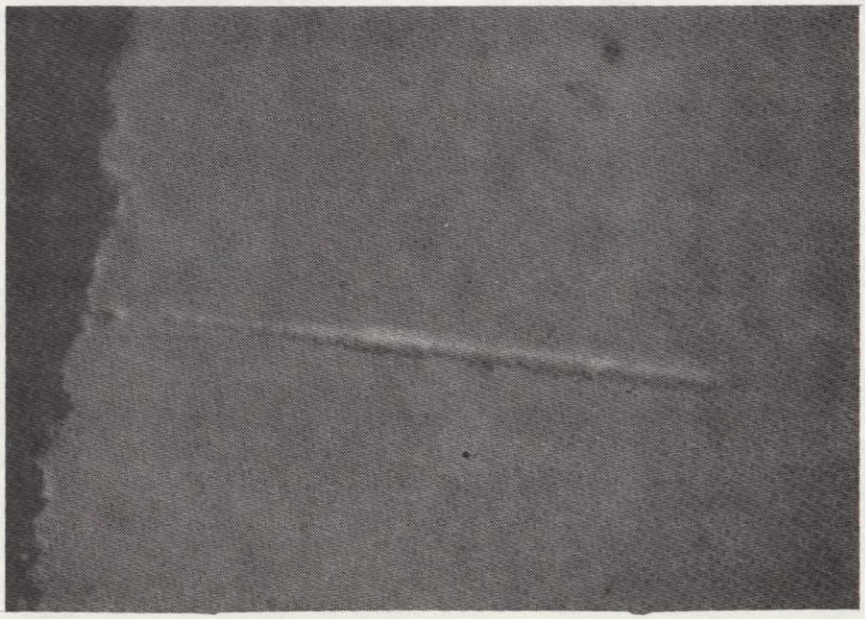

Figure 43. Facet damage observed on high-power LOC laser at the 1200-W/cm operating level. (Facet originally coated with SiO which was removed to obtain this photograph.)

The problem at this level becomes one of obtaining extended lifetimes in units operated at duty factors exceeding those used in the catastrophic damage tests by 100:1. Thus, 350 hour lifetimes become equivalent to 3.5 hour lifetimes.

The techniques employed in attempting to achieve lifetimes of several thousand hours at 1% duty factors have been to take all of those elements that have been observed to offer improved life and to use this to construct the best possible diodes. These led to the production of test diodes of the following characteristics:

Material	Ge doped LOC
Contact form	0.006 inch stripe on p side
Coating	AR on output; HR on back
Die size	0.018 x 0.018 x 0.004 inches
Mounting	Copper header

Diodes for these tests were made from selected cleaved strips with no visible cleavage striae. After careful mounting and inspection, the diodes were placed on life test with 0.5 W per mil of emitting junction width.

Single diode units fabricated in this manner in the first 3 months of the second phase of this program operated as much as 9000 hours at 1/2% duty factor. Stabilizing these characteristics and producing laser arrays encountered very frequent difficulties. It was necessary under what is primarily an RCA-funded effort to produce sizable refinements in each step of the process passing beyond the basic wafer growth. Normal steps in this procedure include stripe contacting, cleaving, coating facets, mounting, sawing, series wiring and testing.

Life tests made, using arrays fabricated and using the care employed with the single diodes, have shown individual diodes dropping in output at periods ranging from 200 hours to 1500 hours. These diodes are observed to degrade over a period of roughly 100 hours per diode. Figure 44 shows life test results for several of the diodes. Examination of the diodes that have degraded reveals the following:

a) No facet damage was observed.

b) No change in electrical characteristic was observed.

c) Threshold was elevated.

d) Quantum efficiency was degraded.

e) The near field pattern becomes spotty.

Catastrophic failure is not seen. The changes observed are those one would expect from degradations in the bulk material, dislocations, color centers, etc.

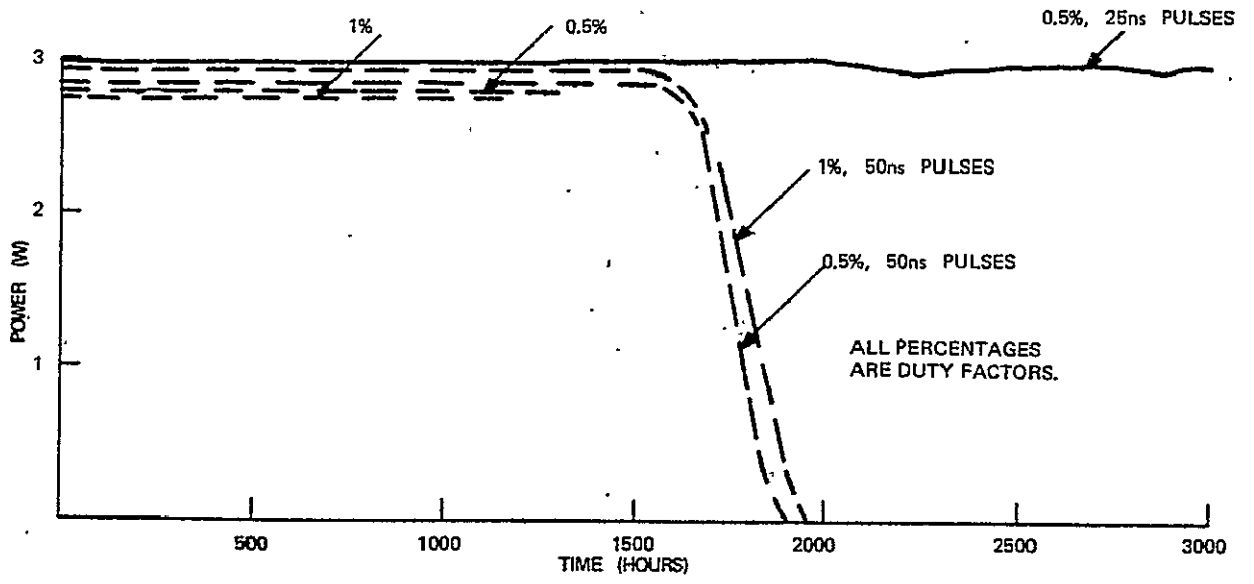

Figure 44. Results of diode life tests.

For further insight into the causes of this degradation and possible remedies, it is instructive to refer to work done previously. A series of experiments was designed to determine the effect on operating life of the presence of heterojunctions and of the Al composition in (AlGa)As heterojunction diodes. The phenomenon studied is gradual degradation, which is known to depend on operating current density and metallurgical factors.

Diodes were sawed into ~100- μm squares from a fully metallized wafer and then bonded with In to an Au-plated Cu heat sink. The wafer contacts consisted of alloyed Sn followed by plated Ni and Au on the n side, with plated Ni and Au on the p side. Four or five diodes were chosen randomly from each wafer and operated continuously at ~100 A/cm^2; the light output at 1000 A/cm^2 was monitored as a function of time with a Si solar cell attached to each diode test assembly. At this current density there was no significant device heating as evidenced by the lack of electroluminescence spectral shift with current increase, so special heat-sink geometries (e.g., stripes) were unnecessary. The operating lifetime for each set was defined as the average time for the output to fall to half its initial value. The test was terminated at about 1000 hours. For those diodes with a half-life greater than 1000 hours, the degradation curve was extrapolated to half-power output to determine the lifetime. Figure 45 illustrates the behavior of a group of four diodes over an extended period of time. Note that the degradation rate is quite uniform; this was usually the case for longer-lived diodes.

The major results of this study are summarized in Figure 46, where we show the half-life of diodes with varying dopants and the peak of the emission wavelengths. The pertinent diode construction details are listed in Table 5 for all the diodes studied.

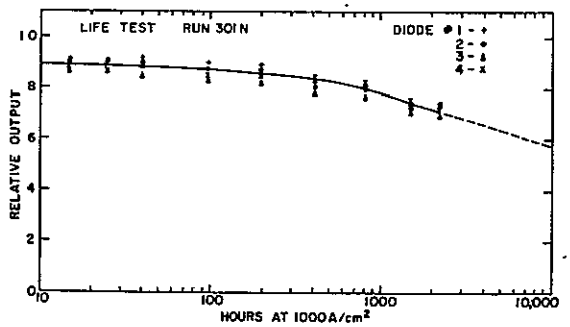

Figure 45. Relative light output as a function of time of broad area contacted incoherent emitters stressed at ~1000 A/cm^2.

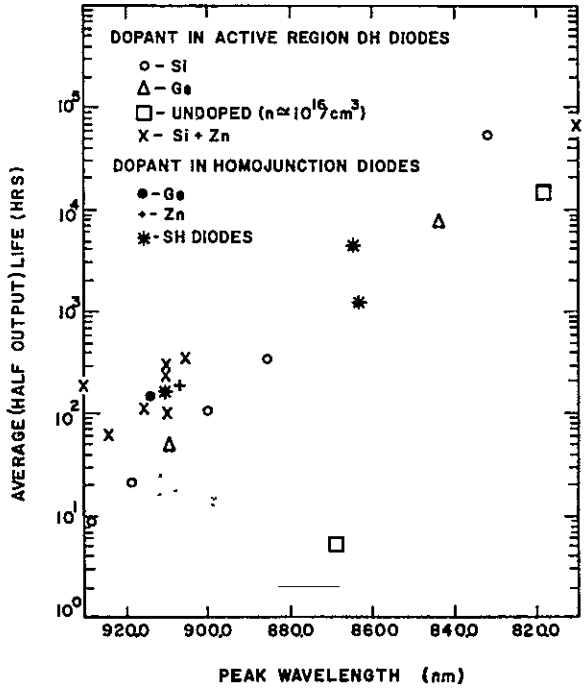

Figure 46. Average (half-output) life of incoherent emitters stressed at ~1000 A/cm^2 as a function of emission wavelength. For each doping type the shift to shorter wavelength represents additions of Al to the recombination region.

The diodes studied were edge-emitting devices with the surfaces fully metallized. It is known from previous work[21] that the spontaneous emission data obtained under such conditions are representative of the entire recombination region in the devices as long as the current density of operation is sufficiently high. A current density of 1000 A/cm^2 satisfies this requirement. The double-heterojunction (DH) $Al_yGa_{1-y}As$/ $Al_xGa_{1-x}As$ ($y>x = 0.1-0.3$) diodes had Ge, Si, Si + Zn, or not intentionally ("undoped")

[21] Henry Kressel and N. E. Byer, "Physical basis of noncatastrophic degradation in GaAs injection lasers," Proc. IEEE, vol. 57, p. 25, January 1969.

TABLE 5. DIODE DETAILS

Designation	Peak Wavelength (nm)	Doping Density in Recombination Region (10^{18} cm^{-3})	Heterojunction Spacing (μm)	Recombination Width (μm)
DH-Si (O)	928.0	10	2.0	2.0
	918.0	10	2.5[a]	1.0
	899.0	1	2.5[a]	0.75
	886.0	1	2.5[a]	1.0
	834.0	10	2.0	2.0
DH-Ge(Δ)	909.0	1	1.4[a]	0.4
	845.0	2	1.0	1.0
DH-undoped (□)	867.0	0.01	1.0	1.0
	820.0	0.01	1.0	1.0
DH-Si-Zn (x)	930.0	10(Si), 1(Zn)	1.5[a]	0.5
	928.0	10(Si), 1(Zn)	4.0[a]	0.5
	920.0	10(Si), 1(Zn)	0.5	0.5
	915.0	10(Si), 1(Zn)	1.5[a]	0.5
	915.0	10(Si), 1(Zn)	2.0[a]	0.5
	915.0	10(Si), 1(Zn)	2.5[a]	0.5
	911.0	10(Si), 1(Zn)	1.5[a]	0.5
	810.0	10(Si), 1(Zn)	2.5[a]	0.5
Homo-Ge (●)	918.0	5		
Zn(†)	910.0	5		
SH (*)	915.0	10(Zn)		2.0
	865.0	10(Zn), 2(Te)		2.0
	865.0	10(Zn), 2(Te)		2.0
Laser test (Fig. 47)	895.0	1 (Te)	2.5[a]	1.0

[a]LOC types.

doped recombination regions. In addition, single-heterojunction and homojunction diodes were tested in order to determine whether the addition of heterojunctions (with the resultant elastic strain in the recombination region) made a detectable contribution to the degradation. The single-heterojunction diodes consisted of an (AlGa)As: Zn layer grown on a melt-grown Si-doped substrate ($n \simeq 2 \times 10^{18}$ cm^{-3}) or on a Te-doped n-type epitaxial layer with the Zn diffused from the p layer into the n-type layer a distance of about 2 μm. The homojunctions were made by the deposition of a Ge- or Zn-doped GaAs epitaxial layer ($p = 5 \times 10^{18}$ cm^{-3}) on an n-type melt-grown GaAs substrate ($n \simeq 2 \times 10^{18}$ cm^{-3}).

The emission wavelength of the diodes, shown in Figure 46, depends on three factors: the doping density, the doping type, and the Al content in the recombination region. For each dopant type tested (illustrated in Figure 46 as differently shaped data points) the doping density was kept about constant while the band gap was increased by the addition of Al to the recombination region. Diodes with GaAs ($x = 0$) recombination regions emit at ~930.0 nm for Si and Si + Zn doping, ~910.0 nm for Ge, and ~870.0 nm for the undoped recombination regions. Data points for each doping type corresponding to emission at progressively shorter wavelengths represent increasing additions of Al to the recombination region.

The conclusions that may be drawn from the data in Figure 46 are as follows:

a) Although there were only a few homojunction wafers tested, there seems to be no significant effect which can be attributed to the presence of heterojunctions in the structure. This is evident from a comparison of the GaAs homojunction or single- and double-heterojunction life with similar active region doping.

b) For the limited range of dopants and diode construction shown in Table 5, the operating lifetime improves significantly with the addition of Al to the recombination region.[22] This is particularly striking in the case of the double-heterojunction diodes with undoped active regions where an improvement by a factor of 10^3 is obtained by changing the recombination region to $Al_{0.1}Ga_{0.9}As$ ($\lambda = 800.0$ nm). These results agree with other laser diode data.[18]

c) For GaAs, Si + Zn- and Ge-doped recombination regions exhibit better life than Si-only and undoped samples.

---

[18] H. Yonezu, K. Kobayashi, K. Minemura, and I. Sakuma, "GaAs-$Al_xGa_{1-x}As$ double heterostructure laser for optical fiber communication system," Technical Digest, 1973 International Electron Devices Meeting, Washington, December 3-5, 1973, p. 324.

[22] Some of these data were reported on by M. Ettenberg, H. F. Lockwood, J. P. Wittke, and H. Kressel, "High radiance, high speed $Al_xGa_{1-x}As$ heterojunction diodes for optical communications," Technical Digest, 1973 International Electron Devices Meeting, Washington, December 3-5, 1973, p. 317.

The above results are indicative of lifetime trends for the specific doping ranges shown and do not indicate the actual limits of what can be achieved. It should be emphasized that it is possible to fabricate heterojunction diodes using GaAs recombination regions with operating lifetimes in the incoherent mode of operation as high as those shown in Figure 46 for (AlGa)As. For example, GaAs diodes with heavily Ge-doped recombination regions ($p > 1 \times 10^{19}$ cm^{-3}) can exhibit an operating life greater than 10^4 hours. However, because of the very heavy Ge doping, these diodes are inefficient lasers.

To examine the correlation between incoherent emission tests and the diode properties in the lasing mode, tests were performed on a group of LOC lasers (with a 2.3-μm heterojunction spacing and a 1-μm Te-doped GaAs recombination region) at 1000 A/cm^2 with periodic tests of the threshold current density and differential quantum efficiency. These were broad-area contacted devices (100 x 300 μm) with cleaved facets to form the Fabry-Perot cavity and sawed sides. Figure 47 shows the results of these tests in the form of plots of normalized threshold current density, differential quantum efficiency, and spontaneous output (at ~1000 A/cm^2) as a function of operating time. The major conclusions from these data are as follows:

a) The lasing properties degrade simultaneously with the spontaneous emission, though at a slower rate. In fact, some diodes which degraded in the spontaneous emission regime hardly changed their threshold current density or differential quantum efficiency. On the average, a factor-of-2 reduction in the spontaneous emission intensity corresponds to a 25% reduction in the differential quantum efficiency and a 15% increase in the threshold current density.

b) There is a great deal of scatter in the correlation between spontaneous and lasing properties. In one diode, No. 2, degradation in the incoherent mode of operation occurred while the lasing properties changed very little. This results from nonuniform degradation within the diode.[21,23] Near-field observation of the diodes in the lasing mode after the degradation test shows that small portions of the lasers are still operating, indicating the nonuniform nature of the degradation for the broad-area devices. This suggests that in narrow stripe geometry diodes, where

[21] Henry Kressel and N. E. Byer, "Physical basis of noncatastrophic degradation in GaAs injection lasers," Proc. IEEE, vol. 57, p. 25, January 1969.

[23] B. C. DeLoach, B. W. Hakki, R. L. Hartman, and L. A. D'Asaro, "Degradation of CW GaAs double-heterojunction lasers at 300 K," Proc. IEEE, vol. 61, p. 1042, July 1973.

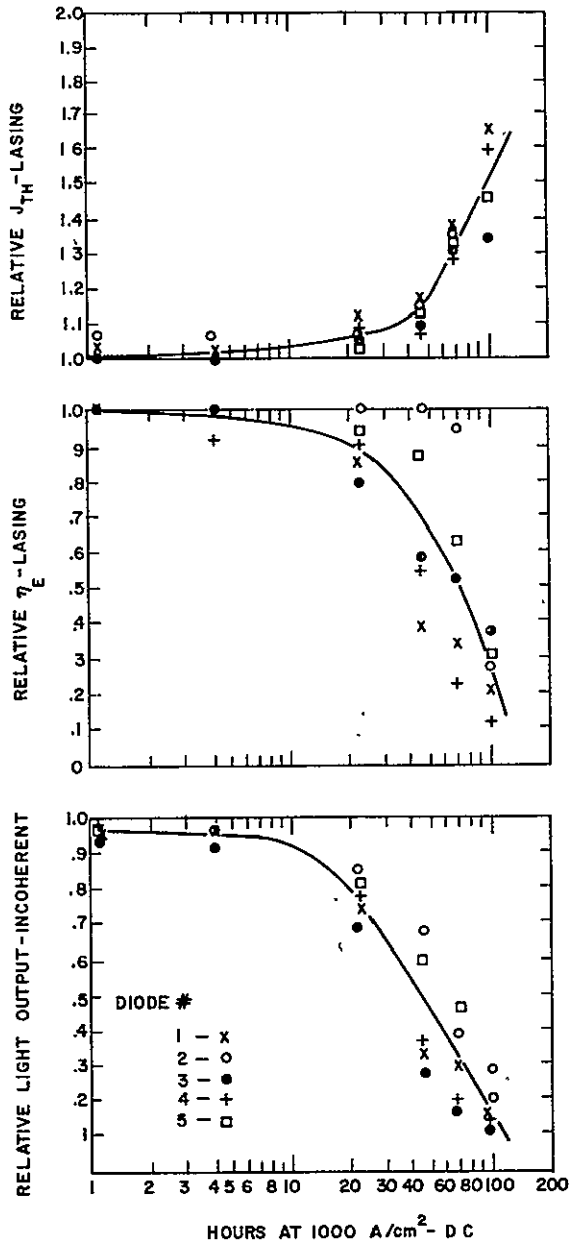

Figure 47. Relative incoherent emission and lasing threshold and efficiency LOC-type lasers as a function of time when stressed at ~1000 A/cm^2. η_e is differential quantum relative to undegraded diode. J_{th} is threshold current density relative to undegraded diode.

only a small portion of the crystal is active, individual diodes may have better life than broad-area diodes similarly operated. In fact, stripe geometry GaAs lasers have been reported with lifetimes above 1000 h.[24,25]

In order to relate this to the pulsed laser tests, note that the average current density of a laser diode of dimensions 0.006 x 0.014 inch operating at 10 A current and 0.5% duty factor, is 100 A per square centimeter. Thus, from Figure 47 it is seen that use of this data indicates bulk damage should be expected by 1000 hours for material of comparable parameters. This could be reduced by alloying to AlGaAs and using the pump bands near 81 μm.

Thus, although lifetimes in excess of 1000 hours can now be seen in a substantial portion of a sample of LOC GaAs diodes for loading of 0.5 W/mil of facet width with pulse lengths of 25 to 50 s, stabilizing the characteristic throughout a sample is expected to be a difficult task requiring much work in the materials. An easier path for laser pump sources for Nd:YAG is expected if shorter wavelengths are employed where incoherent studies reveal greater life. At these wavelengths, CW AlGaAs laser sources have shown lifetimes in excess of 5000 hours without degradation. Mild extrapolations of power levels with indirect coupling (i.e., fiber optics) lead to pumping techniques with a greater expectation of long lifetime.

E. WAVELENGTH MATCHING TO PUMP BANDS

Three techniques have been used to tune the wavelength of emission in GaAs or alloyed GaAs laser diodes:

Temperature tuning

Alloying with AlAs or GaP

Adjustment of the P dopant concentration.

---

[24] H. Yonezu, I. Sakuma, T. Kamejima, M. Ueno, K. Nishida, Y. Nannichi, and I. Hayashi, "Degradation mechanism of (Al·Ga)As double-heterostructure laser diodes," Appl. Phys. Lett., vol. 24, p. 18, January 1, 1974.

[25] R. L. Hartman, J. C. Dyment, C. J. Hwang, and M. Kuhn, "Continuous operation of GaAs-$Ga_{1-x}Al_xAs$ double-heterostructure lasers with 30°C half-lives exceeding 1000 hours," Appl. Phys. Lett., vol. 23, p. 181, August 15, 1973.

The bandgap in GaAs temperature tunes at a rate of 0.22 to 0.3 nm/°C over the temperature range of 77°K to 350°K or more. Figures 48 and 49 show temperature tuning for Si and Zn diode samples. As heat sink temperature is limited to greater than 250°K with room temperature of 300°K, temperature tuning is limited to a maximum of 10 nm from the 300°K value. Part of this may profitably be used to fine tune the emission to the absorption peak.

Alloying with AlAs or GaP allows the emission wavelength to be tuned for a particular wafer, from about 900 nm to less than 800 nm with generally better devices being produced using AlGaAs. The major difficulty is in providing adequate control of the composition of all the layers in the LOC structure to allow reproducible lasers to be constructed for operation in the shorter pump bands. This technology was not selected for this program because of its immaturity.

Variations in dopant and doping level affect the emission wavelength of GaAs. Large doping levels generally produce longer emission wavelengths. Intrinsic GaAs has an emission at $\leq$890 nm at room temperature; highly doped p type GaAs doped with Si can have a laser emission wavelength of greater than 910 nm. Other dopants, including Zn, produce shorter wavelengths, and it has been determined that lasers emitting at approximately 895 nm at room temperature may be constructed using several p-dopants. Throughout a major portion of this contract Zn-doped GaAs lasers were characterized for the arrays. Determination that these lasers appear to be fundamentally limited in lifetime because of Zn in the junction region during this and other work led to the selection of an alternate dopant, Ge, which does not have this limitation but still allows room temperature operation at 895 nm or less. Thus, with temperature tuning, the line of Nd:YAG at 885 nm may be pumped. Because of the availability of high-power low-temperature homojunction arrays, the 868 nm band was selected for some pumping experiments.

During this program, a number of changes in processing of diodes for near room temperature operation were brought about by integration of known techniques. The desired characteristics of the diodes were:

Peak power	3 W
Peak current	10 A
Threshold current	<5 A
Duty factor	1%
Wavelength	890 nm at 300°K (low duty factor)
ΔT at high duty factor	15°K
Dynamic impedance	0.1 ohm
Lifetime	$\geq$10,000 hours at 1% duty factor
Efficiency	10% overall
Emitting width	6×10^{-3} inch.

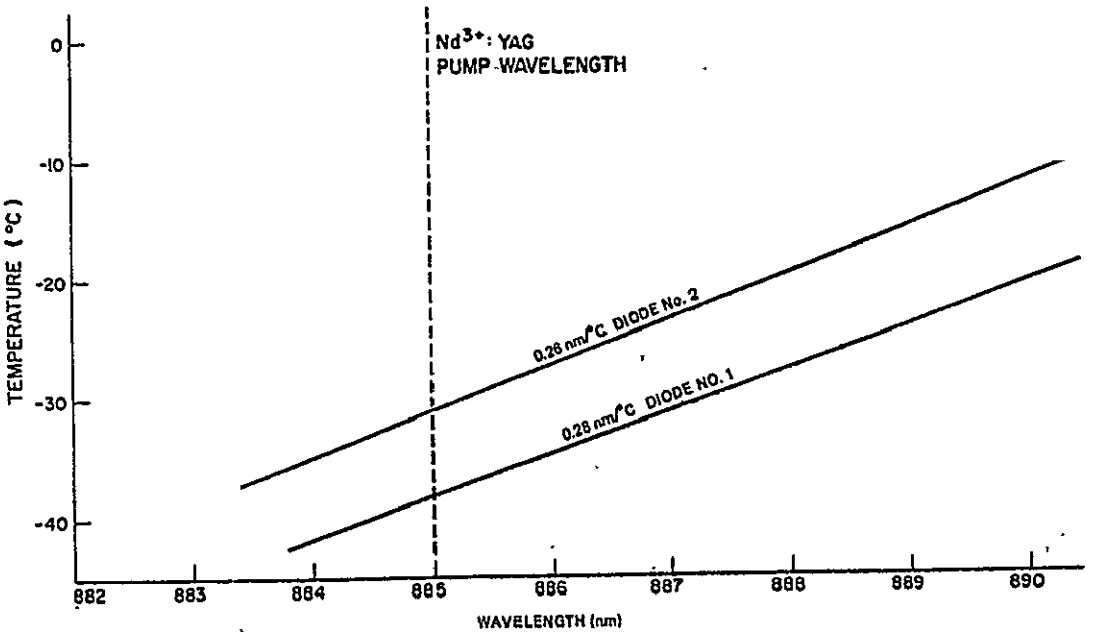

Figure 48. Output wavelength vs temperature of mount for LOC experimental diodes with Si dopant.

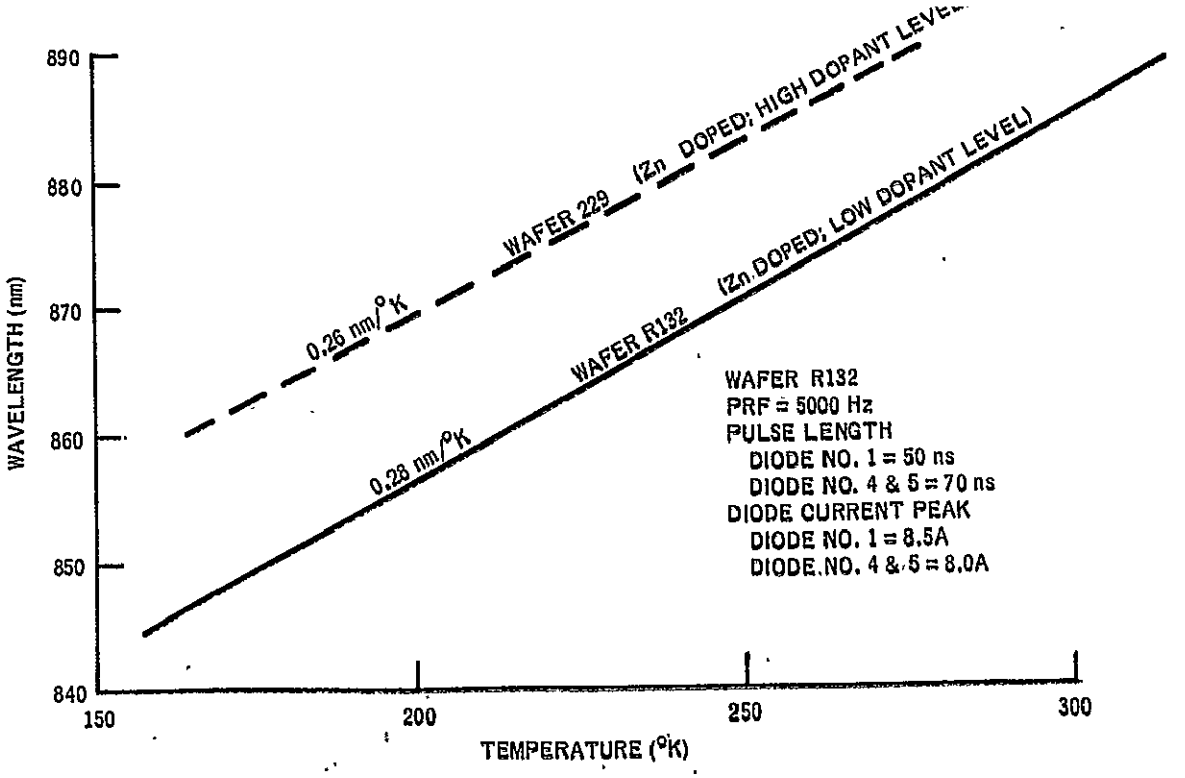

Figure 49. Wavelength vs. temperature for wafer R132.

In general, peak power, drive current and threshold current are closely linked along with quantum efficiency. In order to maximize the quantum efficiency in a LOC diode, one generally desires to operate 3 to 4 times threshold. This can be accomplished either by increasing the drive current or by thinning the waveguide region. Because of the limited drive currents (i.e., 10 A) available from practical high efficiency drive circuitry at the required pulse widths to maintain good life characteristics and because of the observed thresholds for catastrophic facet damage, operation near 2X threshold was chosen for this contract. This led to a light generation layer (p-GaAs) of 1 μm and to the second layer composing the optical cavity (N-GaAs) being approximately 1 μm thick. This, with the proper index difference to the waveguiding layer (AlGaAs) leads to excellent quantum efficiencies and thresholds of 5 A or less for room temperature operation when combined with appropriate doping levels. The threshold characteristics of a number of wafers are summarized in Table 6.

In electrical characteristics, laser diodes possess the normal diode characteristic plus some amount of series resistance. The band gap of the diode is a fundamental characteristic of a particular composition. The resistance is formed of terms from 1) contact resistance which is a measure of the ability to make ohmic contacts on both surfaces of the diode and 2) the resistance of the individual layers of the stack. Reductions in resistance have been made in both these areas during this work. Contacts of very low resistance and high reproducibility continue to be a problem being attacked by using proprietary techniques under RCA funding. Dynamic resistances from 0.05 ohm to 0.5 ohm were observed at various times during this contract. Unfortunately, the particular contact used and the materials on which it was used to produce 0.05 ohm resistance apparently led to lifetime problems. Alternate methods used since that time have failed until recently to achieve reproducible values approaching this.

The primary change made to reduce the resistance within the laser diode structure was in going to the seven-layer LOC structure rather than the four- or five-layer structure. In the seven-layer structure, contact is made to a relatively thick (i.e., 10 μ m) GaAs layer which is exposed by etching off a heavily alloyed AlGaAs layer. This compares to the four- or five-layer structure in which contact is made directly to the p-AlGaAs layer used to form the second waveguide boundary. In this structure, this layer is grown in the last bin of the furnace. Because of this, thickness is difficult to control. The result is a thick uneven layer (i.e., 20 to 40 μm) of p-AlGaAs on the side normally contacted to the mounting block.

This has two deleterious effects:

1) p-AlGaAs has much higher electrical resistivity than p-GaAs which causes the high electrical resistance in these diodes. The p-GaAs layer will continue to dominate the electrical characteristic of the diode. Thinning the layer increases contacting problems and mounting problems (solder thickness must be more carefully controlled). The effect of these changes may

TABLE 6. RESULTS OF WAFER GROWTHS AND TESTS

Wafer No.	No. of Layers	P Dopant	Layer 6 p^+ cap Thick. (μm)	Layer 4 p GaAs Thick. (μm)	Alloy Comp.	Temp. for 885 nm (°K)	Threshold for 885 nm (A)	ΔT at 1% Duty Cycle 877.5 nm (°K)	Slope of EI Curve	Effective Resistance at Operating Current (ohms)	Average Efficiency	
											Ratio of Peak Power Out to Peak Power In (%)	Operating Current (A)
226	4	Zn	-	25	-	248-256	2.4-4.4	15-40	0 27	0.49	5.0	15
229	4	Zn	-	25	-	258-269	4.2-5.5	35-74	0.30	0.53	2.4	15
230	5	Zn	~25	5	-	272-278	5.7-7,5	24-32	0.37	0.70	2.4	15
R132	7	Zn	9.2	1.1	-	293-303	4.2-5.6	4.5-9.0	0.05	0.25	10	15
R133	7	Zn	4.8	1.0	-	298-306	4.5-7.0	2.8-8.8	0.06	0.23	5.0	15
R140	7	Zn	8.0	0.9	Yes	303-340	3.5-4.3	12	0.33	0.6-0.7	8.4	6
R144	7	Zn	10.8	1.0	-	300-322	5.4-10	16	0.05	0.26	5.1	15
R145	7	Zn	4.5	1.0	-	292-308	3.6-4.9	14-18	0.06	0.23	10.6	10
R147	7	Zn	9.1	1.0	-	290-312	3.6-5.3	26	0.13-0.15	0.33	7.0	10

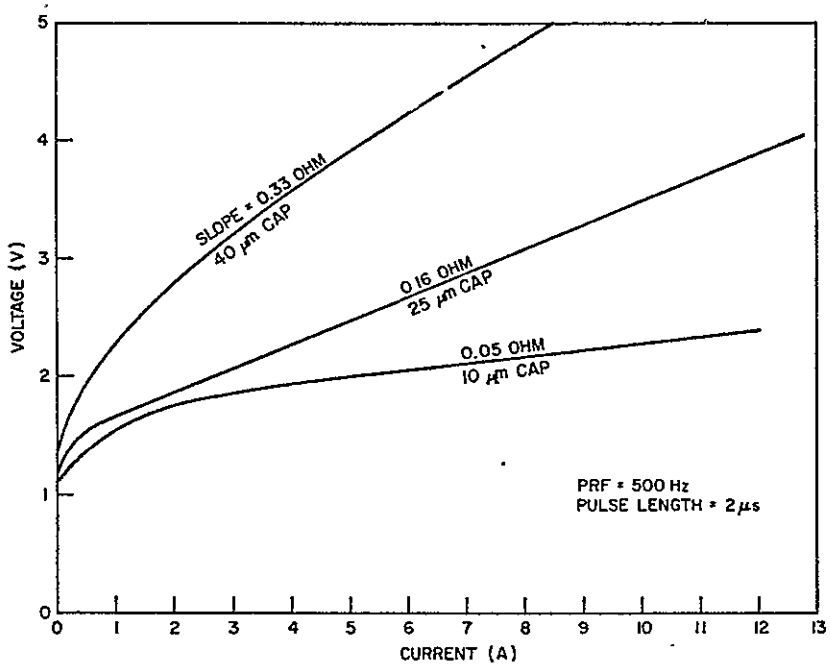

Figure 50. Voltage-current characteristics for typical water.

be observed in Figure 50, which compares the characteristics of diodes with thick Al GaAs top layers to characteristics of diodes with 5 and 10 μm thick GaAs top layers with thin internal AlGaAs p-layers.

2) A similar loss of thermal conductivity occurs in the p-AlGaAs, which is used in mounting the diodes. The temperature rise from the heat sink to the junction is increased substantially for high duty factors. This improvement is indicated by the changes in ΔT in Table 6.

F. ARRAY FABRICATION TECHNIQUES

The subarray processing sequence is illustrated in Figure 51. The metallized wafer is cleaved along the <100> axis to provide slivers of approximately 12 x 480 mils. To one of the cleaved faces, a reflective coating is applied by sequential evaporative techniques. The end-coated GaAs sliver and a beryllium-copper p-contact bar are then simultaneously soldered to a metallized beryllium oxide ceramic block. This structure is subsequently submitted to a multiple-cutting operation wherein the GaAs sliver, the BeCu back bar, and the BeO metallization are simultaneously cut, thereby forming the individual laser cavities. This cutting procedure electrically isolates the individual diodes, but does not disturb their mutual optical

alignment. The series electrical interconnection of the individual diodes is accomplished by using small interconnect wires which are positioned from the top of one diode to the back bar of the adjacent diode. These connections are then soldered simultaneously by exposing the subarray to appropriate temperatures in a controlled environment. Subassemblies are then subjected to evaluation performance tests. To accomplish this, the completed subarray is affixed to a temporary mount for performance tests at the final array test conditions.

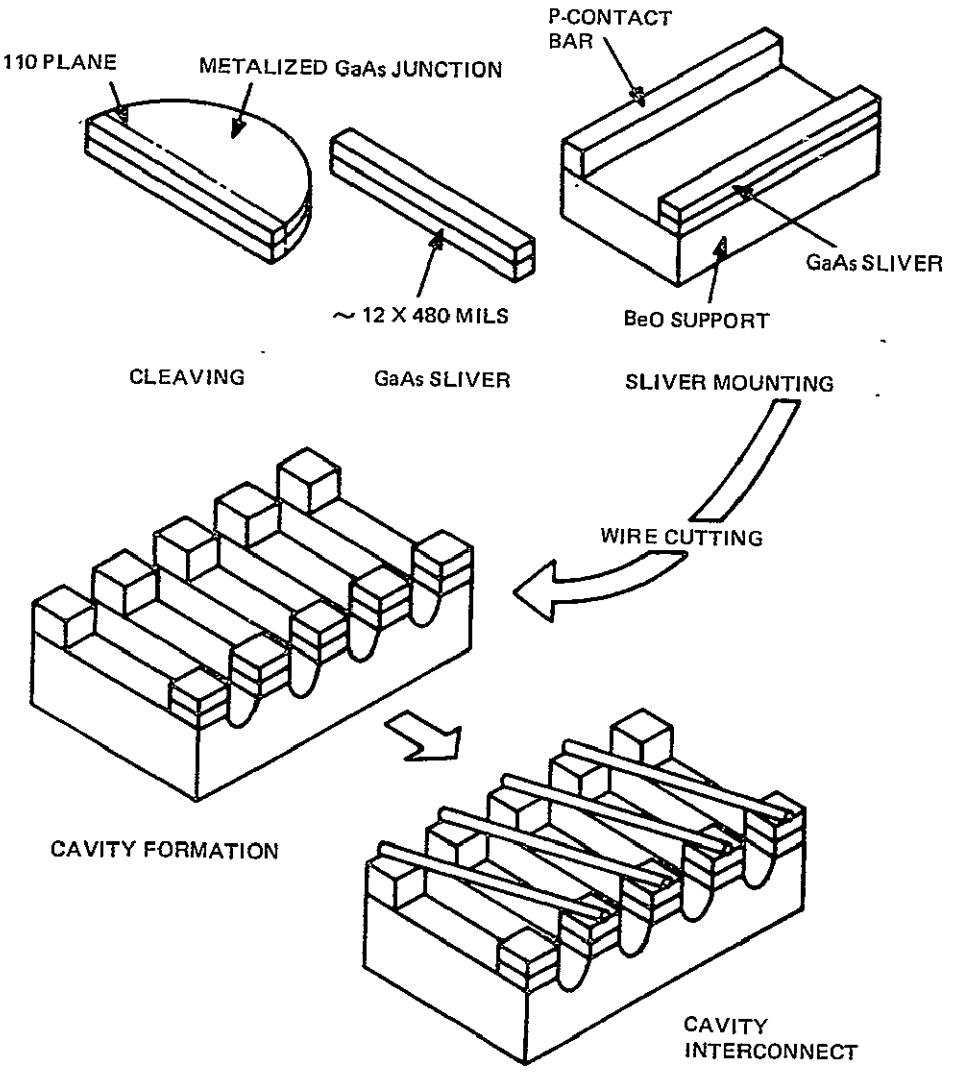

Figure 51. Subarray processes.

Section V

HYBRID DRIVERS FOR INJECTION LASER PUMPED Nd:YAG

A laser diode array driver capable of delivering an adjustable 30-200 ns, 10-A current pulse at 40 V delivered across the array at room temperature was designed and fabricated. The PRF is adjustable up to 500 kHz.

Outstanding features of this pulser are its small size, its high efficiency, its capability for narrow pulse widths, and its high pulse repetition rate. Although the pulser was developed for use with a 10-diode GaAs array, it can be used for operation with as few as one diode and as many as fifteen. The driver employs an RF power transistor in the saturated (switching) mode as the crucial current switching device.

The original driver design, which could deliver pulses as narrow as 45 ns, was subsequently modified to provide 30-ns pulses.

Table 4 includes the circuit specifications chosen as objectives, as well as the circuit performance achieved with the implemented design (Design I) and its subsequent modification (Design II). Figures 52 through 55 show current and voltage waveforms according to conditions specified in Table 7.

A. CIRCUIT OPERATION

Figures 56 and 57 present the two designs for the driver. Overall operation of the circuits is as follows.

A positive-going pulse at the logic level input terminal causes a negative-going pulse at the collector of Q1. The base voltage of Q7 drops from its quiescent +5 level to a level appropriate for turning Q7 on. A positive-going pulse is seen at the collector of Q7 and at the emitter of the emitter follower Q6. If it is assumed that Q4 is off when this positive pulse is present, Q5 can be turned on and saturated by propagation of the pulse through capacitor C5 and resistor R9. Retracing the switching action from Q1 through Q5 in the lower leg of the circuit, it can be seen that a negative-going pulse at collector of Q1 will provide a positive pulse at the collector of Q2, a negative pulse at the base of Q4, resulting in a turnoff of Q4 during the driving of Q5 by the emitter follower stage, Q6. At the trailing edge of the negative-going pulse at the base of Q4, the collector of Q4 drops to a low level as Q4 turns on. Since the voltage across capacitor C5 cannot change instantaneously, the base of Q5 drops below ground, providing negative drive to pull minority carriers from the base emitter junction of Q5 to ensure as short a storage time in Q5 as possible. Smaller pulse widths at greater efficiencies are the result of this "deliberate turnoff" feature. Q5 is a CTC CD6105 chosen for

TABLE 7. PULSER PERFORMANCE

Parameter	Objective	Design I	Design II
Pulse Amplitude	10 A nominal	10 A nominal	10 A nominal
Rise Time	35 ns or less	41 ns	30 ns
Fall Time	25 ns or less	10 ns	8 ns
Pulse Width Range	75-150 ns	45-200 ns	30-200 ns
Maximum Duty Factor	2.5% or greater	5%	5%
Efficiency	55% or greater	58%	67%
Method of Pulse Width Control	Vary input pulse width	Vary input pulse width	Vary input pulse width
Size	Small enough to permit short leads to laser diode loads	3/4 inch × 1 1/2 inches	3/4 inch × 1 1/2 inches
V+ (driver)	Less than 50 V	40 V nominal	40 V nominal
Load: Dummy load (1 ohm in series with 15-V Zener)			
Power supply voltages for both versions: B+ (driver) = 41 V; B+ (predriver) = 9 V			

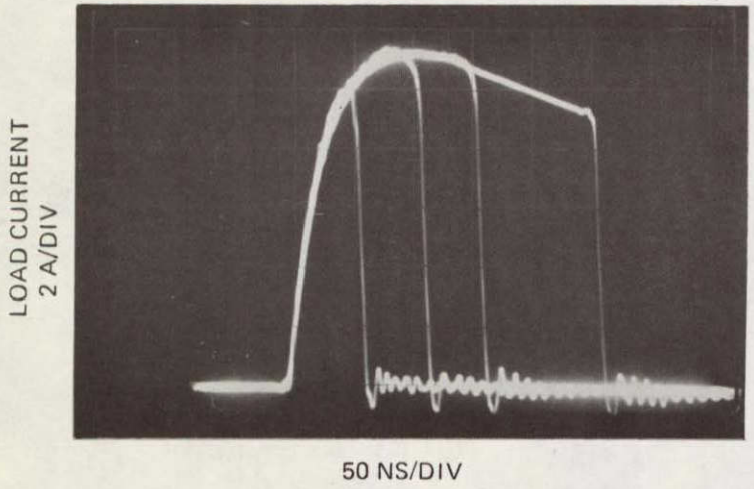

Figure 52. Driver output, Design I, multiexposure showing minimum to maximum pulse width.

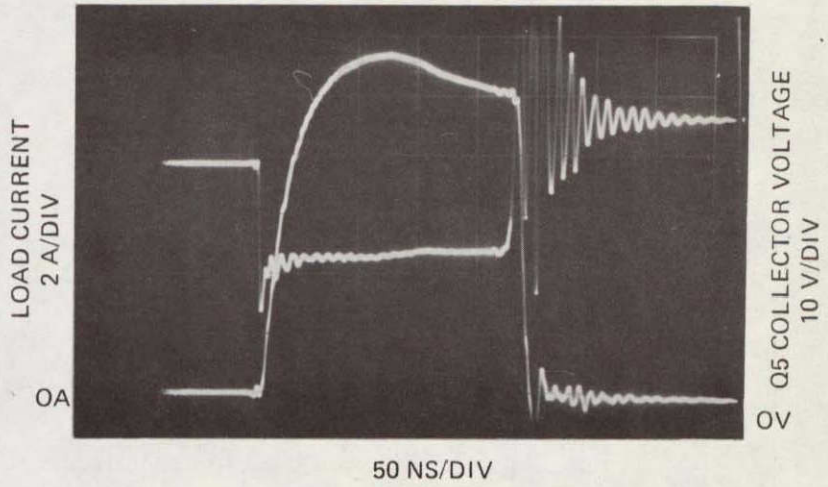

Figure 53. Driver output, Design I, showing load current and switching transistor saturation voltage simultaneously.

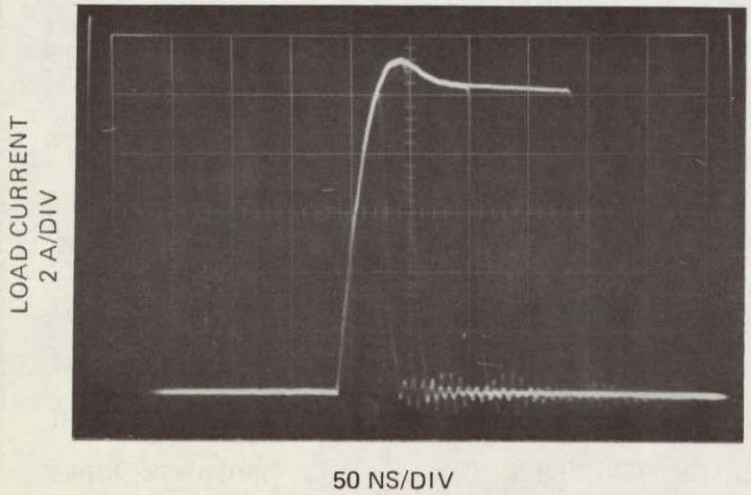

Figure 54. Driver output, Design II, multiexposure showing minimum to maximum pulse width.

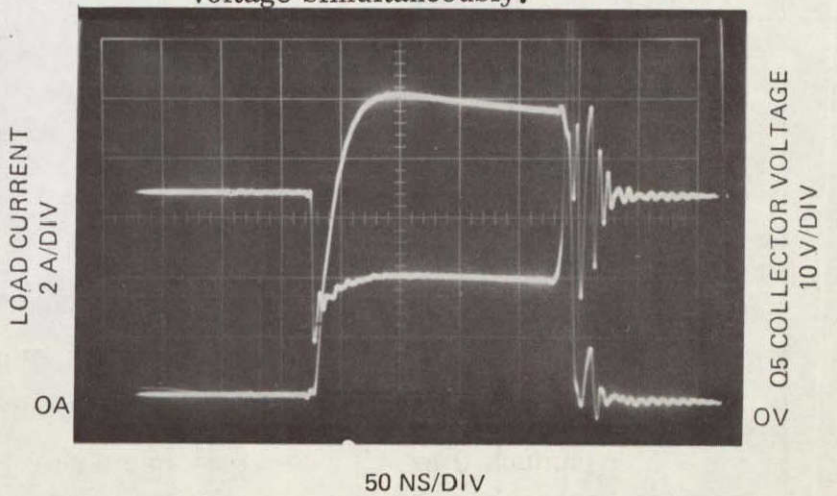

Figure 55. Driver output, Design II, dual trace showing load current and switching transistor saturation voltage.

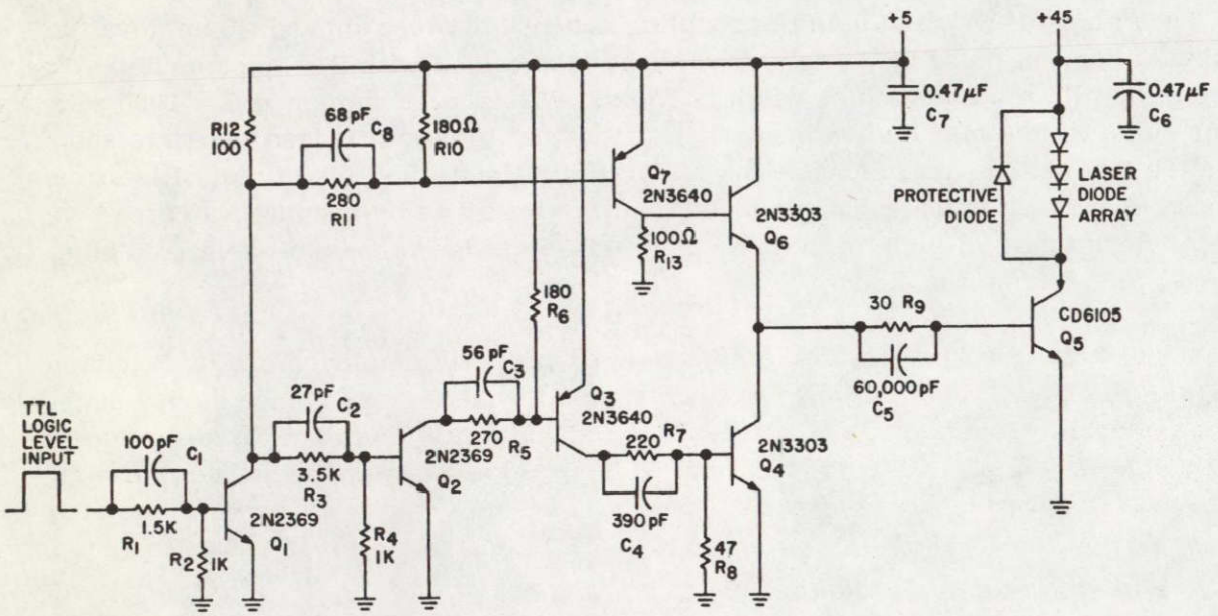

Figure 56. Schematic of laser diode driver, Design I.

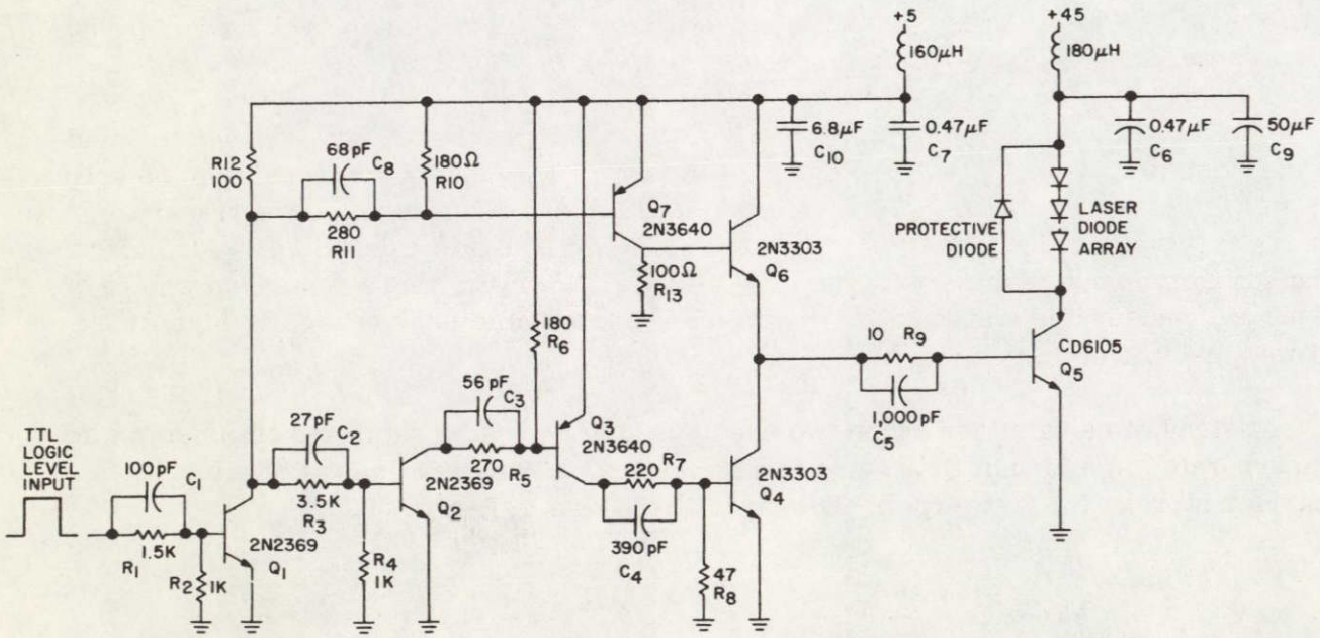

Figure 57. Schematic of laser diode driver, Design II.

its large collector current rating (5 A), small saturation voltage (10 V at 10 A), and fast switching speed (less than 4 ns).

The values of R9 and C5 in the coupling network between Q6 and Q5 achieve the minimum current pulse width delivered at the load; e.g., with R = 30 ohms and C = 60,000 pF, minimum pulse width is 75 ns. With R = 10 ohms and C = 1000 pF, 30-ns pulse widths may be obtained. It is important to note that lead length to and from the laser diode array load is the major limitation to fast rise time. Rise times for a 10-A current pulse can be reduced to as low as 20 ns by keeping short lead lengths (less than 1/2 inch total) or by using low-impedance coaxial cable (10 ohms or less) to and from the diodes.

Most of the previous work on laser diode drivers has employed one or two basic designs. A considerable majority of drivers use a negative resistance device such as an avalanche transistor or SCR to switch high currents (10 to 100 A) at fast speeds (40-ns pulse widths). In such a design a capacitor or delay line discharges through the negative resistance and laser diode load to produce a fast-rise-time (10-ns rise time) high-current pulse. A typical avalanche transistor circuit is shown in Fig. 58.

The chief drawback to a design with a negative resistance device is the limitation on repetition rate, a difficulty caused by two inherent properties of the device. The first is the inability of the device to hold off anode (collector) voltage if voltage is applied too soon after avalanching. The second is the inability to stay nonconductive if anode (collector) voltage rises too fast. This latter property is called "critical rate of rise, dV/dt." Testing of a popular high-current nanosecond SCR demonstrated that this state-of-the-art device cannot be operated above 100 kHz without fear of "latch-on" and laser diode destruction. Difficulty of pulse width control further lowers the practical value of the negative resistance device.

In lieu of the negative resistance device approach, designers have chosen to pulse semiconductor lasers with drivers using conventional transistors operating in the active region. Those who desire narrow pulse width have avoided saturating the transistor in the last stage of the pulser in order to skirt the problem of excessively wide pulses caused by minority carrier storage time effects. However, those designers who have used the unsaturated transistor have suffered reduced efficiency caused by significant power dissipation in the last stage.

Instead of using either of the two previous approaches, a saturated transistor was incorporated in a circuit to provide fast turnon and deliberate removal of minority carrier storage for fast turnoff. The circuit is shown in Figure 56.

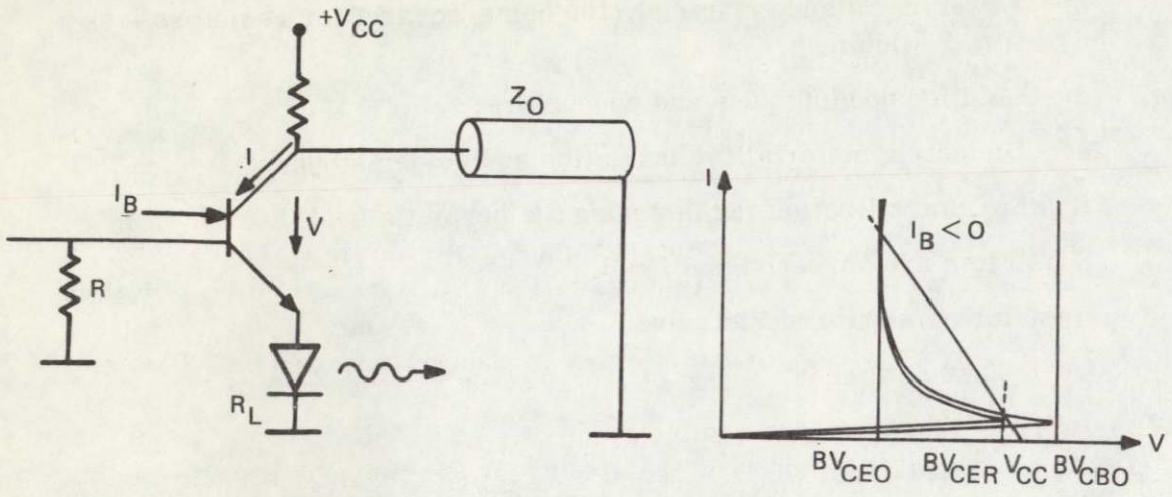

Figure 58. Typical avalanche transistor circuit and operating characteristics.

B. HYBRID THICK FILM MICROCIRCUIT

Because proximity to the diodes and resulting low distributed load inductance are essential to the driver's fast rise time and high current performance, miniaturization in the form of a hybrid thick film microcircuit was chosen. Only by hybridization of a driver into a module, 3/4 x 1-1/2 inches, could convenient packaging of 20 circuits be achieved. The size of a human fist would approximate the volume required for the twenty drivers. An equivalent PC board system would be the size of a shoe box. Proximity of a diode array to its respective driver is no greater than 2-1/4 inches and average distance is only 1 inch. Because the hybrid microcircuit is mounted on an alumina substrate which is metallized and indium soldered to a copper board, heat sinking properties are excellent.

Since technology for making thick film microcircuits is well developed, most of the design rules and fabrication techniques are straightforward, resulting in high yield and faithful reproduction of the breadboarded circuit's performance.

A coarse step-by-step procedure for making the hybrid driver is detailed below:

1) Breadboard circuit is built and desired performance is achieved.
2) Layout of substrate determines where each device should go and how it should be interconnected.
3) Six screens are made.
   a) PtAu (platinum gold) for resistor termination and conductive material.
   b) High resistance (1 kilohm/square) material for resistors greater than 1 kilohm.

c) Lower resistance material (100 ohms/square) for resistors less than 1 kilohm.

d) Gold for bonding pads and conductors.

e) Dielectric material for insulation and solder stops.

f) Seal metallization for fastening the hermetic seal.

4) Substrates are screened and fired.

5) Resistors are trimmed to value.

6) Devices are attached.

7) Prepackaging tests are completed.

8) Hermetic seals are mounted.

9) Hybrid is tested.

A rectangular cover, which protects all the active devices in the hybrid, can be soldered into place over the rectangular-shaped seal metallization. Also, a protective diode is soldered into place from the laser diode out pin to V+. This diode protects the laser diode under test from sustained reverse bias and protects the transistor switch (CD6105) from high voltage breakdown caused by inductive ringing when the switch is turned off.

C. DRIVER-MODE ARRAY INTERFACE

As was previously discussed, a system of packaging and heat sinking has been built to allow for close proximity between driver and array. This system calls for four single hybrid drivers to be indium soldered to a copper board. Five copper boards are then stacked together to achieve the desired configuration. Figure 59 shows a driver with its cover removed mounted on a copper plate adjacent to a laser diode array that it will be driving. The driver has six terminals for external connections:

1) +45 V dc
2) + 5 V dc
3) Ground
4) To laser diode array (+)
5) From laser diode array
6) Logic level.

D. RIPPLE-FIRED LOGIC

Firing multiple drivers sequentially is particularly well suited to a TTL logic system consisting of a clock, divide by, encoding circuits, and an array of one-shots. Such a system can be designed so that the clock frequency can be changed and the pulse width for each output varied individually.

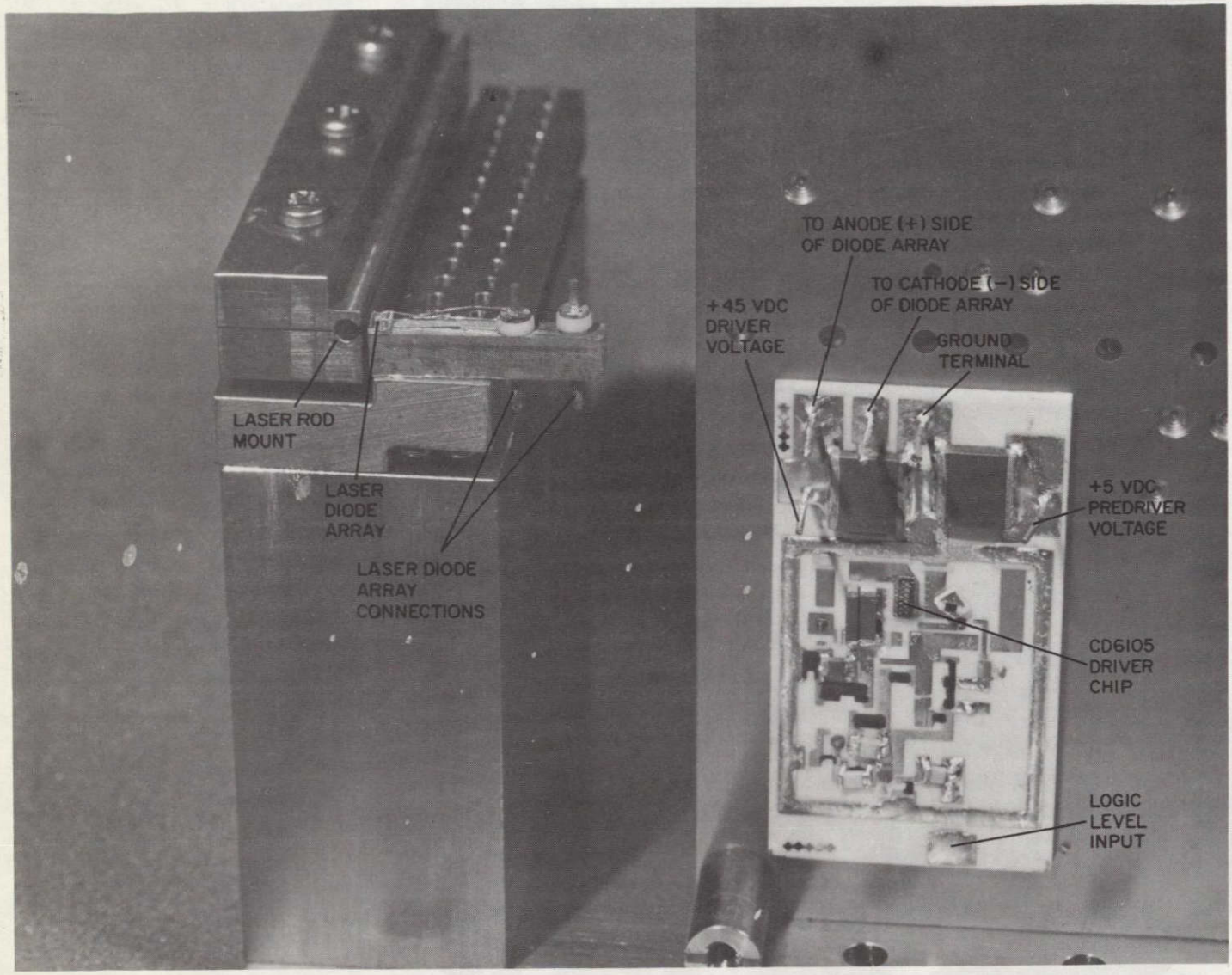

Figure 59. Hybrid driver with cover removed.

The clock feeds its 1-MHz nominal output into the "count to 18" circuit (see Figure 60). The counter is composed of two chips (a 5476 flip-flop and a MC4023 counter). MC4023 is a programmable counter that can be connected to count any number between 2 and 12 except 7 and 11. If the MC 4023 is set to count up to 9, various pins on the chip will give intermediate states of the various internal flip-flops during the count. The output from the 5426 flip-flop may be called Q_* and the states of the flip-flop of the MC4023 may be called Q_0, Q_1, Q_2, Q_3. These five states have inverses associated with them: $\overline{Q}_*$, $\overline{Q}_0$, $\overline{Q}_1$, $\overline{Q}_2$, $\overline{Q}_3$. Depending on the count (from 1 to 18), all five states have different values (either logic high or logic low).

A potentiometer controls the frequency of the clock. The clock varies in frequency from 667 kHz to 2.5 MHz, which causes the frequency range of each driver to be 37 kHz to 139 kHz.

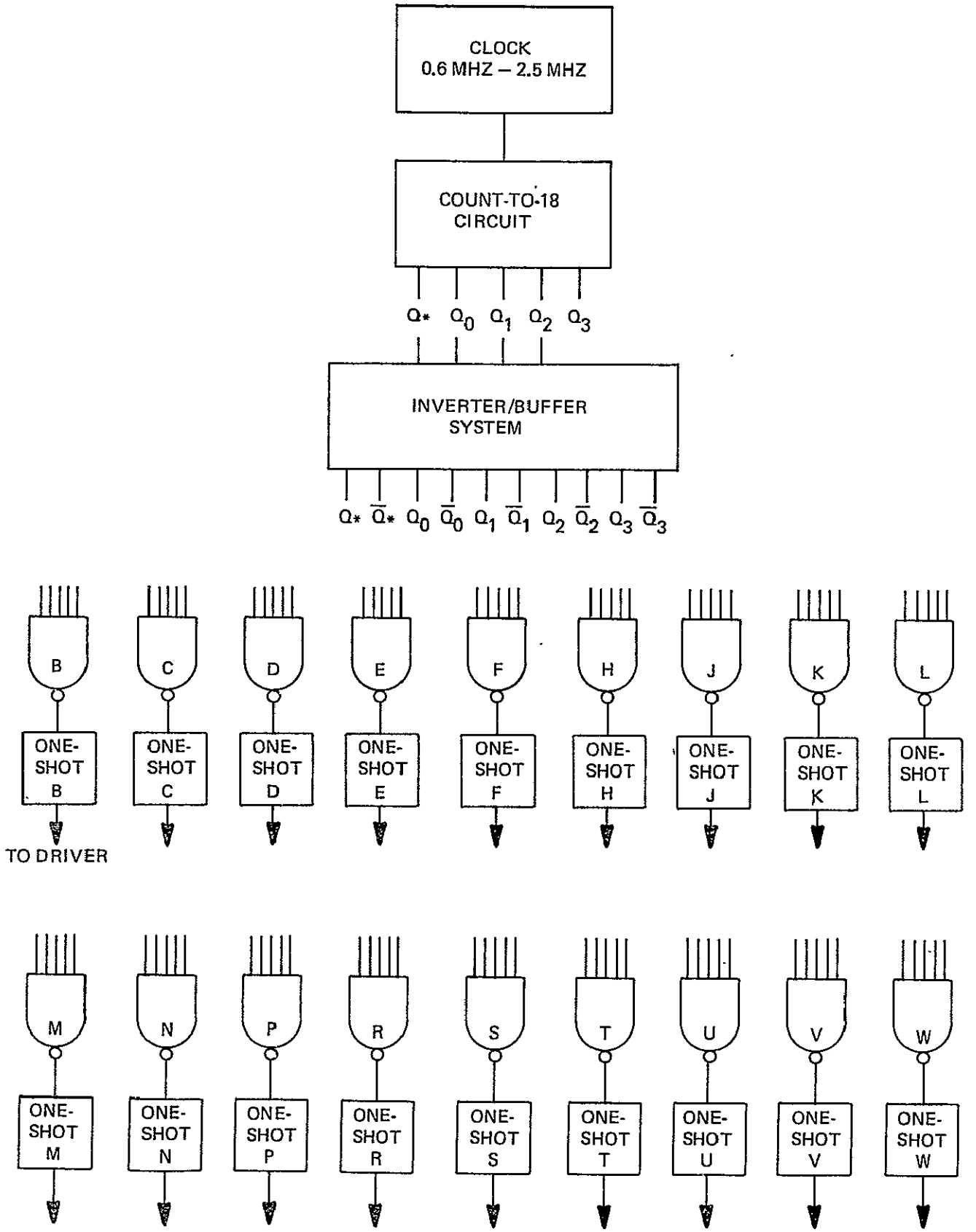

Figure 60. Block diagram of ripple-fired logic system.

Section VI

CONCLUSIONS AND RECOMMENDATIONS

The pumping of Nd:YAG by laser diodes with average power of 125 mW and power efficiency of about 0.25% has been demonstrated to be feasible. Three techniques offer various levels of advantage for use in a long-life system:

Pulsed GaAs LOC diodes operating at 885-nm pump wavelength

Pulsed AlGaAs LOC diodes operating at 806-nm pump wavelength

CW AlGaAs double heterojunction diodes operating at 806-nm wavelength.

CW AlGaAs heterojunction diodes offer proved long life, adequate power efficiency, good wavelength match, and reduced driver problems. The absorption band of Nd in YAG at 806 nm is several times as strong as that at 885 nm. Relatively minor problems are foreseen in producing adequate quantities, arraying techniques, adequate wavelength control, and high efficiency pump coupling. With the present advanced state of the art in CW diodes, this now becomes the prime candidate for a moderate power CW YAG laser. As absorbed powers of approximately 0.6 W can be expected to produce 125 mW output power in a low loss cavity (low concentration rod at 250°K), 40 CW diodes each producing 30 mW can, if efficiently coupled, be expected to pump such a laser.

Pulsed GaAs LOC diodes are conveniently arrayed in numbers up to 10 to 15 diodes for use in ripple fire techniques. They offer stable wavelength properties with adequate power efficiency.

Pulsed AlGaAs LOC diodes (or double heterojunction) can be made to match an optimum pump band of Nd:YAG, but wavelength control to the required level is difficult. Adequate power efficiency seems obtainable. Lifetime properties should be better than GaAs LOC diodes. Arraying techniques duplicate GaAs.

A CW AlGaAs pump should be vigorously pursued for moderate power spacecraft applications because of the basic advantages it will ultimately have in terms of reliability (many fewer vital components), good redundancy in the pump, and relatively high efficiency (up to 1/2% overall).

A recommended arrangement for CW pumping a 1% Nd:YAG laser rod is shown in Figure 61. In this format fiber optics are employed to couple the output energy

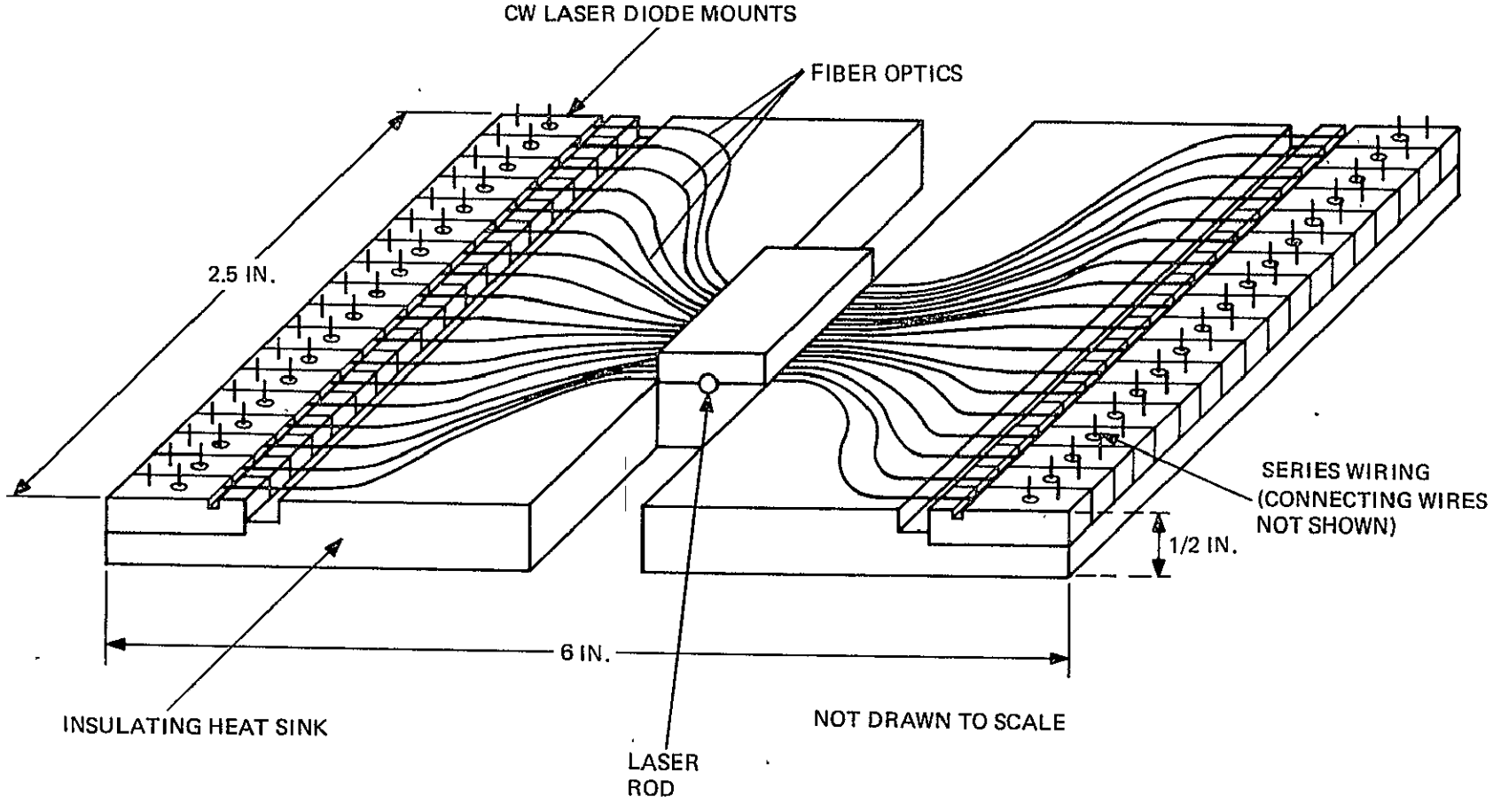

Figure 61. Recommended format for pumping a 1% Nd:YAG laser rod.

of 35 to 40 CW laser diodes into a short (less than 2 cm) laser rod. Total pump power required from the diodes does not exceed 1.2 W. The power coupled by the fiber optics to the rod does not exceed 1 W, with the required absorbed power of 0.6 W. This is feasible within the state of the art on the basis of two premises: 1) quantities of CW laser diodes can be manufactured with characteristics similar to samples currently undergoing life tests, 2) no severe difficulty will be encountered in tuning the wavelength of these diodes to 806 nm ±1 nm at center wavelength. (They are currently operating at approximately 820 nm.)

The operational parameters of such an arrangement are:

Power output:	$\geq$125 mW TEM_{oo}
	$\geq$100 mW at 5000 hours
Power input:	<50W
Heat sink temperature:	$\geq$250°K
Amplitude stability:	± 2% over 100 hours at constant heat sink temperatures
Cooling format:	All conduction cooled
Drive format:	Two series strings, dc regulated power supply
Pump heat sink dimensions: (Feasibility Model)	2.5 inches x 1 inch x 6 inches (0.086 ft^3)

REFERENCES

1. D. Gloge, "Optical fiber end preparation for low loss splices," BSTJ, vol. 52, pp. 1579-89, November 1973.

2. J. A. Koningstein and J. E. Geusic, "Energy levels and crystal field calculations of neodymium in yttrium aluminum garnet," Phys. Rev., vol. 136, pp. 711-716, 2 November 1964.

3. L. J. Rosenkrantz, "GaAs diode-pumped Nd:YAG laser," JAP, vol. 43, pp. 4603-4605, November 1972.

4. R. S. Brandewie and C. L. Telk, "Quantum efficiency of Nd^{3+} in glass, calcium tungstate, and yttrium aluminum garnet," JOSA, vol. 57, pp. 1221-1225, October 1967.

5. R. F. Belt, "Nd concentration in YAG," Laser Focus, vol. 9, p. 51, August 1973.

6. Ronald B. Chesler, "Optimized TEM_{oo} output from a uniformly pumped four-level laser," JQE, vol. QE-8, pp. 493-496, June 1972.

7. Takashi Kushida, "Linewidths and thermal shifts of spectral lines in neodymium-doped yttrium aluminum garnet and calcium fluorophosphate," Phys. Rev., vol. 185, p. 500, 10 September 1969.

8. H. G. Danielmeyer and F. W. Ostermayer, Jr., "Diode-pump-modulated Nd:YAG laser," J. Appl. Phys., vol. 43, pp. 2911-2913, June 1972.

9. H. G. Danielmeyer, "Low-frequency dynamics of homogeneous four-level CW lasers," J. Appl. Phys., vol. 41, pp. 4014-4018, September 1970.

10. J. E. Jackson and R. R. Rice, "Output fluctuations of high-frequency pulse-pumped Nd:YAG laser," J. Appl. Phys., vol. 45, pp. 2353-2355, May 1974.

11. Robert J. Pressley (ed.), Handbook of Lasers. Cleveland: Chemical Rubber Co., 1971, p. 434.

12. M. Ilegems and G. L. Pearson, "Derivation of the Ga-Al-As ternary phase diagram with applications to liquid phase epitaxy," Proc. Second Intl. Gallium Arsenide Symposium, Dallas, 16-18 October 1968, p. 3.

13. H. Kressel, H. F. Lockwood, and J. K. Butler, "Measurements of refractive index step and of carrier confinement at (AlGa)As-GaAs heterojunctions," J. Appl. Phys., vol. 44, p. 4095, September 1973.

14. I. Hayashi, M. B. Panish, P. W. Foy, and S. Sumski, "Junction lasers which operate continuously at room temperature," Appl. Phys. Lett., vol. 17, p. 109, August 1, 1970.

15. H. F. Lockwood, H. Kressel, H. S. Sommers, Jr., and F. Z. Hawrylo, "An efficient large optical cavity injection laser," Appl. Phys. Lett., vol. 17, p. 499, December 1, 1970. H. Kressel, H. F. Lockwood, and F. Z. Hawrylo, "Large-optical-cavity (AlGa)As-GaAs heterojunction laser diode: threshold and efficiency," J. Appl. Phys., vol. 43, p. 561, February 1972.

16. D. B. Keck, R. D. Mauer, and P. C. Schultz, "On the ultimate lower limit of attenuation in glass optical waveguides," Appl. Phys. Lett., vol. 22, p. 307, April 1, 1973.

17. M. Ettenberg, H. F. Lockwood, J. P. Wittke, and H. Kressel, "High radiance, high speed $Al_xGa_{1-x}As$ heterojunction diodes for optical communications," Technical Digest, 1973 International Electron Devices Meeting, Washington, December 3-5, 1973, p. 317. M. Ettenberg, H. Kressel, and H. F. Lockwood, "Degradation of $Al_xGa_{1-x}As$ heterojunction electroluminescent devices," Appl. Phys. Lett., vol. 25, p. 82, July 1, 1974.

18. H. Yonezu, K. Kobayashi, K. Minemura, and I. Sakuma, "GaAs-$Al_xGa_{1-x}As$ double heterostructure laser for optical fiber communication system," Technical Digest, 1973 International Electron Devices Meeting, Washington, December 3-5, 1973, p. 324.

19. H. Kressel, J. K. Butler, F. Z. Hawrylo, H. F. Lockwood, and M. Ettenberg, "Mode guiding in symmetrical (AlGa)As-GaAs heterojunction lasers with very narrow active regions," RCA Review, vol. 32, p. 383, September 1971.

20. P. G. Eliseev, Semiconductor Light Emitters and Detectors (A. Frove, ed.). Amsterdam: North Holland Publishing Co., 1973.

21. Henry Kressel and N. E. Byer, "Physical basis of noncatastrophic degradation in GaAs injection lasers," Proc. IEEE, vol. 57, p. 25, January 1969.

22. Some of these data were reported on by M. Ettenberg, H. F. Lockwood, J. P. Wittke, and H. Kressel, "High radiance, high speed $Al_xGa_{1-x}As$ heterojunction diodes for optical communications," Technical Digest, 1973 International Electron Devices Meeting, Washington, December 3-5, 1973, p. 317.

C 2

23. B. C. De Loach, B. W. Hakki, R. L. Hartman, and L. A. D'Asaro, "Degradation of CW GaAs double-heterojunction lasers at 300 K," Proc. IEEE, vol. 61, p. 1042, July 1973.
24. H. Yonezu, I. Sakuma, T. Kamejima, M. Ueno, K. Nishida, Y. Nannichi, and I. Hayashi, "Degradation mechanism of (Al·Ga)As double-heterostructure laser diodes," Appl. Phys. Lett., vol. 24, p. 18, January 1, 1974.
25. R. L. Hartman, J. C. Dyment, C. J. Hwang, and M. Kuhn, "Continuous operation of GaAs-$Ga_{1-x}Al_xAs$ double-heterostructure lasers with 30°C half-lives exceeding 1000 hours," Appl. Phys. Lett., vol. 23, p. 181, August 15, 1973.

BEST SELLERS

FROM NATIONAL TECHNICAL INFORMATION SERVICE

NTIS

U.S. Service Industries in World Markets: Current Problems and Future Policy Development
PB-262 528/PAT 423p PC$11.00/MF$3.00

Federal Information Processing Standards Register: Guidelines: for Automatic Data Processing Physical Security and Risk Management. Category: ADP Operations. Subcategory: Computer Security
FIPSPUB-31/PAT 97p PC$5.00/MF$3.00

Federal Personnel Management Handbook for Librarians, Information Specialists and Technicians
PB-261 467/PAT 287p PC$9.25/MF$3.00

Handbook for Sampling and Sample Preservation of Water and Wastewater
PB-259 946/PAT 278p PC$9.25/MF$3.00

Historical Trends in Coal Utilization and Supply
PB-261 278/PAT 631p PC$16.25/MF$3.00

Electronic Message Systems for the U.S. Postal Service
PB-262 892/PAT 60p PC$4.50/MF$3.00

Interagency Task Force on Product Liability Legal Study
PB-263 601/PAT 1274p PC$31.25/MF$3.00

NIOSH Analytical Methods for SET P
PB-258 434/PAT 63p PC$4.50/MF$3.00

Interagency Task Force on Product Liability—Briefing Report: Executive Summary
PB-262 515/PAT 56p PC$4.50/MF$3.00

NIOSH Analytical Methods for SET Q
PB-258 435/PAT 40p PC$4.00/MF$3.00

Mini-and Micro Computers in Communications
ADA-031 892/PAT 72p PC$4.50/MF$3.00

Fuel Consumption Study. Urban Traffic Control System (UTCS) Software Support Project
PB-259 003/PAT 71p PC$4.50/MF$3.00

MEDLARS Indexing Manual. (Part I): Bibliographic Principles and Descriptive Indexing, 1977
PB-254 270/PAT 134p PC$6.00/MF$3.00

Coal Transportation Capability of the Existing Rail and Barge Network, 1985 and Beyond
PB-260 597/PAT 152p PC$6.75/MF$3.00

Proceedings of the Workshop on Solar Energy Storage Subsystems for the Heating and Cooling of Buildings, Held at Charlottesville, Virginia on April 16-18, 1975
PB-252 449/PAT 191p PC$7.50/MF$3.00

HOW TO ORDER

When you indicate the method of payment, please note if a purchase order is not accompanied by payment, you will be billed an additional $5.00 *ship and bill* charge. And please include the card expiration date when using American Express.

Normal delivery time takes three to five weeks It is vital that you order by number or your order will be manually filled, insuring a delay. You can opt for *airmail delivery* for $2.00 North American continent; $3.00 outside North American continent charge per item. Just check the *Airmail Service* box. If you're really pressed for time, call the NTIS Rush Handling Service (703)557-4700. For a $10.00 charge per item, your order will be airmailed within 48 hours. Or, you can pick up your order in the Washington Information Center & Bookstore or at our Springfield Operations Center within 24 hours for a $6.00 per item charge.

You may also place your order by telephone or if you have an NTIS Deposit Account or an American Express card order through TELEX. The order desk number is (703) 557-4650 and the TELEX number is 89-9405.

Thank you for your interest in NTIS. We appreciate your order.

METHOD OF PAYMENT

- ☐ Charge my NTIS deposit account no. _____
- ☐ Purchase order no. _____
- ☐ Check enclosed for $_____
- ☐ Bill me. Add $5.00 per order and sign below. (Not available outside North American continent.)
- ☐ Charge to my American Express Card account number

Card expiration date_____

Signature_____

☐ Airmail Services requested

NAME_____

ADDRESS_____

CITY. STATE. ZIP_____

Item Number	Quantity		Unit Price*	Total Price
	Paper Copy (PC)	Microfiche (MF)		

All prices subject to change. The prices above are accurate as of 7/77

Foreign Prices on Request.

Sub Total	
Additional Charge	
Enter Grand Total	

Clip and mail to

NTIS

National Technical Information Service
U.S. DEPARTMENT OF COMMERCE
Springfield, Va. 22161
(703) 557-4650 TELEX 89-9405